arXiv:2605.11473v2 [cs.AI] 3 Nov 2026

TOPPO: Rethinking PPO for Multi-Task Reinforcement Learning with Critic Balancing

Yuanpeng Li
UC Irvine

Gefei Lin
George Washington University

Annie Qu
UC Santa Barbara

Rui Miao[†]
UT Dallas

Code: `https://github.com/NAIVlab/TOPPO`
Training logs: `https://forge.coreweave.com/wandb/liyp1220-uci/TOPPO`

Abstract

Soft Actor-Critic (SAC) and its variants dominate Multi-Task Reinforcement Learning (MTRL) due to their off-policy sample efficiency, while on-policy methods such as Proximal Policy Optimization (PPO) remain underexplored. We diagnose that PPO in MTRL suffers from a previously overlooked issue: critic-side gradient ill-conditioning, which may cause tail tasks to stall while easy tasks dominate the value function's updates. To address this, we propose TOPPO (Tail-Optimized PPO), a reformulation of PPO via Critic Balancing—a set of modules that improve gradient conditioning and balance learning dynamics across tasks. Unlike prior approaches that rely on modular architectures or large models, TOPPO targets the optimization bottleneck within PPO itself. Empirically, on the Meta-World+ MT50 benchmark, TOPPO achieves stronger mean and tail-task performance than prior SAC-family and ARS-family methods while using substantially fewer parameters and reaching their final performance in fewer environment steps. Notably, TOPPO matches or surpasses strong SAC baselines early in training and maintains superior performance at full budget. Ablations confirm the effectiveness of each module in TOPPO and provide insights into their interactions. Our results demonstrate that, with proper optimization, on-policy methods can rival or exceed off-policy approaches in MTRL, challenging the prevailing reliance on SAC and highlighting critic-side gradient conditioning as the central bottleneck.

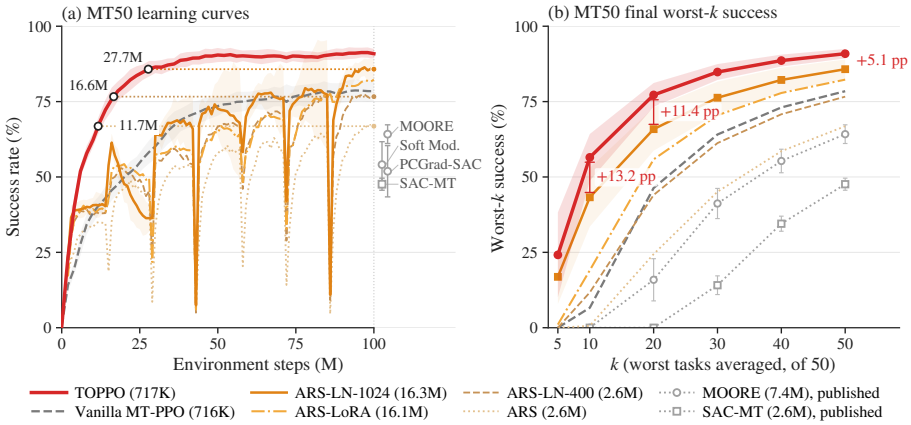


Figure 1: TOPPO (717K params) on Meta-World V2 MT50 outperforms the ARS family at 3.6–22.7× fewer parameters. (a) Training curve (Circles: TOPPO reaching ARS final means). (b) Worst-k tail tasks. Bands are standard deviations.

40th Conference on Neural Information Processing Systems (NeurIPS 2026).

[†]Correspondence to Rui Miao <rui.miao@utdallas.edu>

1 Introduction

Soft Actor-Critic (SAC) [Haarnoja et al., 2018] has been the default backbone for Multi-Task Reinforcement Learning (MTRL), due to its off-policy nature and sample efficiency under online data-collection budgets: the replay buffer reuses past experiences, and the slow target network softens per-task TD-error magnitudes across history so that cross-task gradient imbalance is not directly visible to the optimizer. On Meta-World [Yu et al., 2020b], the canonical multi-task manipulation benchmark, this preference is near-universal: architectural variants (Soft Modularization [Yang et al., 2020], CARE [Sodhani et al., 2021], PaCo [Sun et al., 2022], MOORE [Hendawy et al., 2024], ARS [Cho et al., 2025]) and gradient-aggregation methods (PCGrad [Yu et al., 2020a], CAGrad [Liu et al., 2021], FAMO [Liu et al., 2023], FairGrad [Ban and Ji, 2024], Nash-MTL [Navon et al., 2022], loss-level reweighting [Kendall et al., 2018, Liu et al., 2019]) all build on SAC-style training [McLean et al., 2025]. Despite this, every published non-ARS multi-task SAC method floors at 0% success rate on the ten hardest MT50 tasks, while the strongest ARS variant (ARS-LN-1024) clears the floor only at 43.3% and at a substantially higher parameter cost.

In contrast, on-policy methods such as Proximal Policy Optimization (PPO) [Schulman et al., 2017] remain underexplored in MTRL. The original Meta-World Multi-Task PPO (MT-PPO) baseline scored only $\sim 30\%$ on MT10 with a $(512, 512)$ MLP, and this comparison has not been revisited under architectures matched to modern MTRL methods. PPO is also a useful testbed for cross-task gradient ill-conditioning: its on-policy GAE exposes task imbalance at each minibatch, without replay-buffer smoothing or target-network lag. We therefore revisit MT-PPO with a $[400\times3]$ backbone, matching CAGrad/CARE/PaCo/MOORE, and find that even vanilla MT-PPO lifts the worst-10 tail above the zero floor of prior non-ARS methods while using far fewer parameters.

Although vanilla MT-PPO already breaks the floor, the hardest tasks remain far from solved, and we trace the remaining gap to a self-reinforcing trap on the critic. Early in training, a few easier tasks learn fast and produce large critic gradients, pulling the shared critic network toward features that reduce their TD errors. Harder tasks that contribute little to this aggregate update must then fit their value functions through shared features optimized primarily for other tasks, which biases their advantage estimates rather than simply making them vanish. The actor updates on those tasks then follow this distorted signal; in the online loop, the resulting policies collect worse or less informative rollouts, leaving the next critic update with little useful signal from the same tasks. Crucially, loss-level or actor-side reweighting methods such as DWA [Liu et al., 2019] and UW [Kendall et al., 2018] cannot break this loop when they leave the critic-gradient geometry uncorrected.

Empirically, per-task critic gradient norms span $\sim 497\times$ across tasks, while per-task actor gradient norms span only $\sim 4.1\times$ after per-task advantage normalization (Figure 2). This asymmetry is stable across training, and concurrent benchmarking work also identifies the critic, not the actor,

Table 1: MT-PPO diagnosis, TOPPO module and mechanism. The main failure is critic-side ill-conditioning (D1–D3). The actor row is a residual combiner choice after per-task advantage normalization removes most actor-side scale spread.

Diagnosis	Module / stage	Mechanism and evidence
Critic-side (primary failure)		
D1: Scale Spread	**Per-task value normalizer** value-loss scale; PopArt [van Hasselt et al., 2016, Hessel et al., 2019]	Compresses critic-Gram diagonal scale. Evidence: Figures 3 and D.4, Corollary 1, Table D.1, and Section D.5.
D2: Co-Linear Collapse	**LayerNorm-Critic (LN-c)** critic representation layer [Ba et al., 2016]; RL precedent [Lee et al., 2025, Hansen et al., 2024]	Regularizes the critic feature Jacobian and lowers critic-Gram off-diagonal cosine collapse while leaving scale structure intact. Evidence: Figures 3, D.4 and D.6.
D3: Unfair Aggregation	**FairGrad-Critic (FG-c)** α=1 critic gradient combiner $\mathbf{G}^c\mathbf{w} = \mathbf{w}^{-1}$ [Ban and Ji, 2024, Mo and Walrand, 2000, Kelly, 1997]	Pins the combined-gradient norm at $\sqrt{K}$-level and absorbs positive task-wise rescaling at the aggregator output. Evidence: Theorem 1 and Figures D.7 and D.9.
Actor-side (secondary failure)		
Direction Conflict	**PCGrad-Actor (PCGrad-a)** actor gradient combiner on $\mathbf{g}_i^a$ [Yu et al., 2020a]	Actor norm spread is small, so the actor-side combiner targets negative-cosine pairs rather than scale. Evidence: Figures 2 and D.5 and Table D.2.

as where cross-task gradient conflict concentrates in MT-PPO [Joshi et al., 2025]. The critic ill-conditioning then decomposes into three aspects (Table 1): (D1) per-task gradient-norm spread, (D2) representation-level co-linear collapse in the per-task Gram matrix, and (D3) unfair aggregation of an already-imbalanced gradient set.

To address these three aspects of critic ill-conditioning together with the residual actor-side gradient conflict, we propose TOPPO (Tail-Optimized PPO), which incorporates four modules at four distinct stages of the per-minibatch update (Table 1). PopArt normalizes per-task value targets via a per-task affine head, putting each task's squared TD loss on a comparable scale before the critic gradients are formed. LN-c adds LayerNorm in the critic to improve hidden-feature conditioning. FairGrad (α=1) reweights per-task critic gradients with an α-fair objective, selecting a scale-invariant aggregate critic update. Finally, PCGrad-a handles the remaining actor-side conflict by projecting negative-cosine actor-gradient pairs after advantage normalization.

In our experiments, with only 717K parameters, TOPPO reaches $90.9 \pm 1.6\%$ final-checkpoint mean success on MT50 and $56.5 \pm 7.8\%$ on the worst-10 tail tasks. This is 5.1 and 13.2 points above ARS-LN-1024, the strongest ARS variant, in terms of mean success and worst-10 tail success rates, with $22.7\times$ fewer parameters (Table 2). TOPPO reaches the full-budget mean of ARS-LN-1024 after only $\sim 28\%$ of the environment-step budget (Figure 1(a)).

Summary of contributions. Our main contribution is a critic-centered diagnosis of MT-PPO failure and a stage-specific reformulation across the target, critic, and aggregation pathways.

- We diagnose three major aspects of MT-PPO critic ill-conditioning (D1–D3) and a minor aspect of actor ill-conditioning, and identify their empirical signatures in MT10 (Figures D.4 and D.6).
- We propose TOPPO, a four-module intervention (PopArt, LN-c, FairGrad (α=1), PCGrad-a), applied at distinct stages of the per-minibatch update.
- Theoretically, we show that FairGrad with α=1 fixes the combined-gradient L^2 norm at $\sqrt{K}$ and is invariant to positive task-wise rescaling at the aggregator output, explaining the predictable composition of PopArt and FG-c. We also introduce a projected Newton solver that makes FG-c tractable at K=50 ($\sim$50–1,450$\times$ faster than a generic `scipy` nonlinear-solver baseline).
- We show through experiments on Meta-World+ that TOPPO outperforms existing methods on MT50. Along the ablation study the full stack TOPPO gives the best MT50 headline and tail results, while individual marginal effects depend strongly on the reward regime.

2 Preliminaries

We consider Markov Decision Processes (MDPs) $\{\mathcal{M}_i\}_{i=1}^K$ sharing the same state space $\mathcal{S}$ and action space $\mathcal{A}$ across K tasks indexed by i, with initial state $s_0 \sim \mu_i$, task-specific transition dynamics $P_i(s' \mid s, a)$ and reward $r_i(s, a)$ [Yu et al., 2020b, McLean et al., 2025]. In online MTRL, the agent jointly learns a task-aware policy $\pi_{\boldsymbol{\theta}^a}(a \mid s, i)$ and state-value critic $V_{\boldsymbol{\theta}^c}(s, i)$ with parameters $\boldsymbol{\theta}^a$ and $\boldsymbol{\theta}^c$ shared across all K tasks. The objective is to maximize the average cross-task expected discounted return $\frac{1}{K}\sum_{i=1}^K \mathbb{E}_{\pi_{\boldsymbol{\theta}^a},\, P_i, \mu_i}\big[\sum_t \gamma^t r_i(s_t, a_t)\big]$ with some discount factor $\gamma \in (0, 1)$.

In MT-PPO, for each task i, we collect rollouts $\{(s_t, a_t, r_i(s_t, a_t))\}$ from $\mathcal{M}_i$ under the old policy $\pi_{\boldsymbol{\theta}^a_{\text{old}}}$, then calculate the importance ratio $\rho_t^{(i)}(\boldsymbol{\theta}^a) = \pi_{\boldsymbol{\theta}^a}(a_t \mid s_t, i) \,/\, \pi_{\boldsymbol{\theta}^a_{\text{old}}}(a_t \mid s_t, i)$, the per-task TD residual $\delta_t^{(i)} = r_i(s_t, a_t) + \gamma V_{\boldsymbol{\theta}^c_{\text{old}}}(s_{t+1}, i) - V_{\boldsymbol{\theta}^c_{\text{old}}}(s_t, i)$, the GAE advantage $\hat{A}_t^{(i)} = \sum_{l\geq 0}(\gamma\lambda)^l \delta_{t+l}^{(i)}$, and the return target $\hat{V}_t^{(i),\text{targ}} = \hat{A}_t^{(i)} + V_{\boldsymbol{\theta}^c_{\text{old}}}(s_t, i)$ [Schulman et al., 2016]. The vanilla MT-PPO objective averages per-task losses, each combining a clipped policy surrogate, a squared value loss, and an entropy bonus [Schulman et al., 2017]:

$$
\begin{aligned}
L(\boldsymbol{\theta}) \;&=\; K^{-1}\sum\nolimits_{i=1}^{K} L_i(\boldsymbol{\theta}), \qquad \text{where } L_i(\boldsymbol{\theta}) \;=\; L_i^a(\boldsymbol{\theta}^a) + c_v\, L_i^c(\boldsymbol{\theta}^c) - c_e\, H_i(\boldsymbol{\theta}^a),\\
L_i^a(\boldsymbol{\theta}^a) \;&=\; -\,\mathbb{E}_t\Big[\min\big(\rho_t^{(i)}(\boldsymbol{\theta}^a)\,\hat{A}_t^{(i)},\; \text{clip}(\rho_t^{(i)}(\boldsymbol{\theta}^a), 1{-}\epsilon, 1{+}\epsilon)\,\hat{A}_t^{(i)}\big)\Big], \qquad (1)\\
L_i^c(\boldsymbol{\theta}^c) \;&=\; \mathbb{E}_t\Big[\big(V_{\boldsymbol{\theta}^c}(s_t, i) - \hat{V}_t^{(i),\text{targ}}\big)^2\Big], \qquad H_i(\boldsymbol{\theta}^a) \;=\; \mathbb{E}_t\big[\mathcal{H}(\pi_{\boldsymbol{\theta}^a}(\cdot \mid s_t, i))\big],
\end{aligned}
$$

where $\mathbb{E}_t$ denotes the empirical average over steps in the rollout batch, $c_v, c_e > 0$ are scalar coefficients, and $\mathcal{H}(\bullet)$ is the entropy of a distribution. Per-task advantage normalization (computed

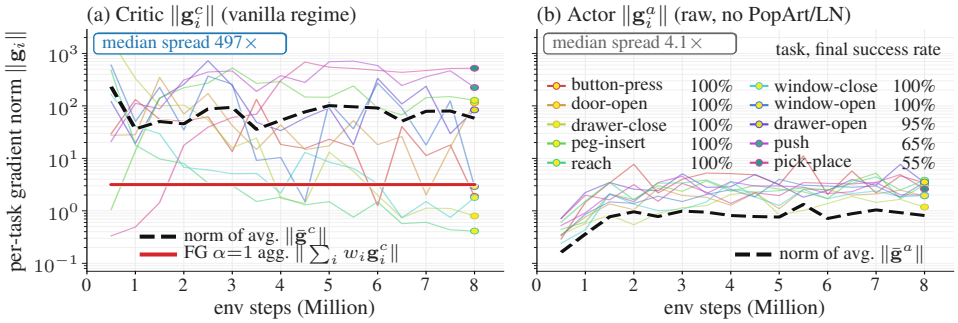


Figure 2: Per-task gradient norms $\|\mathbf{g}_i\|$ (thin lines) on MT10, 0.5–8.0M steps. (a) Critic: the mean update's norm $\|\bar{\mathbf{g}}^c\|$ (dashed) and FG-c (α=1) aggregate $\|\sum_i w_i \mathbf{g}_i^c\| = \sqrt{K}$ (red, Theorem 1). (b) Actor: $\|\bar{\mathbf{g}}^a\|$ (dashed) lies below due to actor gradients $\mathbf{g}_i^a$ partially canceled each other (Figure D.5).

within each task's slice of a minibatch) is applied to $\hat{A}^{(i)}$ before the actor surrogate. This is a task-wise variant of the per-minibatch normalization option studied in PPO implementation analyses [Andrychowicz et al., 2021]. Here it is used to remove actor-side cross-task scale differences, following the MT-PPO convention in Meta-World+ [McLean et al., 2025].

Across all K tasks, $\boldsymbol{\theta}^a$ and $\boldsymbol{\theta}^c$ are shared, so every gradient step must aggregate K per-task gradients over shared parameters into a single update direction. The relative magnitudes and pairwise alignment of these gradients determine whether the aggregated gradient represents the multi-task objective fairly or is dominated by a subset of tasks.

To diagnose the gradient ill-conditioning, we capture the per-task gradients $\mathbf{g}_i^a := \nabla_{\boldsymbol{\theta}^a} L_i^a$ and $\mathbf{g}_i^c := \nabla_{\boldsymbol{\theta}^c} L_i^c$ on the shared parameters for actor and critic, respectively. We omit global scalar coefficients such as c_v because they do not affect cross-task relative geometry. We also consider the Gram matrices $\mathbf{G}^\bullet \in \mathbb{R}^{K\times K}$, $\mathbf{G}_{ij}^\bullet = \langle \mathbf{g}_i^\bullet, \mathbf{g}_j^\bullet \rangle$ ($\bullet \in \{a, c\}$, i.e., actor and critic), where the diagonal $\mathbf{G}_{ii}^\bullet = \|\mathbf{g}_i^\bullet\|^2$ records per-task scale, and the off-diagonal cosines $\mathbf{G}_{ij}^\bullet / \sqrt{\mathbf{G}_{ii}^\bullet \mathbf{G}_{jj}^\bullet}$ record pairwise direction conflict. Throughout, we contrast each aggregator against the default average $\bar{\mathbf{g}}^\bullet = \frac{1}{K}\sum_i \mathbf{g}_i^\bullet$ applied to each shared parameter set for actor and critic.

3 Gradient Ill-conditioning

At each shared-parameter update, MT-PPO aggregates K per-task gradients into a single direction. We diagnose this aggregation along three fairness axes: preventing raw-scale domination, preserving task-specific directions, and allocating update budget according to gradient geometry rather than a few dominant tasks. Vanilla MT-PPO's critic fails along all three axes, as summarized in Table 1 and detailed below.

- **(D1) Per-task scale spread.** Large diagonal entries $\mathbf{G}_{ii}^c$ make the mean $\bar{\mathbf{g}}^c := K^{-1}\sum_i \mathbf{g}_i^c$ inherit the scale of high-gradient tasks, leaving small-gradient tasks with little influence.
- **(D2) Co-linear collapse.** A high mean off-diagonal $|\cos| = |\mathbf{G}_{ij}^c| / \sqrt{\mathbf{G}_{ii}^c \mathbf{G}_{jj}^c}$ for $i \neq j$ indicates that per-task critic gradients have collapsed toward a small set of shared-feature directions, which leaves little task-specific direction for any aggregator to act on and makes $\mathbf{G}^c$ near-singular.
- **(D3) Unfair aggregation.** Even when scale spread and co-linearity are reduced, the default mean update can still allocate most of the combined direction to a few tasks. The aggregation rule therefore needs to be geometry-aware, not merely scale-normalized.

Critic is the dominant issue. In our diagnostics, the per-task gradient-norm spread on the critic, $\max_i \|\mathbf{g}_i^c\| / \min_i \|\mathbf{g}_i^c\|$, is two orders of magnitude larger than the actor-side spread, $\max_i \|\mathbf{g}_i^a\| / \min_i \|\mathbf{g}_i^a\|$, and this gap persists across training (Figure 2; full diagnostics in Sections D.1 and D.3). This asymmetry is expected: per-task advantage normalization absorbs much of the reward-scale variation in the actor surrogate, whereas the critic fits unnormalized value targets unless explicitly corrected. We therefore focus the diagnosis and interventions on the critic side. Actor-side aggregation is secondary in our work, and we use PCGrad [Yu et al., 2020a] as a representative actor-gradient aggregator.

A Self-reinforcing tail trap. Early critic imbalance is damaging because it can turn small initial gaps into a self-reinforcing failure mode. In vanilla MT-PPO, the critic update averages task gradients, so the shared critic parameters $\boldsymbol{\theta}^c$ are driven mainly by tasks with large critic gradients (D1–D3). Small-gradient tasks must then fit their value functions through shared features shaped primarily by other tasks' TD errors, yielding biased advantages $\hat{A}_t^{(i)}$ and distorted actor updates. The resulting policies collect less-informative data, which further reduces useful critic signal for the same tasks in later updates. This feedback loop explains why actor-side reweighting or gradient surgery alone gives limited gains without Critic Balancing. Empirically, vanilla MT-PPO's worst-10 MT50 tasks average only 6.6% success at the training budget, and its five hardest tasks remain below 20% (Tables 2 and D.6). This motivates correcting critic gradient ill-conditioning early in training. See Figure 3 for *early-stage* Gram diagnostics and Figure 6 for TOPPO's effect.

4 Method: TOPPO

To address the gradient ill-conditioning discussed in Section 3, we propose TOPPO, which consists of three critic-side modules and an actor-side gradient aggregator, listed in Table 1 and laid out in Algorithm 1.

On the critic side, a **per-task value normalizer** puts each task's TD loss on the same scale before computing critic-side gradients (D1); **LN-c** (LayerNorm in the critic network) regularizes the hidden-activation conditioning that produces co-linear collapse (D2); **FG-c** (α=1) reweights per-task gradients at the aggregator so that the pre-clipping combined-gradient norm is pinned at $\sqrt{K}$ (D3).

Algorithm 1 TOPPO: a PPO collect-and-update phase. See full version in Algorithm C.1.

Require: Tasks $\{\mathcal{M}_i\}_{i=1}^K$, $\boldsymbol{\theta} = (\boldsymbol{\theta}^a, \boldsymbol{\theta}^c)$ with **[LN-c]** and PopArt $\{(\sigma_i, \mu_i)\}$, repeats R, max grad-norm τ

Rollout $\mathcal{B} = \bigcup_i \mathcal{B}_i$ by $\pi_{\boldsymbol{\theta}^a_{\text{old}}}$; calculate $\hat{A}_t^{(i)}$, $\hat{V}_t^{(i),\text{targ}}$
[PopArt] update (μ_i, σ_i), PopArt-renorm affine head
for $r = 1$ **to** R (recompute adv. if $r > 1$) **do**
  for each stratified minibatch $\mathcal{B}^{\text{mb}} \subset \mathcal{B}$ **do**
    normalize advantages within each task; use critic targets $(\hat{V}_t^{(i),\text{targ}} - \mu_i)/\sigma_i$ as in Section 4.1
    for each i: compute $\mathbf{g}_i^a$ and $\mathbf{g}_i^{c,\text{PopArt}}$ from the actor and PopArt critic losses
    [FG-c] $\mathbf{d}^c \leftarrow \sum_i w_i \mathbf{g}_i^{c,\text{PopArt}}$ from Algorithm C.2
    [PCGrad-a] $\mathbf{d}^a \leftarrow \text{PCGrad}(\{\mathbf{g}_i^a\})$
    rescale $(\mathbf{d}^a, \mathbf{d}^c)$ by $\min(1, \tau/\|(\mathbf{d}^a, \mathbf{d}^c)\|_2)$; Adam step on $\boldsymbol{\theta}$
  end for
end for

On the actor side, per-task advantage normalization makes reward-scale variation much smaller, leaving direction conflict as the main residual issue. Therefore, we apply PCGrad to actor-gradient aggregation (**PCGrad-a**). Empirical comparisons with alternative actor-side aggregators are reported in Section D.1 and Table D.2.

In subsections below, we discuss the three critic-side interventions in more detail.

4.1 Per-task value normalization

In heterogeneous environments the per-task value-target variation can be extreme, so the squared TD loss L_i^c can inherit this variation and spread quadratically across tasks (D1). A per-task value normalizer addresses this by estimating each task's return scale and rescales its value targets, rewards, or prediction errors, so that value losses have comparable scales across tasks. Several normalizers can be used, for example per-task reward normalization, return-based scaling [Schaul et al., 2021], or PopArt [van Hasselt et al., 2016]. We adopt PopArt in this work.

PopArt [van Hasselt et al., 2016, Hessel et al., 2019] normalizes value targets by inserting a per-task affine layer between the shared critic network and the value prediction. For the "Art" (Adaptively Rescaling Targets) part, the shared critic outputs a single normalized scalar $z_{\boldsymbol{\theta}^c}(s, i) \in \mathbb{R}$, and a per-task scale-and-shift (σ_i, μ_i) maps it back to the raw value range by

$$V_{\boldsymbol{\theta}^c}(s, i) \;=\; \sigma_i \, z_{\boldsymbol{\theta}^c}(s, i) + \mu_i, \qquad \text{where } (\mu_i, \sigma_i^2) \;\approx\; \big(\widehat{\mathbb{E}}_t[\hat{V}_t^{(i),\text{targ}}],\; \widehat{\text{Var}}_t[\hat{V}_t^{(i),\text{targ}}]\,\big).$$

These running estimates of each task's target mean and variance are accumulated online via Welford's algorithm [Welford, 1962] (canonical PopArt uses an EMA, see Section B.5). The shared critic is then trained to predict normalized per-step targets $(\hat{V}_t^{(i),\text{targ}} - \mu_i)/\sigma_i$, which have approximately zero mean and unit variance per task by construction, so every task's value-loss sits on the same scale.

The "Pop" (Preserving Outputs Precisely) part is a small bookkeeping step: whenever (μ_i, σ_i) update, the per-task affine head is simultaneously re-parameterized so the raw prediction $V_{\boldsymbol{\theta}^c}(s, i)$ does not jump [van Hasselt et al., 2016], and the underlying critic remains a single shared MLP.

PopArt target normalization acts as a task-wise rescaling of critic gradients. Let $\mathbf{g}_i^{c,\text{PopArt}}$ be the shared-critic gradient from the PopArt-normalized critic loss, and let $\mathbf{g}_i^{c,\text{raw}}$ be the corresponding gradient from the unnormalized-target loss. For shared critic parameters $\boldsymbol{\theta}^c$ and a fixed PopArt statistic σ_i during the update,

$$\mathbf{g}_i^{c,\text{PopArt}} \;=\; \sigma_i^{-2}\, \mathbf{g}_i^{c,\text{raw}}, \tag{2}$$

with one factor of σ_i^{-1} from the normalized residual and another σ_i^{-1} from the chain rule. This rescaling is observed empirically in Figure 3.

4.2 LN-c: LayerNorm on the critic network

Pre-activation LayerNorm [Ba et al., 2016] is applied to the critic's hidden linear layers to stabilize task-wise hidden activation scales before forming $\mathbf{G}^c$. In early-stage critic Gram diagnostics, critic LN reduces the mean off-diagonal $|\cos|$ from 0.34 to 0.20 while roughly preserving diagonal magnitude (Figure 3; full diagnostics in Figures D.4 and D.6). This is consistent with prior RL reports on LayerNorm [Lee et al., 2025, Hansen et al., 2024]. In the MT50 cumulative ablation ladder, LN-c gives the largest single-step gain (Figure 6).

4.3 FairGrad (α=1): per-task critic-gradient aggregation

To address unfair gradient aggregation (D3), we replace the critic-gradient mean aggregation $\frac{1}{K}\sum_i g_i^c$ with FairGrad aggregation $\mathbf{d}^c = \sum_i w_i \mathbf{g}_i^c$ [Ban and Ji, 2024] with task weights $\mathbf{w} = (w_1, \ldots, w_K)^\top \in \mathbb{R}^K_{>0}$. FairGrad downweights tasks whose gradients would otherwise dominate the combined direction, so that small-gradient tasks are not sacrificed to large ones. For example, for orthogonal gradients $\mathbf{g}_1, \mathbf{g}_2$ with norms 10 and 1, the mean direction has cosine 0.995 with $\mathbf{g}_1$, whereas FairGrad with α=1 sets $w_i = 1/\|\mathbf{g}_i\|$, so the two weighted gradients have equal norms.

Formally, FairGrad chooses $\mathbf{d}^c$ within a norm ball to maximize the α-fairness utility $\sum_i U_\alpha(x_i)$ [Mo and Walrand, 2000, Kelly, 1997], where

$$U_\alpha(x) \;=\; \begin{cases} (1-\alpha)^{-1}\, x^{1-\alpha}, & 0 \le \alpha \ne 1, \\ \log x, & \alpha = 1, \end{cases} \tag{3}$$

and $x_i := \langle \mathbf{g}_i^c, \mathbf{d}^c \rangle$ is task i's first-order loss decrease along $\mathbf{d}^c$. Writing $\mathbf{d}^c = \sum_j w_j \mathbf{g}_j^c$ gives $x_i = (\mathbf{G}^c \mathbf{w})_i$, and under the standard FairGrad scaling the KKT condition is $\mathbf{G}^c \mathbf{w} = \mathbf{w}^{-1/\alpha}$ componentwise (Section C.2).

Choice of α. The parameter α in (3) trades total improvement against fairness. We consider a case of conflicting gradients with different magnitudes of norm. As illustrated in Figure 4, take $\mathbf{g}_1, \mathbf{g}_2$ with norms 10 and 1 pointing in nearly opposite directions ($\cos\angle(\mathbf{g}_1, \mathbf{g}_2) = -0.9$). When α=0, $\mathbf{d}$ follows $\mathbf{g}_1$ and locally increases task 2's loss. On another extreme, $\alpha \to \infty$ equalizes the raw decreases x_i, which forces $\mathbf{d}$ to be nearly orthogonal to the large $\mathbf{g}_1$ ($\cos\angle(\mathbf{d}, \mathbf{g}_1) = 0.04$), so the large task barely improves. Our choice α=1 instead equalizes the task contributions $\langle w_i \mathbf{g}_i, \mathbf{d} \rangle = w_i x_i = 1$ by the KKT condition, with the same angle $\cos\angle(\mathbf{d}, \mathbf{g}_1) = \cos\angle(\mathbf{d}, \mathbf{g}_2) = 0.22$. Therefore, even if the two tasks conflict in their critic gradients, both tasks improve slowly in the combined direction $\mathbf{d}$, which can potentially benefit other tasks at the time of the update. Theoretically, at α=1 the KKT condition becomes $\mathbf{G}^c \mathbf{w} = \mathbf{w}^{-1}$, and its solution has two good properties that fail for every other α as explained in Theorem 1 below.

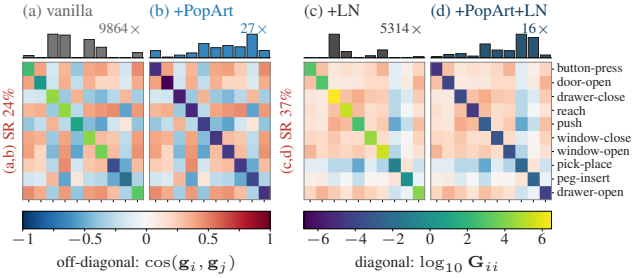


Figure 3: Early-stage ($\sim$0.5M steps) MT10 Gram matrices of critic gradients. Off-diagonal values are $\cos\angle(\mathbf{g}_i^c, \mathbf{g}_j^c)$ and diagonal $\log_{10} \mathbf{G}_{ii}^c$. Histograms: $\|\mathbf{g}_i^c\|/K$ and magnitude-spread ratio. See Figure D.4 for mid/late stages.

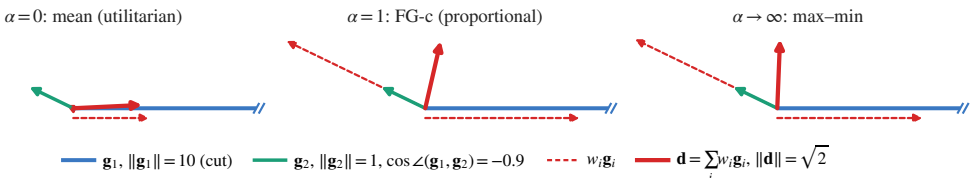


Figure 4: The α-fair update on the two conflicting gradients of Section 4.3. Updates are rescaled to $\|\mathbf{d}\|=\sqrt{K}$ for comparison; $\mathbf{g}_1$ is truncated.

Theorem 1 (FairGrad (α=1): fixed norm and scale invariance)**.** *Let $\mathbf{g}_1,\dots,\mathbf{g}_K\in\mathbb{R}^d$ be linearly independent, with Gram matrix $\mathbf{G}=[\langle\mathbf{g}_i,\mathbf{g}_j\rangle]_{ij}\succ 0$. Let $\mathbf{w}\in\mathbb{R}^K_{>0}$ be the unique positive solution of $\mathbf{G}\mathbf{w}=\mathbf{w}^{-1}$, where the inverse is componentwise. Then $\mathbf{d}=\sum_{i=1}^K w_i\mathbf{g}_i$ has fixed norm $\|\mathbf{d}\|^2=\mathbf{w}^\top\mathbf{G}\mathbf{w}=K$. Moreover, it is invariant to arbitrary positive rescaling. Specifically, for any $\mathbf{c}\in\mathbb{R}^K_{>0}$ and $\tilde{\mathbf{g}}_i=c_i\mathbf{g}_i$, the rescaled Gram matrix $\tilde{\mathbf{G}}$ has positive solution $\tilde{\mathbf{w}}=\mathbf{w}\oslash\mathbf{c}$, and $\sum_i\tilde{w}_i\tilde{\mathbf{g}}_i=\sum_i w_i\mathbf{g}_i$.*

Theorem 1 shows the two properties for the critic update. The fixed norm property ensures that each task contributes $w_ix_i=1$, so $\|\mathbf{d}^c\|^2=K$ and every task receives an equal $1/K$ share of the critic update. The critic gradient thus has the same norm on every minibatch, instead of growing and shrinking with the TD errors of the large-gradient tasks. The scale invariance property ensures that the update depends only on gradient directions, so a task's influence does not shrink with its gradient norm. Importantly, it also lets FG-c absorb PopArt's per-task rescaling, so the two modules compose predictably (Corollary 1). The proof of Theorem 1 is in Section C.4.

Corollary 1 (PopArt rescaling is absorbed at the FairGrad (α=1) output)**.** *Within one PPO minibatch, before PopArt statistics (μ_i,σ_i) are refreshed, PopArt rescales each shared-critic gradient by $\mathbf{g}_i^{c,\mathrm{PopArt}}=\sigma_i^{-2}\mathbf{g}_i^{c,\mathrm{raw}}$ (Eq. (2)). If the raw critic Gram is positive definite, then by Theorem 1 the α=1 FairGrad combined critic gradient is identical on raw and PopArt-rescaled gradients.*

A fast solver. Solving $\mathbf{G}^c\mathbf{w}=\mathbf{w}^{-1}$ is the main computational bottleneck for FG-c. Existing FairGrad/Nash-MTL solvers [Ban and Ji, 2024, Navon et al., 2022] are too slow for per-minibatch critic updates. The fixed-budget SGD solver in Ban and Ji [2024] is faster, but it misses the KKT target on every real critic Gram we tested (Figure C.2). We propose a projected Newton solver with a closed-form diagonal warm start, which reaches the target KKT tolerance with much lower wall-clock time (see Figure 5 and details in Section C.5).

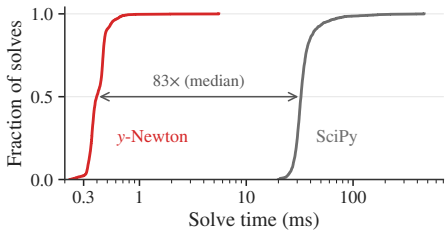


Figure 5: Solve time of FairGrad (α=1) solvers on 1,984 real MT50 Gram matrices (full version in Figure C.1).

5 Experiments

5.1 Setup

Benchmark. We train and evaluate all models on Meta-World V2 [Yu et al., 2020b, McLean et al., 2025], MT10 (K=10) and MT50 (K=50) over all tasks with a task identifier. We use V2 reward throughout the paper unless specifically labeled V1. Beyond Meta-World, in Section E.5, we demonstrate our method to a two-objective humanoid control task [Peng et al., 2021].

Architecture. TOPPO, our PPO-based method, adopts a fully task-shared $[400\times3]$ ReLU MLP, the standard Meta-World multi-task backbone used by most prior works, including the SAC-family in Meta-World+ [McLean et al., 2025] and the structured-RL methods CAGrad / CARE / PaCo / MOORE / FAMO / FairGrad, with separate actor and critic of the same size. The only per-task structure is the input one-hot and the action log standard deviation σ_i. ARS [Cho et al., 2025] uses architectures with deeper $[400\times4]$ MLPs by default, and wider $[1024\times4]$ MLPs for ARS-LN-1024 (a scaled version). Our TOPPO has 685K (MT10) / 717K (MT50) parameters, which on MT50 are 22.5–22.7$\times$ smaller than the strongest ARS variants, ARS-LoRA and ARS-LN-1024 (See Table B.2 and Section B.1).

Training. Our models are trained with 20M (MT10) / 100M (MT50) total environment steps (2M per task), matching the ARS / MOORE / PaCo / Meta-World+ convention. Our TOPPO *headline* configuration is PCGrad-a + FG-c (α=1) + PopArt + LN-c; the *vanilla MT-PPO* baseline removes all four interventions while retaining standard MT-PPO machinery (per-task advantage normalization, stratified minibatches, value clip, post-aggregation $\|\cdot\| \leq 1$ clip), so the contrast isolates the four interventions. Full hyperparameters are in Table B.1; PPO-specific adaptations of SAC-based gradient-surgery methods are in Section B.4.

Baselines and reporting. For comparability, each comparison keeps the reward version and reporting statistic fixed. For V2 reward, we follow the final-checkpoint mean $\pm$ standard deviation (std) protocol of Cho et al. [2025]. Table 2 lists their published numbers (8 seeds in their Tables 1 and 2) alongside our 10-seed reruns of SAC-MT and the four ARS variants with the authors' code and configurations (protocol differences in Section E.1). For the V1 head-to-head with Meta-World+ [McLean et al., 2025], both our rows and the baseline rows follow the Meta-World+ 10-seed final-checkpoint Interquartile Mean (IQM) $\pm$ std (Table 3). The appendix gives parameter counts (Section B.3), step budgets, reporting protocols, and all four success metrics (Tables D.8 to D.10), and per-task success rates (Section D.6).

Code and reproducibility. Code Repository: `https://github.com/NAIVlab/TOPPO`
Training logs: `https://forge.coreweave.com/wandb/liyp1220-uci/TOPPO`

5.2 Main Results

MT50 mean and Worst-k tail tasks. On MT50, TOPPO (90.9% mean, 56.5% worst-10) beats the strongest baseline, ARS-LN-1024 (85.7% mean, 43.3% worst-10), on both metrics: by 5.1 points on the mean (Table 2) and 13.2 points on the worst-10 tail tasks (Table 2), at 22.7$\times$ fewer parameters. SAC-MT and all published non-ARS multi-task SAC methods score 0.0% on the worst-10 tail tasks.

MT10: Saturating performance. The MT10 *final*-checkpoint mean success rate in Table 2 (97.2%) sits 1.2 points below ARS-LoRA (98.4%, within seed variation), but every seed in fact reaches $\geq$ 99% at its own best checkpoint (see per-seed best columns in Table D.10). This gap reflects PPO's well-known late-training instability, for which linear learning-rate annealing is a documented code-level practice [Engstrom et al., 2020, Andrychowicz et al., 2021]. We do not apply such a learning-rate schedule, to keep training-time hyperparameters identical across all our configurations and to align with the published-baseline protocol that reports a single fixed-schedule final-checkpoint number. We report *final* as the headline statistic as it is the most conservative and matches the protocol used in most published baselines (see Table D.9). For more detailed results, see per-seed argmax-step distribution and the full 4-metric breakdown in Tables D.10 and D.11.

Cumulative ladder. Figure 6 traces how the four intervention effects accumulate on MT50. Vanilla MT-PPO with LN-c and PopArt already exceeds ARS-LN-1024 on both the mean and the worst-10 tail tasks (Table 2). Modules FG-c (α=1) and PCGrad-a then add mechanism-aligned residual gains. Adding LN-c is the largest single jump on both metrics. Note that this effect ladder is not a unique additive decomposition, as the three critic interventions interact.

Convergence speed and parameter efficiency. Figure 1(a) shows that on MT50, TOPPO reaches every ARS variant's 100M-step final mean within its first $\sim$28M steps and the published MOORE mean at $\sim$ 11M (full curves in Section D.4). With 22.7$\times$ fewer parameters than ARS-LN-1024, TOPPO sits on the parameter and sample efficiency frontier among the compared V2 methods.

5.3 Ablation and analysis

We isolate each component's contribution via four ablations. Full details are in Section D.1.

Critic-side intervention cube (LN-c $\times$ PopArt $\times$ FG-c, 8 cells $\times$ 10 seeds, MT50 V2). Each component in TOPPO is mechanism-distinct and they interact. The interaction signature suggested by Corollary 1 appears at training outcome scale: *PopArt's worst-10 marginal collapses from* $+6.6$ *points (over LN-c) to* -0.2 *points (over LN-c+FG-c).* This is consistent with FairGrad (α=1) absorbing PopArt's per-task gradient rescaling at the gradient aggregator (Table D.1).

Table 2: Final-checkpoint Meta-World V2 success (%) at 20M/100M steps (MT10/MT50), mean with seed std in gray. Worst-k: mean of each seed's k lowest tasks. Published rows use a different protocol and worst-k aggregation (Section E.1). Params include target networks (Table B.2). Bold: column maximum; –: not reported or not run.

	Params (K)	MT10	MT50					
Algorithm	MT10/MT50	Mean	Worst-5	Worst-10	Worst-20	Worst-30	Worst-40	Mean
Published (Cho et al. [2025], Tables 1 and 2, 8 seeds; ARS-LN-1024 from Table 6; SMT is Cho et al. [2024])								
SAC-MT	2517/2597	69.4 ± 0.8	0.0 ± 0.0	0.0 ± 0.0	0.0 ± 0.0	14.1 ± 3.1	34.5 ± 2.5	47.6 ± 2.0
MT-MH-SAC	2546/2754	77.2 ±11.9	0.0 ± 0.0	0.0 ± 0.0	0.0 ± 0.0	14.1 ± 1.7	34.0 ± 2.0	47.2 ± 1.7
Soft Modularization	3454/3534	74.4 ±10.5	0.0 ± 0.0	0.0 ± 0.0	1.8 ± 3.7	23.7 ±12.3	42.6 ± 9.5	54.1 ± 7.6
PCGrad-SAC	2517/2597	74.8 ±13.7	0.0 ± 0.0	0.0 ± 0.0	0.0 ± 0.0	21.0 ±12.9	39.9 ±10.7	51.9 ± 8.5
PaCo	–	82.4 ±14.2	0.0 ± 0.0	0.0 ± 0.0	4.6 ± 8.2	26.1 ±15.0	44.6 ±11.2	55.6 ± 9.1
MOORE	6890/7403	86.0 ± 4.8	0.0 ± 0.0	0.0 ± 0.0	15.9 ± 7.0	41.2 ± 5.0	55.3 ± 3.9	64.2 ± 3.1
SMT	–	86.8 ± 8.6	0.0 ± 0.0	0.0 ± 0.0	8.0 ± 8.9	26.8 ±13.1	45.0 ± 9.9	56.0 ± 8.0
ARS	2517/2597	97.3 ± 2.1	–	9.1 ± 6.6	26.3 ± 6.1	45.3 ± 4.7	57.5 ± 3.6	65.9 ± 2.9
ARS-LN-400	2530/2611	98.6 ± 1.5	–	21.0 ±11.4	49.1 ± 6.5	64.3 ± 6.2	72.9 ± 4.7	78.3 ± 3.7
ARS-LN-1024	–/16267	–	–	–	–	–	–	88.9 ± 2.6
ARS-LoRA	3878/16123	**99.5** ± 0.8	–	29.3 ± 7.7	58.4 ± 4.5	72.0 ± 3.0	79.0 ± 2.2	83.2 ± 1.8
SAC-MT and ARS family, our runs (10 seeds, Section E.1; SAC critic-balancing ports are in Table E.2)								
SAC-MT	2517/2597	61.7 ± 8.2	0.0 ± 0.0	0.0 ± 0.0	0.0 ± 0.0	10.5 ± 3.8	32.3 ± 3.3	45.8 ± 2.6
ARS	2517/2597	93.9 ± 4.1	0.0 ± 0.0	0.6 ± 1.6	24.4 ± 9.0	45.1 ± 7.8	58.6 ± 6.0	66.8 ± 4.8
ARS-LN-400	2530/2611	96.2 ± 2.4	0.0 ± 0.0	11.7 ± 9.6	44.0 ±11.3	61.2 ± 9.1	70.8 ± 7.1	76.6 ± 5.7
ARS-LN-1024	16062/16267	96.9 ± 2.6	16.9 ± 9.1	43.3 ± 9.8	65.9 ± 7.2	76.3 ± 5.3	82.2 ± 4.0	85.7 ± 3.2
ARS-LoRA	3878/16123	98.4 ± 3.1	1.0 ± 2.8	19.0 ±11.6	55.9 ± 7.6	70.5 ± 5.2	77.9 ± 3.9	82.3 ± 3.1
Ours (10 seeds)								
Vanilla MT-PPO	684/716	85.2 ± 6.5	0.0 ± 0.0	6.6 ± 9.1	46.4 ± 8.0	64.1 ± 5.4	73.1 ± 4.1	78.5 ± 3.3
+LN-c	685/717	96.2 ± 3.4	6.9 ±11.4	42.3 ±10.1	68.9 ± 5.9	79.2 ± 4.0	84.4 ± 3.0	87.5 ± 2.4
+LN-c+PopArt	685/717	96.8 ± 1.5	18.0 ±12.5	48.9 ± 9.0	72.3 ± 5.6	81.5 ± 3.8	86.1 ± 2.8	88.9 ± 2.3
+LN-c+PopArt+FG-c	685/717	94.8 ± 5.1	22.3 ±17.3	52.4 ±11.3	75.1 ± 5.7	83.4 ± 3.8	87.6 ± 2.8	90.1 ± 2.3
TOPPO	685/717	97.2 ± 3.1	**24.2** ±14.1	**56.5** ± 7.8	**77.2** ± 4.0	**84.8** ± 2.6	**88.6** ± 2.0	**90.9** ± 1.6

Per-side combiner asymmetry. Actor-side scale spread is small after per-task advantage normalization, leaving direction conflict as the main residual issue (Figure 2). This motivates our PCGrad-a/FG-c asymmetric design: adding PCGrad-a on top of the critic stack raises MT50 worst-10 from 52.4% to 56.5% and lowers its seed std from 11.3 to 7.8 points (Table 2). FG-a on top of FG-c does not improve on default-actor FG-c (89.2% vs. 90.1%, Table D.2). FG-c vs. PCGrad-c is a tie within seed noise. We adopt FG-c on the critic for the fixed $\sqrt{K}$-norm identity and scale-invariance of Theorem 1 (see all per-side combiners in Section C.3).

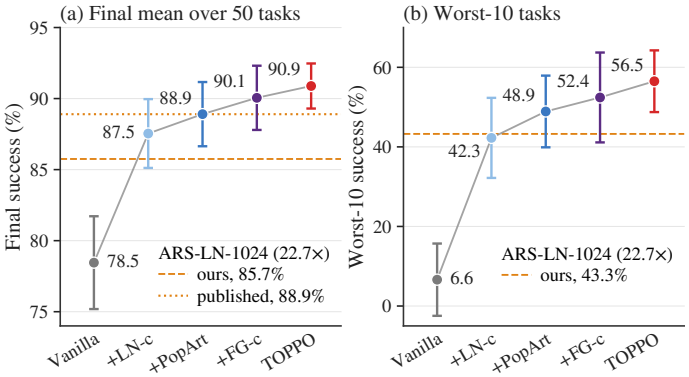


Figure 6: MT50 ablation ladder. (a) Final mean. (b) Final worst-10 tail tasks. n=10 seeds, ± std. Orange: ARS-LN-1024 (dashed: our 10-seed runs. dotted: published)

V1 reward sensitivity. V1 rewards have much wider per-task scale heterogeneity than V2, so PopArt's channels that FG-c does not absorb (running statistics, optimizer state, downstream actor) should matter more. Table 3 confirms this on MT50 V1: the PopArt marginal over LN-c+FG-c is +17.0 IQM points (vs. +0.3 on V2, Table D.3), while FG-c without PopArt slightly hurts (−2.3 points over LN-c). The full stack remains the strongest: TOPPO reaches 79.3% IQM versus 61.8% for the strongest published V1 baseline (MOORE), with 14.5× fewer parameters (learning curves in Figure D.12).

Alternative critic normalizers. We also compare PopArt with reward normalization, return-based scaling [Schaul et al., 2021], and an HL-Gauss critic [Farebrother et al., 2024] on MT50 with LN-c fixed (Sections E.2 and E.3). Reward normalization and PopArt perform about the same under both reward versions: 79.8% vs. 79.5% IQM on V1 with value clipping off (paired $p = 0.64$), and 89.5% vs. 88.9% mean on V2. PopArt is thus one valid per-task value normalizer rather than a superior one. We keep it as default because it changes neither the reward nor the actor objective.

Table 3: Meta-World V1 (MT50): final-checkpoint IQM $\pm$ std (10 seeds). Top: our V1 ablation. Bottom: published Meta-World+ baselines. Match step: first common checkpoint at which TOPPO's seed IQM reaches the published value.

Method	Params	Success rate %	TOPPO step to match	Backbone
Ours: Vanilla MT-PPO	716K	45.2 $\pm$ 2.4	–	[400]×3
+LN-c	717K	64.3 $\pm$ 3.1	–	[400]×3
+LN-c +FG-c	717K	62.0 $\pm$ 2.7	–	[400]×3
+LN-c +PopArt	717K	76.5 $\pm$ 2.0	–	[400]×3
+LN-c +PopArt +FG-c	717K	79.0 $\pm$ 1.2	–	[400]×3
TOPPO	717K	**79.3** $\pm$ 1.3	–	[400]×3
Meta-World+ MT50 SAC-family V1 baselines [McLean et al., 2025]				
MT-MH-SAC	2031K	31.9 $\pm$ 2.7	4M (4%)	[400]×3 shared, per-task heads
Soft Modularization	8030K	60.6 $\pm$ 3.9	14M (14%)	routing [256]×4×4
MOORE	10385K	61.8 $\pm$ 2.7	14M (14%)	[400]×3, 6 experts
PaCo	33909K	18.6 $\pm$15.4	4M (4%)	[400]×3, K=20
PCGrad-SAC	2031K	45.8 $\pm$ 5.9	6M (6%)	[400]×3 shared, per-task heads

6 Conclusion

We rethink PPO for MTRL under a vanilla shared MLP. Our results show that earlier conclusions drawn from MT-PPO's $\sim 30\%$ MT10 success rate in the original Meta-World benchmark [Yu et al., 2020b] underestimated PPO by confounding the choice of optimizer family with the condition of the critic. We identify critic-side gradient ill-conditioning as the main failure mode: large per-task scale spread, representation-level co-linear collapse, and unfair aggregation of imbalanced gradients. TOPPO targets these failures with PopArt, critic LayerNorm, and critic-side FairGrad (α=1), linked by the scale-invariance result of Theorem 1 and Corollary 1. With a compact shared MLP, TOPPO outperforms the SAC- and ARS-family baselines on MT50, most clearly on the tail tasks, while using far fewer parameters and reaching their final performance in fewer environment steps.

Limitations. We do not claim empirical dominance of FG-c over all critic-side combiners: FG-c and PCGrad-c are tied within seed noise under LN-c+PopArt, and we adopt FG-c for the property in Theorem 1. We also did not exhaustively test actor-side aggregator choices beyond the per-side cube in Table D.2 and the actor sweep in Section E.6. Therefore, PCGrad-a should be read as a mechanism-aligned working choice rather than an optimal actor combiner. Our reported architecture also uses separate actor and critic networks. If an actor–critic model uses a shared feature extractor before branching into policy and value heads, assigning critic-side balancing and actor-side surgery on the shared parameters becomes a coupled design choice that requires separate study. Our evidence covers task-conditioned, state-based MTRL, not visual inputs, missing task IDs, or unlabeled tasks. TOPPO also costs more computation per environment step: 19.8 versus 8.7 RTX-3090 hours per 100M steps for vanilla MT-PPO (Section E.4). Porting the critic-balancing to MTSAC gives no reliable final gain (Section E.1), so our claims are limited to the on-policy PPO setting.

Potential use cases. The same critic-side ill-conditioning can arise in other PPO settings where one shared critic fits value targets of different scales, such as multi-objective control. In PPO-based humanoid walk steering with an adversarial motion prior [Peng et al., 2021], applying the critic-side stack to the task and style rewards substantially improves motion style, with a tradeoff against task return (Section E.5).

Future work. Our study uses compact shared MLPs, where per-task critic gradients show large scale spread and strong co-linearity. In much larger networks, per-task gradients are closer to orthogonal, so cross-task interference, and with it the benefit of critic-side balancing, may shrink. Adapting it to model scale is left for future work.

Acknowledgments and Disclosure of Funding

Miao's research is partially supported by Texas AI Research Institute. Qu's research is partially supported by NCI Grant R01CA297869 and NSF Grant DMS 2627378.

References

Marcin Andrychowicz, Anton Raichuk, Piotr Stańczyk, Manu Orsini, Sertan Girgin, Raphaël Marinier, Léonard Hussenot, Matthieu Geist, Olivier Pietquin, Marcin Michalski, Sylvain Gelly, and Olivier Bachem. What matters for on-policy deep actor-critic methods? a large-scale study. In *International Conference on Learning Representations*, 2021. arXiv:2006.05990.

Jimmy Lei Ba, Jamie Ryan Kiros, and Geoffrey E. Hinton. Layer normalization. *arXiv preprint arXiv:1607.06450*, 2016.

Hao Ban and Kaiyi Ji. Fair resource allocation in multi-task learning. In *Proceedings of the 41st International Conference on Machine Learning*, volume 235 of *Proceedings of Machine Learning Research*, pages 2715–2731. PMLR, 2024. arXiv:2402.15638.

Tony F. Chan, Gene H. Golub, and Randall J. LeVeque. Algorithms for computing the sample variance: Analysis and recommendations. *The American Statistician*, 37(3):242–247, 1983. doi: 10.1080/00031305.1983.10483115.

Zhao Chen, Vijay Badrinarayanan, Chen-Yu Lee, and Andrew Rabinovich. GradNorm: Gradient normalization for adaptive loss balancing in deep multitask networks. In *Proceedings of the 35th International Conference on Machine Learning*, volume 80 of *Proceedings of Machine Learning Research*, pages 794–803. PMLR, 2018.

Myungsik Cho, Jongeui Park, Suyoung Lee, and Youngchul Sung. Hard tasks first: Multi-task reinforcement learning through task scheduling. In *Proceedings of the 41st International Conference on Machine Learning*, volume 235 of *Proceedings of Machine Learning Research*, pages 8556–8577. PMLR, 2024.

Myungsik Cho, Jongeui Park, Jeonghye Kim, and Youngchul Sung. ARS: Adaptive reward scaling for multi-task reinforcement learning. In *Proceedings of the 42nd International Conference on Machine Learning*, volume 267 of *Proceedings of Machine Learning Research*, pages 10583–10601. PMLR, 2025. OpenReview id U0mI6M7lvI; code at `https://github.com/ms-cho/Adaptive-Reward-Scaling-ARS-for-MTRL`.

Logan Engstrom, Andrew Ilyas, Shibani Santurkar, Dimitris Tsipras, Firdaus Janoos, Larry Rudolph, and Aleksander Madry. Implementation matters in deep policy gradients: A case study on PPO and TRPO. In *International Conference on Learning Representations*, 2020. arXiv:2005.12729.

Jesse Farebrother, Jordi Orbay, Quan Vuong, Adrien Ali Taïga, Yevgen Chebotar, Ted Xiao, Alex Irpan, Sergey Levine, Pablo Samuel Castro, Aleksandra Faust, Aviral Kumar, and Rishabh Agarwal. Stop regressing: Training value functions via classification for scalable deep RL. *arXiv preprint arXiv:2403.03950*, 2024. URL `https://arxiv.org/abs/2403.03950`.

Tuomas Haarnoja, Aurick Zhou, Pieter Abbeel, and Sergey Levine. Soft actor-critic: Off-policy maximum entropy deep reinforcement learning with a stochastic actor. In *Proceedings of the 35th International Conference on Machine Learning*, volume 80 of *Proceedings of Machine Learning Research*, pages 1861–1870. PMLR, 2018.

Nicklas Hansen, Hao Su, and Xiaolong Wang. TD-MPC2: Scalable, robust world models for continuous control. In *International Conference on Learning Representations*, 2024. arXiv:2310.16828.

Ahmed Hendawy, Jan Peters, and Carlo D'Eramo. Multi-task reinforcement learning with mixture of orthogonal experts. In *International Conference on Learning Representations*, 2024. arXiv:2311.11385.

Matteo Hessel, Hubert Soyer, Lasse Espeholt, Wojciech Czarnecki, Simon Schmitt, and Hado van Hasselt. Multi-task deep reinforcement learning with PopArt. In *Proceedings of the AAAI Conference on Artificial Intelligence*, volume 33, pages 3796–3803, 2019. arXiv:1809.04474.

Viraj Joshi, Zifan Xu, Bo Liu, Peter Stone, and Amy Zhang. Benchmarking massively parallelized multi-task reinforcement learning for robotics tasks. *Reinforcement Learning Journal*, 2025. arXiv:2507.23172; presented at the Reinforcement Learning Conference (RLC) 2025.

Frank P. Kelly. Charging and rate control for elastic traffic. *European Transactions on Telecommunications*, 8(1):33–37, 1997.

Alex Kendall, Yarin Gal, and Roberto Cipolla. Multi-task learning using uncertainty to weigh losses for scene geometry and semantics. In *IEEE Conference on Computer Vision and Pattern Recognition*, pages 7482–7491, 2018.

Vitaly Kurin, Alessandro De Palma, Ilya Kostrikov, Shimon Whiteson, and M. Pawan Kumar. In defense of the unitary scalarization for deep multi-task learning. In *Advances in Neural Information Processing Systems*, 2022.

Hojoon Lee, Dongyoon Hwang, Donghu Kim, Hyunseung Kim, Jun Jet Tai, Kaushik Subramanian, Peter R. Wurman, Jaegul Choo, Peter Stone, and Takuma Seno. SimBa: Simplicity bias for scaling up parameters in deep reinforcement learning. In *International Conference on Learning Representations*, 2025. arXiv:2410.09754.

Bo Liu, Xingchao Liu, Xiaojie Jin, Peter Stone, and Qiang Liu. Conflict-averse gradient descent for multi-task learning. In *Advances in Neural Information Processing Systems*, volume 34, 2021.

Bo Liu, Yihao Feng, Peter Stone, and Qiang Liu. FAMO: Fast adaptive multitask optimization. In *Advances in Neural Information Processing Systems*, 2023. arXiv:2306.03792.

Shikun Liu, Edward Johns, and Andrew J. Davison. End-to-end multi-task learning with attention. In *IEEE Conference on Computer Vision and Pattern Recognition*, pages 1871–1880, 2019.

Reginald McLean, Evangelos Chatzaroulas, Luc McCutcheon, Frank Röder, Tianhe Yu, Zhanpeng He, K.R. Zentner, Ryan Julian, J K Terry, Isaac Woungang, Nariman Farsad, and Pablo Samuel Castro. Meta-world+: An improved, standardized, RL benchmark. In *Advances in Neural Information Processing Systems Datasets and Benchmarks Track*, 2025. arXiv:2505.11289.

Jeonghoon Mo and Jean Walrand. Fair end-to-end window-based congestion control. *IEEE/ACM Transactions on Networking*, 8(5):556–567, 2000.

John F. Nash. The bargaining problem. *Econometrica*, 18(2):155–162, 1950.

Aviv Navon, Aviv Shamsian, Idan Achituve, Haggai Maron, Kenji Kawaguchi, Gal Chechik, and Ethan Fetaya. Multi-task learning as a bargaining game. In *Proceedings of the 39th International Conference on Machine Learning*, volume 162 of *Proceedings of Machine Learning Research*, pages 16428–16446. PMLR, 2022.

Xue Bin Peng. MimicKit: A reinforcement learning framework for motion imitation and control. *arXiv preprint arXiv:2510.13794*, 2025. URL `https://arxiv.org/abs/2510.13794`.

Xue Bin Peng, Pieter Abbeel, Sergey Levine, and Michiel van de Panne. DeepMimic: Example-guided deep reinforcement learning of physics-based character skills. *ACM Transactions on Graphics*, 37 (4), 2018. doi: 10.1145/3197517.3201311. URL `https://arxiv.org/abs/1804.02717`.

Xue Bin Peng, Ze Ma, Pieter Abbeel, Sergey Levine, and Angjoo Kanazawa. AMP: Adversarial motion priors for stylized physics-based character control. *ACM Transactions on Graphics*, 40(4), 2021. doi: 10.1145/3450626.3459670. URL `https://arxiv.org/abs/2104.02180`.

Tom Schaul, Georg Ostrovski, Iurii Kemaev, and Diana Borsa. Return-based scaling: Yet another normalisation trick for deep RL. *arXiv preprint arXiv:2105.05347*, 2021. URL `https://arxiv.org/abs/2105.05347`.

John Schulman, Philipp Moritz, Sergey Levine, Michael Jordan, and Pieter Abbeel. High-dimensional continuous control using generalized advantage estimation. In *International Conference on Learning Representations*, 2016. arXiv:1506.02438.

John Schulman, Filip Wolski, Prafulla Dhariwal, Alec Radford, and Oleg Klimov. Proximal policy optimization algorithms. *arXiv preprint arXiv:1707.06347*, 2017.

Shagun Sodhani, Amy Zhang, and Joelle Pineau. Multi-task reinforcement learning with context-based representations. In *Proceedings of the 38th International Conference on Machine Learning*, volume 139 of *Proceedings of Machine Learning Research*, pages 9767–9779. PMLR, 2021. arXiv:2102.06177.

Lingfeng Sun, Haichao Zhang, Wei Xu, and Masayoshi Tomizuka. PaCo: Parameter-compositional multi-task reinforcement learning. In *Advances in Neural Information Processing Systems*, volume 35, 2022. arXiv:2210.11653.

The Newton Contributors. Newton: GPU-accelerated physics simulation for robotics and simulation research, 2025. URL `https://github.com/newton-physics/newton`. Version 1.3.0.

Hado P. van Hasselt, Arthur Guez, Matteo Hessel, Volodymyr Mnih, and David Silver. Learning values across many orders of magnitude. In *Advances in Neural Information Processing Systems*, volume 29, 2016. arXiv:1602.07714.

B. P. Welford. Note on a method for calculating corrected sums of squares and products. *Technometrics*, 4(3):419–420, 1962. doi: 10.1080/00401706.1962.10490022.

Jiayi Weng, Huayu Chen, Dong Yan, Kaichao You, Alexis Duburcq, Minghao Zhang, Yi Su, Hang Su, and Jun Zhu. Tianshou: A highly modularized deep reinforcement learning library. *Journal of Machine Learning Research*, 23(267):1–6, 2022. URL `http://jmlr.org/papers/v23/21-1127.html`.

Ruihan Yang, Huazhe Xu, Yi Wu, and Xiaolong Wang. Multi-task reinforcement learning with soft modularization. In *Advances in Neural Information Processing Systems*, volume 33, 2020. arXiv:2003.13661.

Tianhe Yu, Saurabh Kumar, Abhishek Gupta, Sergey Levine, Karol Hausman, and Chelsea Finn. Gradient surgery for multi-task learning. In *Advances in Neural Information Processing Systems*, volume 33, 2020a.

Tianhe Yu, Deirdre Quillen, Zhanpeng He, Ryan Julian, Karol Hausman, Chelsea Finn, and Sergey Levine. Meta-world: A benchmark and evaluation for multi-task and meta reinforcement learning. In *Proceedings of the Conference on Robot Learning*, volume 100 of *Proceedings of Machine Learning Research*, pages 1094–1100. PMLR, 2020b. arXiv:1910.10897.

Appendix Contents

A Extended Related Work **14**

B Implementation Details **15**

B.1 Detailed experimental setup 15

B.2 Hyperparameters and architecture 16

B.3 Parameter audit (source-counted) 18

B.4 PPO-specific adaptations of SAC-based gradient-surgery methods 19

B.5 PopArt: implementation note (Welford full-sample statistics) 20

C Theoretical Details **20**

C.1 TOPPO pseudocode 20

C.2 α-fairness family and KKT derivation 21

C.3 Aggregator family taxonomy and cone containment 22

C.4 Proof of Theorem 1 (scale invariance) 23

C.5 y-Newton solver derivation and benchmark protocol 23

D Additional Experimental Results **28**

D.1 Detailed ablation results 28

D.2 Diagnostic dump-run provenance 29

D.3 Mechanism evidence figures 30

D.4 Headline V2 learning curves 36

D.5 V1 reward sensitivity 36

D.6 Per-task success rates 38

D.7 Cross-paper reporting-protocol map 44

E Extended Experiments and Robustness Checks **46**

E.1 SAC-family baselines under a common evaluation protocol 46

E.2 Normalizer alternatives and value clipping 48

E.3 Composing a categorical critic with scale normalization 49

E.4 Measured computation cost 50

E.5 AMP humanoid: a two-objective control stress test 51

E.6 Actor aggregation and fairness sensitivity 53

A Extended Related Work

Structure-based multi-task RL. Architectural interventions form one line of multi-task RL: Soft Modularization [Yang et al., 2020], CARE [Sodhani et al., 2021], PaCo [Sun et al., 2022], and MOORE [Hendawy et al., 2024]. The original Meta-World paper [Yu et al., 2020b] reported MT-PPO

at $\sim 30\%$ on MT10, anchoring a community shift to SAC backbones for subsequent multi-task RL methods (CARE, PaCo, MOORE, PCGrad-SAC, ARS [Cho et al., 2025]); benchmarks have largely standardized on the SAC stack [McLean et al., 2025]. We hold the architecture fixed at a vanilla shared MLP and revisit the SAC–PPO comparison without architectural additions. Concurrent work [Joshi et al., 2025] observes via cross-task gradient cosine that conflicts dominate on the critic in MT-PPO and bypasses the critic via Monte-Carlo returns, whereas we diagnose a complementary scale-imbalance axis ($497\times$ critic vs. $4.1\times$ actor per-task gradient-norm spread) and address it with the three critic-side modules of Table 1.

Imbalance interventions across pipeline layers. *Per-task gradient aggregation:* scalar-signal reweighting (loss-level: uncertainty weighting [Kendall et al., 2018], DWA [Liu et al., 2019], FAMO [Liu et al., 2023]; per-task gradient-norm: GradNorm [Chen et al., 2018]) is Gram-blind; direction surgery uses Gram inner products (PCGrad [Yu et al., 2020a], CAGrad [Liu et al., 2021]); α-fairness reweighting solves $\mathbf{G}\mathbf{w} = \mathbf{w}^{-1/\alpha}$ on the full Gram (FairGrad [Ban and Ji, 2024]; at $\alpha{=}1$ equivalent to Nash bargaining [Navon et al., 2022], Remark C.1). Kurin et al. [2022] argue that across supervised MTL benchmarks and Meta-World multi-task SAC, the simple uniform sum of losses (unitary scalarization) matches specialized multi-task optimizers once standard regularization is matched; our diagnostic evidence (Figure 2: critic per-task gradient-norm spread $497\times$) is on MT-PPO specifically, a regime they do not test, where FairGrad ($\alpha{=}1$) provably absorbs per-task gradient rescaling (Theorem 1 and Corollary 1). The Kurin SAC result is consistent with our PopArt-removed ablations on V1 (which has wider per-task return scale heterogeneity, Table D.3) showing that direction-only loss-level signals fall short once the critic-side per-task scale spread is load-bearing. Section C.3 positions these methods as different points in the same shared cone $\mathrm{cone}^{+}\{\mathbf{g}_i\}$; only FairGrad ($\alpha{=}1$) carries the scale-invariance of Theorem 1 that links it to PopArt via Corollary 1. *Value-target normalization* (PopArt [van Hasselt et al., 2016, Hessel et al., 2019]; ARS rescales the per-task reward fed into the Bellman target [Cho et al., 2025]) and *representation regularization* (LayerNorm [Ba et al., 2016], applied in deep RL by Lee et al. [2025], Hansen et al. [2024]) are standard; Corollary 1 restricts the new PopArt→FG-c content to PopArt's per-task gradient-rescaling effect $c_i = \sigma_i^{-2}$.

B Implementation Details

B.1 Detailed experimental setup

This appendix expands the main-text Section 5.1 with the full benchmark, architecture, training, and evaluation description; hyperparameter values are tabulated in Table B.1 (Section B.2), PPO-specific adaptations of SAC-based gradient-surgery methods are documented in Section B.4, the source-counted parameter audit against published baselines is in Section B.3, and cross-paper protocol differences are mapped in Section D.7.

Benchmark and observations. We use Meta-World 3.0.0 [Yu et al., 2020b, McLean et al., 2025] with V2 reward semantics throughout the paper unless explicitly labeled V1. The K tasks (reaching, picking, pushing, opening doors, peg-insertion, etc.) share the same continuous observation space $\mathcal{S}$ and continuous action space $\mathcal{A}$; what varies across tasks is the reward function and the dynamics. The agent receives the state concatenated with a one-hot task identifier of length K as input, and is trained on all K tasks simultaneously via stratified minibatches. Meta-World offers two reward variants: V1 is the original per-task reward set from Yu et al. [2020b] with substantial per-task scale heterogeneity, while V2 [McLean et al., 2025] redesigns the per-task rewards with PPO solvability and comparable per-task scales as explicit design criteria. We evaluate TOPPO on *both* variants. Published V2 mean/worst-k and V1 IQM baseline values match our reporting statistic but not our full environment and evaluation protocol. Our SAC-MT and ARS runs share TOPPO's Meta-World 3.0.0 environment and evaluation protocol (Section E.1). V2 carries the headline (MT50 V2 is the main number; MT10 V2 saturates near ceiling and is reported for completeness, Section 5.2); V1 is the sensitivity sweep that also tests Corollary 1's scope under heterogeneous per-task return scales (Section D.5).

Architecture. Actor and critic are separate networks of identical $[400, 400, 400]$ shape (full architecture in Table B.1); this is the standard SAC-family Meta-World+ backbone used by CAGrad [Liu et al., 2021], CARE [Sodhani et al., 2021], PaCo [Sun et al., 2022], MOORE [Hendawy et al., 2024],

FAMO [Liu et al., 2023], and FairGrad [Ban and Ji, 2024], while the ARS codebase [Cho et al., 2025], including its SAC-MT baseline, is the architectural outlier with a deeper $[400 \times 4]$ default or a wider $[1024 \times 4]$ ARS-LN-1024 variant. The task-specific quantities are the input one-hot, an $|\mathcal{A}|$-dimensional action log-stddev per task, and, when PopArt is enabled, two trainable scalar affine parameters (W_i, b_i) per task together with running-statistic buffers (μ_i, σ_i). The actor mean and the pre-PopArt scalar value projections are shared; there are no task-specific hidden subnetworks, expert mixtures, LoRA adapters, or routers. Headline parameter counts are 685K (MT10) and 717K (MT50); per-component breakdowns and ratios against published baselines are tabulated in Table B.2 (Section B.3).

Training pipeline. Our PPO implementation builds on Tianshou 2.0.0 [Weng et al., 2022] (`https://github.com/thu-ml/tianshou`; MIT License). Stratified minibatch sampling guarantees the per-task gradients $\mathbf{g}_i^a$, $\mathbf{g}_i^c$ on the shared parameters are well-defined every minibatch. Per-task advantage normalization (zero-mean unit-variance computed within each task's slice of a minibatch) is applied before the actor surrogate; this task-wise adaptation of a PPO implementation option is the actor-side mechanism that drives the actor-critic asymmetry diagnosed in Section 3. The headline and intervention configurations retain PPO's value clip and a post-aggregation gradient-norm clip. Additional normalizer ablations explicitly vary value clipping; HL-Gauss uses an unclipped cross-entropy critic loss.

Evaluation protocol. All of our reported success rates come from *evaluation* rollouts under the deterministic policy mean (no exploration noise), not training rollouts; published baseline rows retain their original evaluation protocols. Following the Meta-World convention [Yu et al., 2020b, McLean et al., 2025], at each evaluation checkpoint the agent is rolled out once per training goal position per task: 50 goal positions $\times$ K tasks $=$ 500 episodes per evaluation on MT10 and 2,500 on MT50. A per-task "success rate" is the fraction of those episodes whose success flag is 1 at *any* step during the episode (the default Meta-World success criterion inherited from the benchmark code, not a termination-only criterion); the reported scalar is the cross-task mean of per-task success rates.

Reporting choices. We run 10 seeds and report final-checkpoint success rates. To match each baseline's published convention, we report mean $\pm$ std against the V2 baselines from Cho et al. [2025] (Table 2) and IQM $\pm$ std against the Meta-World+ V1 baselines (Table 3); for our rows, both views are computed from the same 10-seed run set. Table 2 lists SAC-MT and the ARS family as run by us for 10 seeds (Section E.1), under our evaluation protocol rather than the published one. The full 4-metric breakdown of every reported configuration is in Table D.10, cross-paper convention conversions are in Section D.7, and per-task breakdowns are in Section D.6.

Compute resources. Each MT10 and MT50 V2 headline run trained one seed on one GPU with 16 CPU cores: an NVIDIA RTX 3090 for every MT10 seed and for MT50 seeds 3–9, and an NVIDIA H200 NVL for MT50 seeds 0–2. The allocated host memory was 24 GB per MT10 run and 32–64 GB per MT50 run. Including its 51 evaluations, one MT10 20M-step seed took 5–8 wall-clock hours, and one MT50 100M-step seed took 23–32 hours on an RTX 3090 and about 14 hours on the H200 NVL. On the RTX 3090, five MT50 seeds took 23–24 hours each; the other two were preempted once, resumed from a checkpoint, and took 31–32 hours from start to finish. The ten MT50 V1 TOPPO runs each used one NVIDIA Tesla V100 (32 GB) with 12 CPU cores and 64 GB of host memory, and with the same evaluation schedule each took 40–43 hours. These are end-to-end durations of the runs above rather than controlled measurements; Section E.4 reports controlled timings with evaluation disabled and their scope. The headline schedule includes 51 evaluation checkpoints during training (one every 2 epochs across 100 epochs, plus initialization); evaluation environment steps are excluded from the 20M / 100M training budget. TOPPO reaches strong performance well before the full budget is exhausted (Section 5.2 and Figure 1); the full schedule is reported to match the published reporting protocol, while shorter runs can be sufficient when strict final-checkpoint comparability is not required.

B.2 Hyperparameters and architecture

Inherited from Meta-World+. The PPO numerical hyperparameters in Table B.1 (loss coefficients, GAE λ, clip range, learning rate, PPO repeats per collect, minibatch size, gradient-norm clip, MLP backbone, per-rollout step counts and total environment-step budgets) follow

the Meta-World+ companion repository [McLean et al., 2025] (`https://github.com/rainx0r/metaworld-algorithms`); we do not separately tune these values. The realized minibatch count changes under our stratified sampler, as detailed below. The one substantive deviation from their MT50 example config is that we keep value clipping on (their MT50 example disables it). Per-task advantage normalization and stratified minibatch sampling are PPO-side multi-task adaptations on top of this baseline (Section B.4); FairGrad / PCGrad / CAGrad / PopArt / LayerNorm hyperparameters are listed under their respective entries below.

Table B.1: Production hyperparameters for the headline experiments. Normalizer and actor-combiner ablations in Section E state their overrides separately. The three FairGrad solver entries below the per-side α rows ($y_{\max}$, η, max Newton iters) are fixed solver constants, not swept.

Parameter	MT10	MT50
Shared backbones with task-local action scale and PopArt affine		
actor $\boldsymbol{\theta}^a$ hidden sizes	$[400, 400, 400]$	$[400, 400, 400]$
actor output projection	shared $\mathrm{Linear}(400, \lvert\mathcal{A}\rvert)$ for μ	shared $\mathrm{Linear}(400, \lvert\mathcal{A}\rvert)$ for μ
critic $\boldsymbol{\theta}^c$ hidden sizes	$[400, 400, 400]$	$[400, 400, 400]$
critic output projection	shared $\mathrm{Linear}(400, 1)$ for V	shared $\mathrm{Linear}(400, 1)$ for V
per-task action log-stddev	$\lvert\mathcal{A}\rvert$ params per task	$\lvert\mathcal{A}\rvert$ params per task
PopArt affine (W_i, b_i)	2 params per task	2 params per task
task identity input	one-hot, length $K = 10$	one-hot, length $K = 50$
activation	ReLU	ReLU
LayerNorm placement (TOPPO)	critic hidden layers only	critic hidden layers only
Training		
epochs	100	100
env steps per epoch	200,000	1,000,000
env steps per collect	100,000	500,000
PPO repeats per collect	16	16
minibatch size (= step/32)	3,125	15,625
minibatch sampling	stratified	stratified
realized minibatches per repeat	31	31
learning rate (Adam)	3×10^{-4}	3×10^{-4}
max gradient norm (post-aggregation)	1.0	1.0
discount γ	0.99	0.99
PPO		
GAE λ	0.97	0.97
clip range ϵ	0.2	0.2
value clip	enabled	enabled
value loss weight c_v	0.001	0.001
entropy bonus c_e	0.005	0.005
per-task advantage normalization	enabled	enabled
recompute advantage per repeat	enabled	enabled
FairGrad (when active)		
actor α_a	2.0	2.0
critic α_c	1.0	1.0
solver y-cap $y_{\max}$	50	50
solver Newton tol η	10^{-2}	10^{-2}
solver max Newton iters	50	50
Evaluation		
eval episodes per task	50	50
seeds reported	10	10

LayerNorm placement notes.

- Pre-activation LN on hidden `Linear` layers of critic network only; actor hidden layers are LN-free.
- SimBa/TD-MPC2-style symmetric LN [Lee et al., 2025, Hansen et al., 2024] (LN on both actor and critic hidden layers) is the natural baseline; TOPPO deliberately uses critic-only LN. The symmetric-LN ablation is discussed with the intervention results in Section D.1.
- LN-enabled critic hidden `Linear` uses `bias=False`; the LayerNorm affine parameters remain trainable, and the critic output projection retains its bias.

B.3 Parameter audit (source-counted)

Convention. Throughout the paper, every "parameter count" refers to the *total number of model parameters held in memory during training, including target copies and excluding optimizer state*. This measures model storage, not total GPU memory, which also includes activations, gradients, optimizer states, and framework buffers. For our PPO this is just actor + critic (no target network). For SAC-style baselines this is actor + 2×critic + 2×target_critic + α, where the twin Q-critics are stacked on a `num_critics`=2 axis and the Polyak-averaged target copy is updated by EMA rather than gradient descent. We include the target copy because it occupies the same GPU memory as the live critic. A trainable-only accounting removes the target critic ensemble from each SAC row in Table B.2; ARS-LoRA holds two target ensembles and also freezes its base network during LoRA training, leaving 820K (MT10) / 8,235K (MT50) trainable parameters. For example, on MT50, ARS-LN-1024 drops from 16,267K resident to 9,758K trainable parameters, still 13.6× TOPPO's 717K; TOPPO remains the smallest model under either accounting.

Provenance. Numbers in Table B.2 were not lifted from the corresponding papers (most do not report scalar parameter counts); they were obtained by instantiating each method's example configuration in code and summing the leaves of the parameter pytree. ARS-paper baselines (SAC-MT, MT-MH-SAC, Soft Modularization, PCGrad-SAC, MOORE, ARS, ARS-LN, ARS-LoRA) come from the official ARS JAX/Flax release [Cho et al., 2025] (`https://github.com/ms-cho/Adaptive-Reward-Scaling-ARS-for-MTRL`); the Meta-World+ MT-family rows (MT-MH-SAC, PCGrad-SAC, Soft Modularization, MOORE, PaCo) come from the companion `metaworld-algorithms` JAX repository [McLean et al., 2025] (`https://github.com/rainx0r/metaworld-algorithms`).

Cross-implementation caveat. Same-named methods can differ between the two source codebases. For example, MOORE is 6,890K (MT10) / 7,403K (MT50) in the ARS reproduction (4 orthogonal 400-wide experts on a SAC-MT backbone) and 6,810K (MT10) / 10,385K (MT50) in the Meta-World+ reproduction (4 experts at MT10, 6 at MT50, plus per-task output heads). We never mix counts across implementations within a single comparison row: Table 2 uses the ARS-paper figures for every V2 baseline (matching the published success rates, which come from Tables 1, 2, and 6 of Cho et al. [2025]; our SAC-MT and ARS runs use the same architectures and therefore the same counts), and Table 3 uses the Meta-World+ figures for V1 baselines.

Headline ratios. TOPPO at the headline configuration (LN-c + PopArt on the critic; FG-c on the critic gradient aggregator adds 0 parameters) is 685K (MT10) / 717K (MT50). LN-c adds $3 \times 400 = 1{,}200$ parameters net of dropped hidden-layer Linear biases; PopArt adds $2K$ trainable scalar affine parameters. Their combined increment is 1,220 parameters on MT10 and 1,300 on MT50. The no-LN-c, no-PopArt rung (the vanilla MT-PPO entry in Table 2) has rounded counts 684K / 716K. Rounded ratios below all use the MT50 headline denominator (717K):

- vs. ARS default (2,597K): we are 27.6% (1/3.6×).
- vs. ARS-LN-1024 (16,267K): we are 4.4% (1/22.7×).
- vs. ARS-LoRA (16,123K): we are 4.4% (1/22.5×).
- vs. PaCo K=20 in Meta-World+ (33,909K): we are 2.1% (1/47.3×).
- vs. MOORE in Meta-World+ (10,385K): we are 6.9% (1/14.5×).

Full table: Table B.2.

Table B.2: **Source-counted parameter audit (training-memory totals).** TOPPO (685K MT10 / 717K MT50) is $1/3.6\times$ ARS, $1/22.7\times$ ARS-LN-1024, and $1/47.3\times$ PaCo K=20 at MT50, supporting the "smaller-and-better" framing. The ARS-paper block [Cho et al., 2025] and Meta-World+ block [McLean et al., 2025] are non-identical reimplementations of same-named methods; counts are never mixed within a comparison row (see Section B.3).

Method (architecture)	Parameters (MT10)	Parameters (MT50)	Notes
Ours: TOPPO $[400 \times 3]$	685K	717K	headline; FG-c aggregator adds 0 params
Ours: Vanilla MT-PPO $[400 \times 3]$	684K	716K	no LN-c, no PopArt (Vanilla MT-PPO rung in Table 2)
ARS paper: SAC-MT	2,517K	2,597K	actor $+2\times$critic $+2\times$target $+\alpha$
MT-MH-SAC	2,546K	2,754K	+per-task output head
Soft Modularization	3,454K	3,534K	task-embed + 2 modules $\times$ depth 2
PCGrad-SAC	2,517K	2,597K	PCGrad arch-identical to SAC-MT
MOORE	6,890K	7,403K	4 orthogonal 400-wide experts
ARS	2,517K	2,597K	SAC-MT backbone; differs only in loss
ARS-LN-400	2,530K	2,611K	+LN-c
ARS-LN-1024	16,062K	16,267K	$22.7\times$ our MT50 baseline
ARS-LoRA	3,878K	16,123K	base + LoRA + 2 targets
PaCo / SMT	–	–	not implemented in ARS reference repo
Meta-World+: MT-MH-SAC / PCGrad-SAC	1,759K	2,031K	shared $[400]\times3$ torso, per-task heads
Soft Modularization	3,454K	8,030K	(depth, num_modules) = (2,2) MT10 / (4,4) MT50
MOORE	6,810K	10,385K	4 experts MT10 / 6 experts MT50
PaCo (K=5 / K=20)	8,476K	33,909K	compositional Dense; K parameter sets

B.4 PPO-specific adaptations of SAC-based gradient-surgery methods

Provenance. PCGrad, CAGrad, and FairGrad are formulated as generic per-task gradient operators and evaluated primarily on supervised MTL benchmarks (CityScapes / NYUv2 / QM9); their Meta-World evaluations all use SAC (PCGrad / CAGrad on MT10 and MT50; FairGrad on MT10 only) [Yu et al., 2020a, Liu et al., 2021, Ban and Ji, 2024]. Porting to PPO requires per-task loss decomposition, per-task backward, and a per-side combiner choice (Section 4); the standard PPO machinery (GAE, ratio clip, value clip, Adam, $[400\times3]$ MLP) is unchanged, and the four interventions of Section 4 (Table B.1) are the entire delta from vanilla MT-PPO. This subsection documents the few items that are not pinned down by the table or the method section.

Baseline hyperparameters preserved verbatim. We do not re-tune any baseline's published hyperparameters. CAGrad $c = 0.5$ (MT50) and $c = 0.9$ (MT10) per Liu et al. [2021]; PCGrad has no solver hyperparameters; per-side FairGrad α is in Table B.1.

Solver call frequency. Whereas the SAC originals invoke the solver once per environment step, PPO invokes it once per minibatch inside each rollout's PPO-epoch loop. Although the nominal minibatch size is the collect size divided by 32, the stratified sampler allocates integer quotas of 312 or 313 samples per task and stops when any task cannot fill its quota. With $10{,}000$ collected transitions per task, this yields $\lfloor 10{,}000/313 \rfloor = 31$ minibatches per repeat, dropping the remaining $1/32$ of the collected batch from that repeat. Thus $16 \times 31 = 496$ combiner calls occur per collect on each enabled side, or $99{,}200$ calls across 200 collects at the full budget. This realized count is also recorded by the real-Gram benchmark in Section C.5.

Task-local parameters bypass surgery. Only the shared actor and critic backbone parameters feed the per-side combiner. The task-local action log-stddev and PopArt affine parameters (W_i, b_i) receive the mean of the per-task gradients, bypassing FairGrad and PCGrad. They are reassembled with the combined shared gradients before the global norm clip and Adam update. The actor/critic partition is exposed to the combiner by a parameter-filter helper that slices the per-task gradient list to each side's flat slab before invoking it. Code paths for a feature-shared preprocess net ($\boldsymbol{\theta}_{\text{pre}}$) and per-task mu/value heads (`mu_heads`, `value_heads`) exist but are empty in every reported config.

FairGrad-specific containment. The released solver does not add a ridge term to the Gram matrix. It floors Gram diagonals at $\varepsilon = 10^{-8}$ for the warm-start calculation, caps Newton log-weights at $y_{\max} = 50$, and floors final weights at ε. The SciPy fallback has a positive lower bound but no upper weight bound. These numerical safeguards and the absolute stopping tolerance can break the exact scale-invariance and fixed-norm identities of Theorem 1; the theorem concerns an exact positive KKT solution. Per-task weights, contributions, residuals, and fallback use are logged, and the reassembled gradient is clipped to norm at most 1 before Adam. See Section C.5 for the numerical distinction.

B.5 PopArt: implementation note (Welford full-sample statistics)

Our PopArt implementation updates the per-task running statistics (μ_i, σ_i) via Chan–Golub–LeVeque parallel Welford merges [Welford, 1962, Chan et al., 1983] over the full per-task return history. Canonical PopArt [van Hasselt et al., 2016, Eq. 4] presents both options—$\beta_t = 1/t$ recovers the full-history sample mean, while a constant-rate EMA at β is the recommended choice for non-stationary settings; the multi-task PopArt setup of Hessel et al. [2019] adopts the constant-β EMA. Our Welford accumulator therefore matches the $\beta_t = 1/t$ branch of canonical PopArt rather than the constant-β branch typically used in deep RL. After each collect of n_{batch} return targets for task i with batch mean $\bar{R}_i$ and batch sum-of-squared-deviations M_2^{batch}:

$$\begin{aligned} n_{\text{new}} &\leftarrow \text{count}[i] + n_{\text{batch}}, \qquad \delta \leftarrow \bar{R}_i - \mu_i, \\ \mu_i &\leftarrow \mu_i + \delta \cdot \tfrac{n_{\text{batch}}}{n_{\text{new}}}, \\ M_2[i] &\leftarrow M_2[i] + M_2^{\text{batch}} + \delta^2 \cdot \tfrac{\text{count}[i]\, n_{\text{batch}}}{n_{\text{new}}}, \\ \sigma_i &\leftarrow \max\!\big(\sqrt{M_2[i]/n_{\text{new}}},\, \sigma_{\min}\big), \qquad \text{count}[i] \leftarrow n_{\text{new}}, \end{aligned} \tag{B.1}$$

with $\sigma_{\min} = 10^{-2}$. The PopArt renormalization that adjusts (W_i, b_i) to preserve V_i^{raw} across (μ_i, σ_i) updates runs identically to canonical PopArt and is unaffected by the choice of estimator.

The effective update rate is $n_{\text{batch}}/n_{\text{new}}$, which decays as $\sim 1/n$ and becomes small after many collects. This estimates the cumulative return distribution over training. The released EMA alternative instead uses a per-sample decay $\beta = 3 \times 10^{-4}$, implemented as the exact closed-form composition of sequential updates within each rollout batch. It therefore emphasizes recent targets, including their order within a collect.

Effect on the paper's claims. The results in Tables 2 and D.1 use Welford PopArt; the EMA cohorts are reported separately. The exact KKT invariance in Theorem 1 applies to either estimator's positive scaling only when the gradient-rescaling premise of Corollary 1 holds: an unclipped squared loss, or equivalent raw and normalized clipping thresholds and active branches. It does not establish equality of the two estimators' training trajectories or bound their performance difference. In particular, the two estimates can differ from the first collect: with $10{,}000$ targets per task, the EMA retains approximately $(1-\beta)^{10{,}000} \simeq 0.050$ of its prior state and nonuniformly weights the new targets, whereas Welford averages the first batch uniformly. Estimator effects therefore require direct ablation, including under V1, rather than an assumed early-training equivalence.

C Theoretical Details

C.1 TOPPO pseudocode

Algorithm C.1 expands the compact Algorithm 1 (Section 4) with the bookkeeping that the main-text version folds into surrounding loop headers, mirroring the released implementation. Relative to our vanilla MT-PPO baseline, TOPPO adds critic LayerNorm, PopArt, and the per-side gradient combiners FG-c / PCGrad-a. Stratified minibatching and per-task advantage normalization are already present in that baseline. Per-task backward passes supply the combiner inputs. PPO's GAE, ratio clipping, advantage recomputation, global gradient-norm clipping, and Adam update are retained. With PopArt enabled, value clipping operates in normalized value coordinates.

Algorithm C.1 TOPPO: a PPO collect-and-update phase.

Require: Tasks $\{\mathcal{M}_i\}_{i=1}^K$, shared params $\boldsymbol{\theta} = (\boldsymbol{\theta}^a, \boldsymbol{\theta}^c)$ with **[LN-c]**, task-local action log-stddev and PopArt affine (W_i, b_i), PopArt statistics (μ_i, σ_i), repeats R, minibatch size b, clip ϵ, max gradient norm τ

Rollout $\mathcal{B} = \bigcup_i \mathcal{B}_i$ under $\pi_{\boldsymbol{\theta}^a_{\text{old}}}$ (uniform per task); calculate per-task GAE $\hat{A}_t^{(i)}$ and value targets $\hat{V}_t^{(i),\text{targ}}$ on raw returns

[PopArt] update (μ_i, σ_i) via Welford on $\{\hat{V}_t^{(i),\text{targ}}\}$ (Eq. (B.1)) and PopArt-renormalize the per-task affine head so raw V is preserved *(Section 4.1)*

for $r = 1$ **to** R **do**

  if $r > 1$ **then**

    recompute $\hat{A}_t^{(i)}, \hat{V}_t^{(i),\text{targ}}$ on $\mathcal{B}$ under current $V_{\boldsymbol{\theta}^c}$

  end if

  for each task-stratified minibatch $\mathcal{B}^{\text{mb}} \subset \mathcal{B}$ of size b **do**

    normalize advantages within each task slice of $\mathcal{B}^{\text{mb}}$; map critic targets to PopArt space $(\hat{V}_t^{(i),\text{targ}} - \mu_i)/\sigma_i$ as in Section 4.1

    for $i = 1$ **to** K such that $\mathcal{B}_i^{\text{mb}} \neq \emptyset$ **do**

      $L_i \leftarrow L_i^a(\boldsymbol{\theta}^a) + c_v L_i^{c,\text{PopArt}}(\boldsymbol{\theta}^c) - c_e H_i(\boldsymbol{\theta}^a)$ on $\mathcal{B}_i^{\text{mb}}$ *(Eq. (1))*

      backward $\mathbf{g}_i \leftarrow \nabla_{\boldsymbol{\theta}} L_i$ and cache flat actor and PopArt critic slabs $(\mathbf{g}_i^a, \mathbf{g}_i^{c,\text{PopArt}})$

    end for

    [FG-c (α=1)] solve $\mathbf{G}^c\mathbf{w} = \mathbf{w}^{-1}$ via Algorithm C.2, then $\mathbf{d}^c \leftarrow \sum_i w_i \mathbf{g}_i^{c,\text{PopArt}}$ *(Section 4.3)*

    [PCGrad-a] $\mathbf{d}^a \leftarrow \text{PCGrad}(\mathbf{g}_1^a, \ldots, \mathbf{g}_K^a)$ *actor-side surgery*

    reassemble $(\mathbf{d}^a, \mathbf{d}^c)$ with averaged task-local gradients; clip the full vector to norm τ and take an Adam step on all trainable parameters

  end for

end for

C.2 α-fairness family and KKT derivation

This appendix expands Section 4.3 with three pieces deferred from the main text: (i) the interpretation of U_α in Eq. (3) as a one-parameter fairness family, (ii) the precise meaning of "per-task contribution x_i" in Eq. (C.1) and the canonical scaling that pins down $\mathbf{w}$ in the FairGrad program, and (iii) the derivation, via a strictly convex unconstrained program, of the KKT condition $\mathbf{G}^c\mathbf{w} = \mathbf{w}^{-1/\alpha}$ stated in Section 4.3.

Family interpretation. U_α [Mo and Walrand, 2000, Kelly, 1997] is strictly concave on $\mathbb{R}_{>0}$ for every $\alpha > 0$, and as α varies over $(0, \infty)$ it interpolates classical social-welfare rules: utilitarian sum as $\alpha \to 0^+$ (each unit of x_i has equal marginal value), Nash bargaining at $\alpha = 1$ [Nash, 1950] (the log-utility / geometric-mean solution), and Rawlsian max-min as $\alpha \to \infty$ (the smallest x_i dominates). Larger α thus up-weights small-share agents — equivalently, in our setting, gives more aggregator budget to tasks whose contribution to the combined critic gradient is currently small.

Per-task contribution and the canonical scaling. Write $\mathbf{d} := \sum_i w_i \mathbf{g}_i^c$ for the combined critic gradient. "Per-task contribution" refers to the inner product

$$x_i \;:=\; \mathbf{g}_i^{c\top}\mathbf{d} \;=\; (\mathbf{G}^c\mathbf{w})_i, \tag{C.1}$$

i.e. how much task i's gradient agrees with the combined direction; $x_i > 0$ is the linearized loss decrease task i obtains under a unit step along $\mathbf{d}$. The bare welfare $\sum_i U_\alpha((\mathbf{G}^c\mathbf{w})_i)$ has no interior maximizer along positive rays $\mathbf{w} \mapsto t\mathbf{w}$ (for $0 < \alpha \leq 1$ it grows without bound as $t \to \infty$; for $\alpha > 1$ it approaches its supremum 0 only in that limit), so a normalization is needed to pin down a canonical $\mathbf{w}$. Geometrically, $\mathbf{w}^\top\mathbf{G}^c\mathbf{w} = \|\mathbf{d}\|^2$, so any normalization of $\mathbf{w}$ corresponds to a choice of $\|\mathbf{d}\|$. Throughout the paper we adopt the *canonical scaling* that yields the dimensionless KKT $\mathbf{G}^c\mathbf{w} = \mathbf{w}^{-1/\alpha}$ used in Section 4.3, Theorem 1, and Corollary 1; for $\alpha = 1$, this canonical $\mathbf{w}$ satisfies $\|\mathbf{d}\|^2 = \mathbf{w}^\top\mathbf{G}^c\mathbf{w} = K$ rather than 1 (Theorem 1).

Derivation of the FairGrad KKT condition. For $\alpha = 1$ (the headline critic setting), the canonical-scaling solution is the unique minimizer of the strictly convex unconstrained program

$$\min_{\mathbf{w}\in\mathbb{R}^K_{>0}} \quad \Phi_1(\mathbf{w}) \;:=\; \tfrac{1}{2}\,\mathbf{w}^\top \mathbf{G}^c \mathbf{w} \;-\; \sum_{i=1}^{K} \log w_i. \tag{C.2}$$

Strict convexity follows from $\nabla^2\Phi_1(\mathbf{w}) = \mathbf{G}^c + \mathrm{diag}(w_i^{-2}) \succ 0$ on $\mathbb{R}^K_{>0}$ (since $\mathbf{G}^c \succ 0$ by the linear-independence assumption); existence and uniqueness then follow because $\Phi_1(\mathbf{w}) \to +\infty$ both on $\partial\mathbb{R}^K_{>0}$ (via $-\sum_i \log w_i \to +\infty$ as any $w_i \to 0^+$) and as $\|\mathbf{w}\| \to \infty$ (via $\mathbf{w}^\top\mathbf{G}^c\mathbf{w} \geq \lambda_{\min}(\mathbf{G}^c)\|\mathbf{w}\|^2$). Stationarity $\nabla\Phi_1(\mathbf{w}^*) = \mathbf{0}$ reads $\mathbf{G}^c\mathbf{w}^* - (\mathbf{w}^*)^{-1} = \mathbf{0}$, i.e. the dimensionless KKT

$$\mathbf{G}^c\mathbf{w}^* \;=\; (\mathbf{w}^*)^{-1} \quad \text{(componentwise)},$$

stated in Section 4.3, on which Theorem 1 and Corollary 1 build. This canonical solution coincides with the constrained α-fairness program $\max \sum_i \log((\mathbf{G}^c\mathbf{w})_i)$ subject to $\mathbf{w}^\top\mathbf{G}^c\mathbf{w} = K$: the constraint value K is precisely what makes the Lagrange multiplier equal 1 at the optimum, eliminating the rescaling step needed under the conventional unit-norm normalization $\mathbf{w}^\top\mathbf{G}^c\mathbf{w} = 1$. The unconstrained form Eq. (C.2) avoids carrying a Lagrange multiplier through the derivation. For general $\alpha > 0$, the same construction with $\sum_i \log w_i$ replaced by $\frac{\alpha}{\alpha-1}\sum_i w_i^{1-1/\alpha}$ ($\alpha \neq 1$) gives the KKT $\mathbf{G}^c\mathbf{w} = \mathbf{w}^{-1/\alpha}$ via the same stationarity calculation; the boundary argument is replaced by gradient blow-up $\partial\Phi_\alpha/\partial w_i = (\mathbf{G}^c\mathbf{w})_i - w_i^{-1/\alpha} \to -\infty$ as $w_i \to 0^+$, which still forces an interior minimizer. The KKT couples per-task scale (diagonal $\mathbf{G}^c_{ii}$, how loud each task is on its own) with direction conflict (off-diagonals, how compatibly two tasks pull).

C.3 Aggregator family taxonomy and cone containment

Theorem C.1 (Shared cone containment)**.** *Let* $\mathrm{cone}^+\{\mathbf{g}_1,\ldots,\mathbf{g}_K\} := \{\sum_i w_i\mathbf{g}_i : w_i \geq 0\}$ *denote the closed conic hull (non-negative combinations) of the per-task gradient set. The combined gradient produced by FairGrad (any* $\alpha > 0$*), PCGrad [Yu et al., 2020a], CAGrad [Liu et al., 2021], FAMO [Liu et al., 2023], DWA [Liu et al., 2019], and uncertainty weighting [Kendall et al., 2018] lies in* $\mathrm{cone}^+\{\mathbf{g}_1,\ldots,\mathbf{g}_K\}$.

Proof. For FairGrad/FAMO/DWA/UW, the combined gradient is $\sum_i w_i\mathbf{g}_i$ with $w_i \geq 0$ by construction (FairGrad's KKT solves on $\mathbb{R}^K_{>0}$ for $\alpha > 0$; FAMO/DWA/UW use loss-level reweighting with non-negative weights, so $\nabla\sum_i w_i L_i = \sum_i w_i\mathbf{g}_i$). For CAGrad, the combined gradient is $\sum_i(\frac{1}{K} + w_i^*\lambda^*)\,\mathbf{g}_i$ with $w_i^* \geq 0$ on the simplex and $\lambda^* \geq 0$ [Liu et al., 2021], so the coefficient on each $\mathbf{g}_i$ is $\geq \frac{1}{K} > 0$. For PCGrad, induct over the projection schedule. Let $S_{<k}$ denote the (ordered) set of tasks already projected against in task i's inner loop before step k. Base case ($k = 0$): $\mathbf{g}_i' = \mathbf{g}_i$, with coefficient 1 on $\mathbf{g}_i$ and $\mu_{i,m} = 0$ for all $m \neq i$. Inductive step: at step k with $\mathbf{g}_i' = \mathbf{g}_i + \sum_{m\in S_{<k}} \mu_{i,m}\mathbf{g}_m$ ($\mu_{i,m} \geq 0$), the projection is taken against the *original* $\mathbf{g}_{j_k}$ (Yu et al., 2020a, Algorithm 1); if $\langle\mathbf{g}_i', \mathbf{g}_{j_k}\rangle \geq 0$ no update; else the update adds $-\langle\mathbf{g}_i', \mathbf{g}_{j_k}\rangle/\|\mathbf{g}_{j_k}\|^2 > 0$ to the (non-negative) coefficient on $\mathbf{g}_{j_k}$. Invariant preserved; final $\mathbf{g}_i^{\mathrm{PC}}$ is a non-negative combination of $\{\mathbf{g}_1,\ldots,\mathbf{g}_K\}$. The combined gradient $\mathbf{g}^{\mathrm{PC}} = \frac{1}{K}\sum_i \mathbf{g}_i^{\mathrm{PC}}$ is then a non-negative combination of the same set, hence in $\mathrm{cone}^+\{\mathbf{g}_1,\ldots,\mathbf{g}_K\}$. □

Remark C.1 (FG at α=1 recovers Nash-MTL). At α=1, the welfare is $\sum_i \log u_i$, where $u_i = \mathbf{g}_i^\top\mathbf{d} > 0$ is the task's linearized improvement [Nash, 1950, Kelly, 1997, Mo and Walrand, 2000]. Under the canonical norm constraint $\|\mathbf{d}\|_2^2 \leq K$, maximizing this welfare over feasible directions gives the Nash bargaining direction used by Nash-MTL [Navon et al., 2022]. The norm constraint is necessary: the unconstrained log-welfare is unbounded under positive scaling. At canonical scaling, both formulations yield $w_i(\mathbf{G}\mathbf{w})_i = 1$, underlying Theorem 1; their numerical solvers and practical stopping criteria differ.

Implication. Theorem C.1 reframes the gradient-aggregation design space: methods differ in which point inside the same shared cone they select, not in the cone itself. FAMO/DWA/UW pick a Gram-blind point; PCGrad picks a point determined by $\mathrm{sign}(\mathbf{G}_{ij})$ via random-order projection; CAGrad picks the solution of a constrained QP on $\mathbf{G}$; FairGrad picks the α-fairness KKT solution on the full Gram. Among these, only α=1 FG carries the closed-form $\sqrt{K}$-norm identity and scale-invariance of Theorem 1.

C.4 Proof of Theorem 1 (scale invariance)

We write $\mathbf{w}^*$ for the theorem's $\mathbf{w}$ throughout, reserving $\mathbf{w}$ as the optimization variable. Thus $\mathbf{w}^* \in \mathbb{R}^K_{>0}$ denotes the unique positive solution of the $\alpha = 1$ KKT $\mathbf{G}\mathbf{w} = \mathbf{w}^{-1}$. Fix any $\mathbf{c} \in \mathbb{R}^K_{>0}$, set $\tilde{\mathbf{g}}_i := c_i \mathbf{g}_i$ and $D := \mathrm{diag}(\mathbf{c})$, and write $\tilde{\mathbf{G}} := D\mathbf{G}D$ for the rescaled Gram. We proceed in four steps.

Step 1 (existence and uniqueness). The KKT $\mathbf{G}\mathbf{w} = \mathbf{w}^{-1}$ is the $\alpha = 1$ specialization of the strictly convex unconstrained program (C.2), which admits a unique positive minimizer by the argument given there. Since D is invertible and $\mathbf{G} \succ 0$, congruence yields $\tilde{\mathbf{G}} = D\mathbf{G}D \succ 0$; applying the same argument to (C.2) with $\mathbf{G}$ replaced by $\tilde{\mathbf{G}}$ gives a unique positive solution of the rescaled KKT $\tilde{\mathbf{G}}\tilde{\mathbf{w}} = \tilde{\mathbf{w}}^{-1}$.

Step 2 (norm identity $\| \sum_i w_i^* \mathbf{g}_i \|^2 = K$). Componentwise, $(\mathbf{G}\mathbf{w}^*)_i = 1/w_i^*$, hence $w_i^*(\mathbf{G}\mathbf{w}^*)_i = 1$ for every i. Summing,

$$(\mathbf{w}^*)^\top \mathbf{G}\mathbf{w}^* \;=\; \sum_{i=1}^{K} w_i^* (\mathbf{G}\mathbf{w}^*)_i \;=\; K.$$

Expanding the quadratic form via $\mathbf{G}_{ij} = \langle \mathbf{g}_i, \mathbf{g}_j \rangle$ gives

$$\Big\| \sum_i w_i^* \mathbf{g}_i \Big\|^2 \;=\; \sum_{i,j} w_i^* w_j^* \langle \mathbf{g}_i, \mathbf{g}_j \rangle \;=\; (\mathbf{w}^*)^\top \mathbf{G}\mathbf{w}^* \;=\; K.$$

Step 3 (scale invariance at $\alpha = 1$). Define $\tilde{\mathbf{w}} := \mathbf{w}^* \oslash \mathbf{c}$, i.e. $\tilde{w}_i = w_i^*/c_i$. We verify that $\tilde{\mathbf{w}}$ solves the rescaled KKT and preserves the combined update.

(3a) Rescaled KKT. Using $\tilde{\mathbf{G}}_{ij} = c_i c_j \mathbf{G}_{ij}$ and $c_j \tilde{w}_j = w_j^*$,

$$(\tilde{\mathbf{G}}\tilde{\mathbf{w}})_i \;=\; c_i \sum_j \mathbf{G}_{ij}\,(c_j \tilde{w}_j) \;=\; c_i \sum_j \mathbf{G}_{ij}\, w_j^* \;=\; c_i\,(\mathbf{G}\mathbf{w}^*)_i \;=\; \frac{c_i}{w_i^*} \;=\; \frac{1}{\tilde{w}_i}.$$

Hence $\tilde{\mathbf{G}}\tilde{\mathbf{w}} = \tilde{\mathbf{w}}^{-1}$, and by Step 1's uniqueness $\tilde{\mathbf{w}}$ is the rescaled FairGrad output.

(3b) Combined-update preservation. Direct substitution gives

$$\sum_i \tilde{w}_i \tilde{\mathbf{g}}_i \;=\; \sum_i \frac{w_i^*}{c_i}\,(c_i \mathbf{g}_i) \;=\; \sum_i w_i^* \mathbf{g}_i.$$

(In fact, combined-update preservation already pins down $\tilde{\mathbf{w}}$: any $\tilde{\mathbf{w}} \in \mathbb{R}^K_{>0}$ with $\sum_i \tilde{w}_i \tilde{\mathbf{g}}_i = \sum_i w_i^* \mathbf{g}_i$ satisfies $\sum_i (c_i \tilde{w}_i - w_i^*)\mathbf{g}_i = 0$, and linear independence of $\{\mathbf{g}_i\}$ forces $\tilde{w}_i = w_i^*/c_i$.)

Step 4 (necessity of $\alpha = 1$). Fix $0 < \alpha \neq 1$ and suppose, for contradiction, that the FairGrad output is invariant under all positive task-wise rescalings. The combined-update preservation argument in Step 3b uses only linear independence and is independent of α, so by hypothesis the rescaled solution must again be $\tilde{w}_i = w_i^*/c_i$, where now $\mathbf{w}^*$ solves the original α-fairness KKT $(\mathbf{G}\mathbf{w}^*)_i = (w_i^*)^{-1/\alpha}$. The same factoring as in Step 3a then yields

$$(\tilde{\mathbf{G}}\tilde{\mathbf{w}})_i \;=\; c_i\,(\mathbf{G}\mathbf{w}^*)_i \;=\; c_i\,(w_i^*)^{-1/\alpha} \;=\; c_i\,(c_i\,\tilde{w}_i)^{-1/\alpha} \;=\; c_i^{\,1-1/\alpha}\,\tilde{w}_i^{-1/\alpha}.$$

The rescaled α-fairness KKT requires the right-hand side to equal $\tilde{w}_i^{-1/\alpha}$, so $c_i^{\,1-1/\alpha} = 1$ must hold for every $\mathbf{c} \in \mathbb{R}^K_{>0}$, which forces $1 - 1/\alpha = 0$, i.e. $\alpha = 1$. Hence $\alpha = 1$ is the unique exponent in the family for which the FairGrad output is invariant under arbitrary positive task-wise rescalings.

Remark C.2 (Value clipping). PPO value clipping is applied before forming $\mathbf{G}^c$, so clipped-out samples contribute zero to the realized minibatch gradients. We log the clip-hit fraction from this actual PPO value update, not from a counterfactual unclipped objective. This does not affect Theorem 1, which is an algebraic statement about the positive-definite Gram matrix passed to the FG-c solver.

C.5 y-Newton solver derivation and benchmark protocol

This appendix expands Section 4.3 with derivations.

Setup and Newton step derivation. Reparameterize $\mathbf{w} = e^{\mathbf{w}_y}$ (positivity automatic; search variable on $\mathbb{R}^K$). The shipped solver applies Armijo backtracking to the residual norm itself rather than its square. Tier 1 declares convergence when $\|F(\mathbf{w}_y)\| \le \eta = 10^{-2}$. The internal routine also exposes a second tolerance 10^{-8}, but the two stopping tests are joined by a logical OR, so the tighter test is redundant with the production defaults. A tighter diagnostic replay must lower the operative absolute threshold as well. The y-space residual and Jacobian are

$$F(\mathbf{w}_y) = \mathbf{G}^c \exp(\mathbf{w}_y) - \exp(-\mathbf{w}_y/\alpha), \tag{C.3}$$

$$J(\mathbf{w}_y) = \mathbf{G}^c \mathrm{diag}(\exp(\mathbf{w}_y)) + \tfrac{1}{\alpha}\mathrm{diag}(\exp(-\mathbf{w}_y/\alpha)). \tag{C.4}$$

The componentwise derivative

$$\frac{\partial F_i}{\partial w_{y,j}} \;=\; \mathbf{G}^c_{ij}\, \exp(w_{y,j}) \;+\; \frac{1}{\alpha}\, \delta_{ij}\, \exp(-w_{y,i}/\alpha)\,, \tag{C.5}$$

assembles to (C.4); in code, J is built by broadcasting $\exp(\mathbf{w}_y)$ along the columns of $\mathbf{G}^c$ plus a diagonal increment, avoiding explicit `diag` materialization. The full procedure — diagonal warm-start, damped y-Newton with Armijo line search, and the two fallback tiers — is given in Algorithm C.2.

Exact identities versus finite-tolerance solves. For returned positive weights $\widehat{\mathbf{w}}$, define the KKT residual $\boldsymbol{r} = \mathbf{G}^c\widehat{\mathbf{w}} - \widehat{\mathbf{w}}^{-1}$ at $\alpha = 1$. The realized combined gradient satisfies

$$\left\|\sum_i \widehat{w}_i \mathbf{g}^c_i\right\|_2^2 = K + \widehat{\mathbf{w}}^\top \boldsymbol{r}, \qquad \left|\|\widehat{\mathbf{d}}\|_2^2 - K\right| \le \|\widehat{\mathbf{w}}\|_2\, \|\boldsymbol{r}\|_2. \tag{C.6}$$

Thus an absolute residual below 10^{-2} does not itself guarantee a norm close to $\sqrt{K}$ when weights are large, nor does it establish scale invariance of the numerical solver. A task-wise rescaling also rescales the residual coordinates, changing which iterates satisfy an absolute threshold. The exact identities in Theorem 1 concern a positive KKT solution before the global clip and Adam update. Gram-diagonal floors, weight bounds, and fallbacks add further numerical differences; SciPy's success flag is a termination status, not a certificate that the specified KKT tolerance was met. The fixed-minibatch PopArt corollary additionally requires the unclipped squared-loss rescaling identity, or matching raw and normalized clipping thresholds and active branches.

Closed-form warm-start (uniqueness).

Proposition C.1 (Diagonal closed form)**.** *If $\mathbf{G}^c$ is diagonal with strictly positive entries, the unique positive solution of the FG-KKT is $w_i^{diag} = G_{ii}^{-\alpha/(\alpha+1)}$.*

Proof. Diagonal $\mathbf{G}^c$ decouples the KKT into $G_{ii}w_i = w_i^{-1/\alpha}$. Multiply by $w_i^{1/\alpha}$: $G_{ii}\, w_i^{1+1/\alpha} = 1$, so $w_i = G_{ii}^{-\alpha/(\alpha+1)}$. The map $w \mapsto G_{ii}w - w^{-1/\alpha}$ is strictly increasing on $\mathbb{R}_{>0}$ (derivative $G_{ii} + (1/\alpha)w^{-1-1/\alpha} > 0$) — solution unique. □

Why the warm-start matters.

- Proposition C.1 is exact for diagonal positive Grams before numerical floors are applied. For non-diagonal Grams it is an initialization heuristic; strong cross-coupling can prevent fast convergence, as the historical synthetic stress case in Table C.1 illustrates.
- On small-norm rows, the unguarded diagonal solution grows as $G_{ii}^{-\alpha/(\alpha+1)}$. The production initialization instead uses $\max(G_{ii}, 10^{-8})$, so at $\alpha = 1$ it starts no higher than 10^4, followed by the y-cap. It does not initialize arbitrarily small rows at their exact diagonal solution.
- When Newton fails its stopping test, its last finite iterate initializes SciPy. The logs distinguish `used_scipy_fallback` from a final uniform `solver_fallback`. In the archived real-Gram benchmark below, Newton terminates in a median of 2 iterations (maximum 19); this is an empirical early-training result, not a bound on all Grams.

Algorithm C.2 y-space projected damped Newton solver for the FG-KKT $\mathbf{G}^c\mathbf{w} = \mathbf{w}^{-1/\alpha}$, with two fallback tiers. Called once per PPO minibatch (Section B.4).

Require: Critic Gram $\mathbf{G}^c \in \mathbb{R}^{K\times K}_{\succ 0}$ (fp64), exponent $\alpha > 0$, residual target $\eta = 10^{-2}$, soft cap $y_{\max} = 50$, max outer iters $N = 50$, max Armijo backtracks $B = 30$, Armijo $c_1 = 10^{-4}$

Ensure: Positive weights $\mathbf{w}$ and logged residual/fallback status; Tier 1 accepts $\|F(\mathbf{w}_y)\| \le \eta$, while Tier 2 uses SciPy's termination flag

$\mathbf{w}_y \leftarrow -\frac{\alpha}{\alpha+1}\log\max(\mathrm{diag}(\mathbf{G}^c),\, \varepsilon)$ {diagonal warm-start (Proposition C.1); ε guards $\log 0$}
$\mathbf{w}_y \leftarrow \mathrm{clip}(\mathbf{w}_y,\, -y_{\max},\, y_{\max})$ {soft cap}
for $k = 1$ **to** N **do**
  $F \leftarrow \mathbf{G}^c \exp(\mathbf{w}_y) - \exp(-\mathbf{w}_y/\alpha)$ {eq. (C.3)}
  if $\|F\| \le \eta$ **then**
    return $\exp(\mathbf{w}_y)$
  end if
  $J \leftarrow \mathbf{G}^c \cdot \mathrm{diag}(\exp(\mathbf{w}_y)) + \frac{1}{\alpha}\,\mathrm{diag}(\exp(-\mathbf{w}_y/\alpha))$ {eq. (C.4)}
  solve $J\,\mathbf{d} = -F$ in fp64
  $t \leftarrow 1$; *accepted* $\leftarrow$ `false`
  for $j = 1$ **to** B **do**
    $\mathbf{w}_y^{\text{trial}} \leftarrow \min(\mathbf{w}_y + t\,\mathbf{d},\, y_{\max})$
    $F^{\text{trial}} \leftarrow \mathbf{G}^c \exp(\mathbf{w}_y^{\text{trial}}) - \exp(-\mathbf{w}_y^{\text{trial}}/\alpha)$
    if $\|F^{\text{trial}}\| < (1 - c_1 t)\,\|F\|$ **then**
      $\mathbf{w}_y \leftarrow \mathbf{w}_y^{\text{trial}}$; *accepted* $\leftarrow$ `true`; **break out of inner loop**
    end if
    $t \leftarrow t/2$
  end for
  if *not accepted* **then**
    break out of outer loop {Armijo exhausted; pass current $\mathbf{w}_y$ to Tier 2}
  end if
end for
Tier 2: Newton did not reach η → SciPy least-squares warm-started from $\exp(\mathbf{w}_y)$
$\mathbf{w} \leftarrow$ `least_squares`$\big(x \mapsto \mathbf{G}^c x - x^{-1/\alpha},\ x_0{>}\varepsilon \text{ from } \exp(\mathbf{w}_y),\ \text{bounds}{=}(\varepsilon, \infty)\big)$
if `res.success` and $\mathbf{w}$ is finite **then**
  return $\mathbf{w}$
end if
Tier 3: SciPy also failed → uniform fallback, flag failure to online diagnostics
return $\mathbf{1}_K/K$

Newton step in the small-norm regime.

- Row i with $\mathbf{G}^c_{i,:} \to 0$: $F_i \to -\exp(-w_{y,i}/\alpha)$, $J_{ii} \to (1/\alpha)\exp(-w_{y,i}/\alpha)$.
- Newton step: $\Delta w_{y,i} = -F_i/J_{ii} \to \alpha$ — exactly α in the row-deficient limit $\mathbf{G}^c_{i,:} \to 0$.
- Under a full Newton step in this limiting regime, a uniform cold start $w_y = -\log K$ would require approximately $\lceil (y^* + \log K)/\alpha \rceil$ steps to reach a target log-weight y^*. Backtracking and coupling can alter this count, and an absolute residual test can stop much earlier while the small-norm task's contribution remains inaccurate. This is why residual termination and exact task balancing must be distinguished.

fp64 throughout.

- Gram computation, residual, line search, final per-task contribution sum: all fp64.
- Squaring very small fp32 gradients can enter the subnormal range or underflow (a 10^{-22} component has square 10^{-44}, below the smallest normal fp32 value). Forming the Gram in fp64 preserves a wider exponent range.
- The Newton branch caps w_y at 50, giving $w \le e^{50} \approx 5 \times 10^{21}$ on that branch. SciPy's fallback is not subject to this upper cap.

- The weighted contribution sum is accumulated in fp64 to reduce underflow, overflow, and cancellation risk, then cast back to the training dtype. This improves numerical robustness without restoring an exact KKT guarantee.

Real-Gram benchmark. The release includes `solverbench_rfv1.csv`, containing 1,984 solves on real MT50 V1 Gram matrices from seed 0 of default-actor FG-c ($\alpha = 1$) with PopArt and LN-c. The capture covers the first 2M training steps (4 collects $\times 16$ repeats $\times 31$ minibatches), with evaluation disabled, on one RTX 3090 and 16 CPU cores. Each production Gram was also solved by a SciPy `least_squares` reference initialized at $1/K$, with positive lower bound 10^{-12}; its solution was discarded. Both timings exclude Gram formation. Recomputing the archived CSV gives median solve times of 0.397 ms for Newton and 32.520 ms for SciPy, a median per-solve speedup of $82.97\times$ and an aggregate-time ratio of $87.07\times$. All 1,984 Newton rows record convergence and all SciPy rows record success. These are recorded solver statuses. The CSV does not include Newton residuals or the Gram matrices, so it does not independently certify each KKT solution or support arbitrary solver replay. The capture covers early training on one host; it is not a full-training or end-to-end speedup. Production telemetry additionally includes fp64 Gram formation; broader wall-clock measurements are in Section E.4.

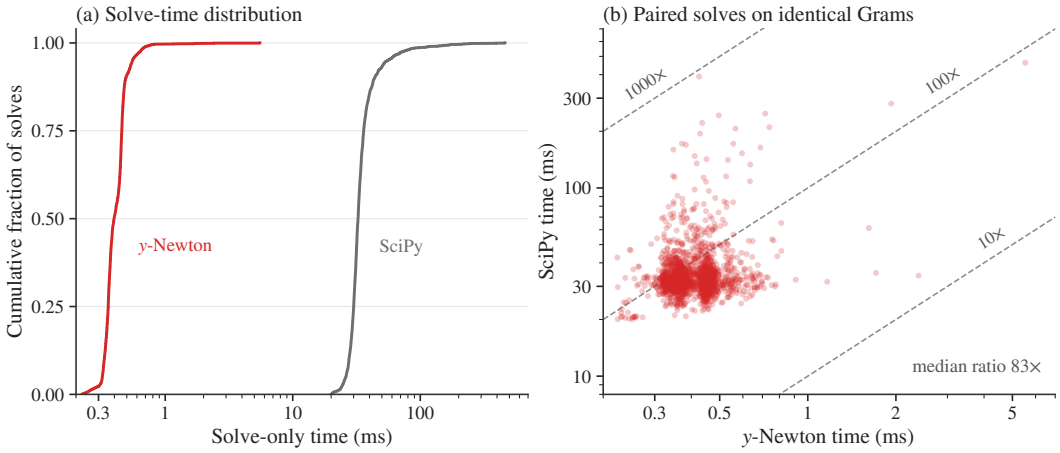


Figure C.1: Solve-only timing on 1,984 real $K = 50$, $\alpha = 1$ Gram matrices from the first 2M MT50 V1 steps of one seed. (a) Empirical cumulative distributions of solve time for y-Newton (red) and the SciPy `least_squares` reference (gray). (b) Paired times, one dot per matrix; dashed lines mark $10\times$, $100\times$, and $1000\times$ ratios, and the median paired ratio is $83\times$. Timings exclude Gram formation, gradient extraction, recombination, and environment interaction, so they do not measure end-to-end training speedup.

Real MT10 Grams with the SGD solver. Because the MT50 capture keeps no Gram matrices, the residual comparison in Figure C.2 uses archived MT10 gradient snapshots instead. Four MT10 runs (default actor or FG-c, each with PopArt, with or without LN-c) stored the full per-task critic gradients of one minibatch every five collects, from collect 5 to collect 80 or 95; this gives 67 critic Grams (K=10, formed in fp64), with a median per-task norm spread of $276\times$ (maximum 3.0×10^4). On each Gram we ran the FairGrad-paper SciPy reference, the FairGrad-RL SGD solver (learning rate 0.1, momentum 0.5, 20 iterations), and the production y-Newton solver, and report the median of 5 timed solves and the absolute KKT residual $\|\mathbf{G}^c\mathbf{w} - \mathbf{w}^{-1}\|_2$. SGD misses the target $\eta = 10^{-2}$ on all 67 Grams (residual ≈ 2.6), while SciPy and Newton reach it on all 67; Newton's median solve time is 0.024 ms versus 2.08 ms for SciPy (median paired ratio $126\times$). These solves were timed offline on one CPU host, separately from the production timings above, so absolute times in Figure C.2 should not be compared with Figures C.1 and 5.

Historical synthetic benchmark protocol. The selected-scenario benchmark in Table C.1 serves as a numerical stress comparison. Its timing ratios describe those selected host-specific measurements and are not a general range for production speedup.

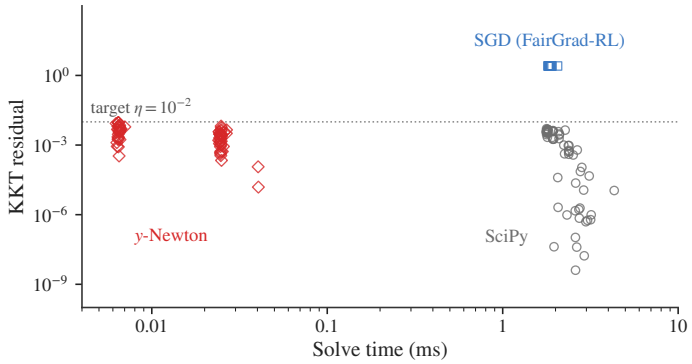


Figure C.2: Solve time and absolute KKT residual of the FairGrad-paper SciPy reference, the FairGrad-RL SGD solver, and production y-Newton on 67 real MT10 critic Gram matrices (K=10, α=1), one marker per Gram and solver. The dotted line marks the target $\eta = 10^{-2}$; SGD misses it on every Gram.

- Synthetic Gaussian per-task gradients $\mathbf{g}_i \in \mathbb{R}^D$ with $D = 1024$ and $\alpha = 1$ (matching the critic-side default of Section 4); Gram $\mathbf{G}^c = [\mathbf{g}_i^\top \mathbf{g}_j]_{ij}$ assembled in fp64.
- Five synthetic regimes spanning the (per-task norm spread, off-diagonal structure) plane: well-conditioned K=50 at spread 1×; heterogeneous K=10 with random-direction small-norm rows at $10^6\times$ spread; and three high-spread K=50 regimes at $10^8\times$ spread distinguished by structure: random Gaussian, orthogonal-to-active single small-norm row, and orthogonal-to-active 25% small-norm rows. The orthogonal cases are constructed proxies, not captured training Grams.
- Four solvers per regime: SciPy `least_squares` (verbatim FairGrad-paper reference, `bounds=(0,`∞`)`, no $\max(x, \varepsilon)$ clip), SGD+momentum (verbatim FairGrad-RL release, `lr=0.1`, `momentum=0.5`, `niter=20`, track-best), y-Newton with uniform cold start, and y-Newton with the diagonal warm-start of Proposition C.1 (our production solver).
- Each (solver × regime) cell timed 7× with warm timing (first run discarded); we report the median.
- Speedup is the ratio of SciPy to Newton-warm median wall times; the table separately discloses residuals, including the warm-start stress case that misses the target. A timing ratio alone does not establish equal solution accuracy.
- The release also archives a broader 85-row synthetic sweep with speedups from 9.2× to 6,914× and median 74.4×. This host-dependent spread should not be collapsed into the selected table's narrower range. We use the real-Gram benchmark above for the primary practical solver-cost estimate.
- The release includes the table's generator, `selected_regimes_a1.py`. A single-threaded rerun on a different host reproduces the SGD and y-Newton residuals to the printed digits, except row 2's cold start ($2.6{\cdot}10^{-9}$ vs. $2.7{\cdot}10^{-9}$); the timings differ, as do SciPy's residuals in several rows, although every SciPy residual remains below the 10^{-2} target.

Table C.1: **Historical selected synthetic FairGrad benchmarks** ($\alpha = 1$)**.** Median solve time and absolute KKT residual for five synthetic Gram regimes. These are host- and regime-specific measurements, not a bound on speedup or measurements of training Grams. The target is $\eta = 10^{-2}$; $^\times$ denotes that the upstream fixed-budget SGD solver does not reach it. Row 3's warm Newton solve also misses the target, so its speedup does not compare equally converged solutions. The recorded MT50-Gram benchmark in Section C.5 provides the primary practical timing evidence.

	Wall time per solve (ms)				KKT residual at termination				
Regime	scipy (FG paper)	SGD (FG-RL)	y-N (cold)	y-N (warm)	scipy (FG paper)	SGD (FG-RL)	y-N (cold)	y-N (warm)	Speedup
K=50, spread 1×	14.5	10.6$^\times$	0.43	0.30	$1.8{\cdot}10^{-13}$	$5.0{\cdot}10^{1}$	$3.4{\cdot}10^{-7}$	$2.4{\cdot}10^{-5}$	48×
K=10, rand, spread 10^6	195	9.0$^\times$	0.64	0.14	$7.7{\cdot}10^{-10}$	$5.2{\cdot}10^{6}$	$2.7{\cdot}10^{-9}$	$4.8{\cdot}10^{-5}$	**1,442×**
K=50, rand, spread 10^8 (stress test)	733	10.1$^\times$	0.84	7.7	$5.6{\cdot}10^{-7}$	$5.6{\cdot}10^{1}$	$6.2{\cdot}10^{-3}$	$2.0{\cdot}10^{-2}$ (rand stall)	95× (rand-stall)
K=50, ⊥, spread 10^8 (orthogonal synthetic)	288	10.2$^\times$	0.84	0.22	$9.3{\cdot}10^{-11}$	$5.6{\cdot}10^{1}$	$6.2{\cdot}10^{-3}$	$3.2{\cdot}10^{-5}$	**1,344×**
K=50, ⊥ 25%, spread 10^8	27.4	10.2$^\times$	0.93	0.21	$5.3{\cdot}10^{-3}$	$7.8{\cdot}10^{1}$	$7.9{\cdot}10^{-3}$	$\mathbf{4.7{\cdot}10^{-5}}$	131×

D Additional Experimental Results

D.1 Detailed ablation results

This appendix expands the main-text ablation summary (Section 5.3) with the underlying tables and per-cell analysis.

Critic-side intervention cube (V2). Table D.1 reports the 2×2 PopArt×FG-c sub-cube of the intervention cube (LN-c on, actor=default); the cumulative ladder and per-axis mechanism mapping are in Table 2 and Figure 6 and Section 5.3. Two scope caveats matter for reading the table: the observed PopArt-marginal collapse signature is at training-outcome scale, not a direct verification of the per-minibatch identity, and the table does not show that every non-aggregation channel of PopArt has zero effect. The synthetic per-minibatch verification of Theorem 1 is in Figure D.9 (Section D.3); the training-time analog at the aggregator-output level is the (c)≡(d) coincidence in Figure D.7. The complementary regime, in which PopArt's marginal remains large with FG-c on, is the V1 sweep below.

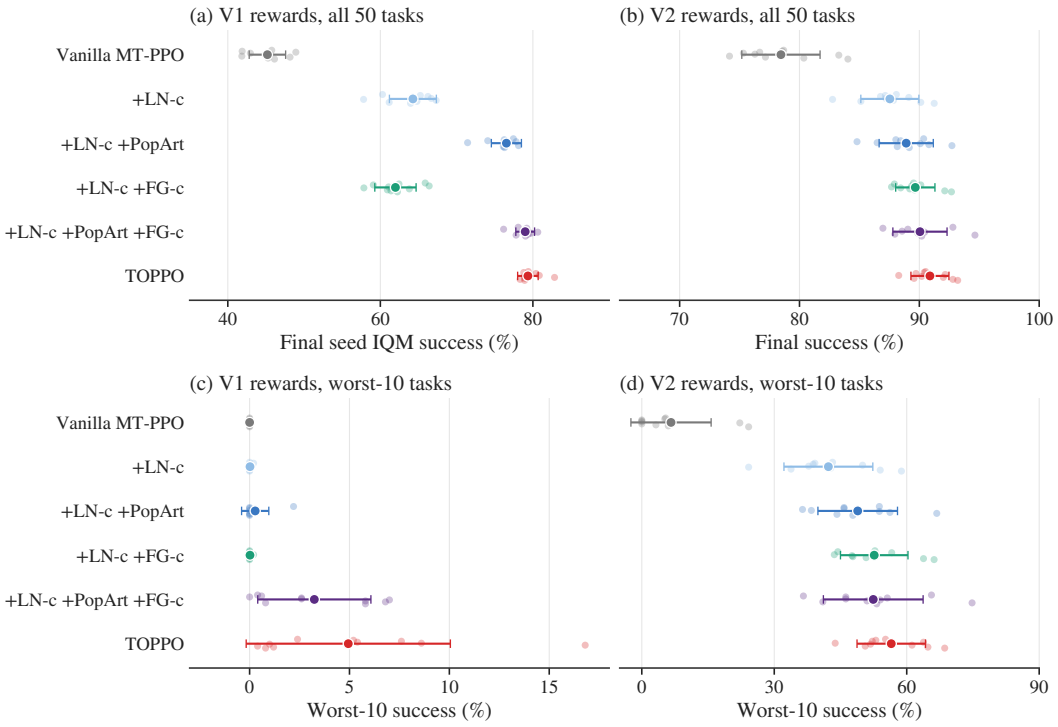


Figure D.1: Reward-regime dependence of the six intervention configurations, ten seeds at 100M transitions. (a) V1 seed IQM and (b) V2 seed mean of final success over 50 tasks; (c, d) seed mean of each seed's worst-10 success. Large markers are these centers, whiskers the untrimmed sample std, and pale points the ten seeds. Colors match Figure 6; +LN-c +FG-c (teal) is a branch, not a cumulative step. Axis ranges differ between panels.

LayerNorm placement ablation. On MT10 with PopArt held fixed (default actor and critic combiners, 10 seeds), symmetric LN on both actor and critic reaches $93.06 \pm 4.61\%$ final mean vs. $96.76 \pm 1.52\%$ for critic-only LN — a 3.70-point mean drop with $\sim 3\times$ wider seed std. We attribute this tentatively to PPO's clipped policy ratio: LN on actor pre-activations changes the mapping from hidden features to the action-mean projection across minibatch updates, which can inflate $|\log \pi(a|s)/\pi_{\text{old}}(a|s)|$ and trigger the ratio clip more frequently; the critic has no analogous ratio constraint. Given the MT10 result we did not extend symmetric LN to a 10-seed MT50 sweep.

Per-side combiner asymmetry. Table D.2 reports the per-side cube. PCGrad-a's contribution is concentrated on the tail tasks: switching the actor combiner from default to PCGrad on +LN-

Table D.1: **PopArt $\times$ α=1 FG-c interaction on MT50.** The 2×2 sub-cube isolates whether adding FG-c absorbs PopArt's worst-10 marginal at training-outcome scale, the signature predicted by Corollary 1; the deltas below the table are consistent with a collapse from rows 1→2 to rows 3→4. All rows use actor=default with LN-c on; 10 seeds, final checkpoint, 100M env steps.

Configuration	PopArt	FG-c	MT50 mean	MT50 worst-10
+LN-c (base)	–	–	$87.5_{\pm 2.4}$	$42.3_{\pm 10.1}$
+LN-c +PopArt	✓	–	$88.9_{\pm 2.3}$	$48.9_{\pm 9.0}$
+LN-c +FG-c	–	✓	$89.7_{\pm 1.6}$	$52.6_{\pm 7.6}$
+LN-c +PopArt +FG-c	✓	✓	$90.1_{\pm 2.3}$	$52.4_{\pm 11.3}$

Δ_{PopArt} without FG-c (rows 1→2): +1.36 mean and $+\mathbf{6.64}$ worst-10 points.
Δ_{PopArt} with FG-c (rows 3→4): +0.39 mean and $-\mathbf{0.22}$ worst-10 points.

c+PopArt+FG-c lifts MT50 worst-10 tail tasks from $52.42 \rightarrow 56.50$ ($+4.08$ points), on top of the $+0.83$-point final-mean gain and worst-10 seed-std reduction already reported in Section 5.3 and Table 2. We expect the FG-c-only properties of Theorem 1 (exact-KKT combined-gradient norm $\sqrt{K}$ and PopArt absorption via Corollary 1) to matter more in environments with more extreme per-task return-scale heterogeneity than V2 (McLean et al., 2025 App. E.3), even when the headline V2 FG-c vs. PCGrad-c gap is within seed noise; both combiners select different points in the same shared cone $\text{cone}^+\{\mathbf{g}_i^c\}$ (Theorem C.1, Section C.3).

Table D.2: **Per-side combiner asymmetry on MT50 (10 seeds, 100M steps).** Holding $[400\times3]$ MLP, PopArt, and LN-c fixed, we vary only the per-side gradient combiner; the asymmetric PCGrad-a + FG-c (α=1) row has the highest means, matching the diagnosis that critic gradients suffer scale spread ($497\times$, addressed by scale-invariant FG, Theorem 1) while actor gradients exhibit direction conflict at modest scale spread ($4.1\times$, addressed by PCGrad). FG-c and PCGrad-c are within seed noise (gaps $< \sigma$) and lie in the same shared cone (Theorem C.1); we adopt FG-c for its scale-invariance guarantee.

Actor method	Critic method	MT50 best	MT50 final	MT50 IQM
default	default	$90.7_{\pm 1.8}$	$88.9_{\pm 2.3}$	89.0
default	FG (α=1)	$91.2_{\pm 2.1}$	$90.1_{\pm 2.3}$	89.7
PCGrad	**FG (α=1)**	$\mathbf{92.1}_{\pm 1.7}$	$\mathbf{90.9}_{\pm 1.6}$	**90.8**
FG (α=2)	FG (α=1)	$90.5_{\pm 2.0}$	$89.2_{\pm 2.2}$	89.2
PCGrad	PCGrad	$91.9_{\pm 1.5}$	$90.5_{\pm 1.4}$	90.4
CAGrad	CAGrad	$90.7_{\pm 1.3}$	$89.4_{\pm 1.4}$	89.2

D.2 Diagnostic dump-run provenance

The historical mechanism figures (Figures 2, 3 and D.4 to D.7) are derived from MT10 gradient-snapshot dump runs that are *separate* from the headline 10-seed sweep used for the success-rate tables. Each dump run instruments `MultiTaskPPO` to write per-task flat actor and critic gradients (plus PopArt σ_i, FairGrad weights when on, long-EMA per-task success rate) to disk every 5 collects ($\sim$0.5M env steps, $\sim$27 MB of uncompressed fp32 gradients per snapshot) for offline replay. The figures use four such dumps, one per intervention cell:

- **default mean aggregation + PopArt + no LN** — backs the no-LN columns of Figures 3 and D.4.
- **default mean aggregation + PopArt + LN-c** — backs the LN-c columns of Figures 3 and D.4, all of Figures 2 and D.5 (so the $497\times$ vs. $4.1\times$ critic-vs-actor spread is read off the same minibatches).
- **FG (α=2 actor / α=1 critic) + PopArt + no LN** — backs all four panels of Figure D.7 and the first two columns of Figure D.6.
- **FG (α=2 actor / α=1 critic) + PopArt + LN-c** — supplies the LN-c FG-trained comparison in Figure D.6.

Cols (a, b) of Figure D.7 and the no-PopArt rows of Figure D.4 rescale the dumped PopArt gradients by σ_i^2 at fixed network weights. For unclipped squared loss this reconstructs the corresponding raw-loss gradient. For clipped losses it corresponds to matched raw-unit clipping thresholds, not necessarily the fixed numerical clip width of an independently trained no-PopArt baseline. Thus the

figure labels "vanilla" and "no PopArt" in these reconstructed cells denote counterfactual gradient units, rather than separate untreated training trajectories. The $497\times$ critic spread in Figure 2 uses this same reconstruction; actor gradients come directly from the same snapshots. Figure D.7 cols (c, d) additionally rely on offline tight-tolerance FairGrad replay ($\eta = 10^{-13}$ on the y-space Newton solver, vs. production training $\eta = 10^{-2}$); these offline replays visualize the exact-solution identity. The production absolute tolerance does not imply a relative error bound of $O(10^{-2})$, particularly at small gradient scales (Section C.5).

D.3 Mechanism evidence figures

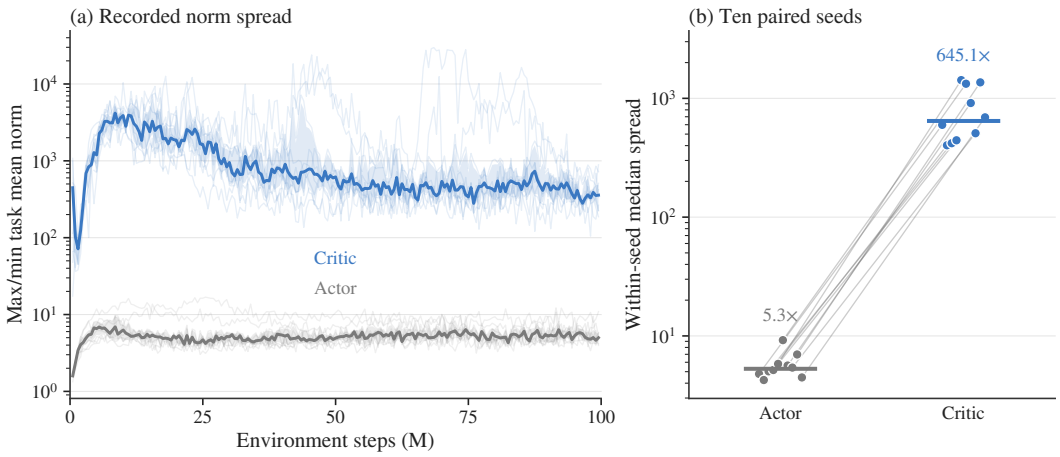


Figure D.2: Recorded task-gradient norm spread (max/min task mean norm) in the ten MT50 V2 TOPPO seeds. (a) Thin lines are individual seeds; the band and thick line are the across-seed interquartile range and median of per-flush ratios. Missing records are not imputed. (b) Each seed's temporal median on the 191 shared logger steps (4.5–99.5M), with a gray line joining its actor and critic values; bars and labels are across-seed medians. PopArt is active; these measurements do not isolate an untreated failure mechanism.

Critic Gram heatmaps, intervention ablation across stages (Figure D.4).

- PopArt (cols a→b, c→d) preserves off-diagonal cosines exactly (closed-form identity from per-task σ^{-2} rescaling) and compresses the diagonal magnitude palette in the early/late stages. The MID-row LN-c pair shows a transient inversion ($525\times \to 1428\times$) attributable to the Welford-accumulated σ_i lagging mid-training return-distribution shifts.
- LN (cols a→c, b→d) reduces mean absolute off-diagonal cosine (early-stage mean off-diag $|\cos|$ from 0.34 no-LN to 0.20 with LN-c on the F3 default-mean dump; the matched FG-trained dump in Figure D.6 reads $0.24 \to 0.10$) while leaving the diagonal magnitude palette roughly intact — a representation-level intervention, not a target-side fix.
- Per-task gradient-norm spread $\max_i \|\mathbf{g}_i^c\| / \min_i \|\mathbf{g}_i^c\|$ (vanilla, σ^2-inverted) up to $\sim 10{,}000\times$ at early training, decaying to $\sim 200\times$ by mid-training and rebounding to $\sim 700\times$ by late training under noLN — still orders of magnitude worse than the actor's 2.7–$4.6\times$ across the same training stages (Figure D.5).

LN $\times$ FG: algebraically orthogonal critic-Gram health metrics (Figure D.6). Each mechanism targets one health metric and leaves the other un-redressed — LN-c modifies $\mathbf{G}^c$ but does not systematically reduce top-1 weighted contribution mass (which drifts $0.45 \to 0.57$ on this matched-seed pair, within cross-snapshot variability), while FG-c modifies only $\mathbf{w}$ and so cannot change cosine structure within a fixed snapshot. The two operations therefore affect different diagnostic quantities; these observations do not establish that both are necessary for a given success rate.

FairGrad (α=1) equalizes per-task contribution; offline replay illustration of Corollary 1 (Figure D.7). The (c)≡(d) coincidence is an offline replay illustration of Corollary 1, complementary

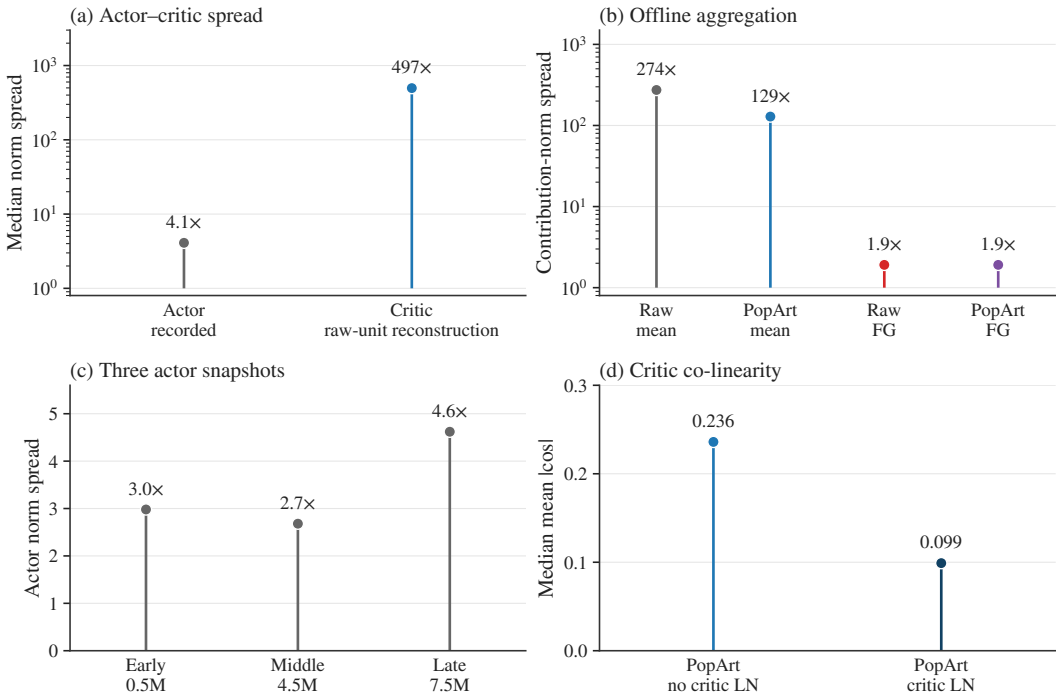


Figure D.3: Redrawn MT10 scalar diagnostics from the preserved numerical summaries, one lollipop per archived value, colored as in the source figures. (a) Median actor and critic task-norm spread. (b) Median contribution-norm spread for raw or PopArt gradients under mean or FairGrad (FG) aggregation. (c) Actor norm spread at three snapshots. (d) Median mean absolute critic cosine without and with critic LN. Raw-unit values reconstruct loss units within PopArt-trained runs; FG denotes offline tight-KKT replay. The panels summarize different recorded diagnostics, not a single common experiment, and carry no uncertainty estimate. Absolute cosine measures co-linearity rather than negative-conflict frequency. The archived heatmaps and traces follow for context.

to the synthetic per-minibatch verification of Theorem 1 in Figure D.9; offline tight-tolerance replay methodology in Section D.2.

Synthetic verification and finite-tolerance behavior (Figure D.9). We independently solve the KKT system after each positive rescaling of a fixed set of ten linearly independent synthetic vectors. The tight solver uses normalized coordinates $z_i = \|\mathbf{g}_i\| w_i$, with residuals checked in the original KKT equations. At $\alpha = 1$, the observed aggregate-vector difference is at floating-point scale; this is numerical agreement, not a bitwise-identity claim. A separate sweep through the released production solver shows how an absolute stopping tolerance can break scale invariance for small gradients.

Recorded production aggregate norms. The ten MT50 headline runs log the realized critic aggregate before global clipping. The median absolute relative deviation of the logged mean norm from $\sqrt{50}$ is 1.15%, while logged minibatch extrema span 5.29–12.00 (Figure D.10). These measurements distinguish exact KKT properties from the numerical updates actually used for the reported results.

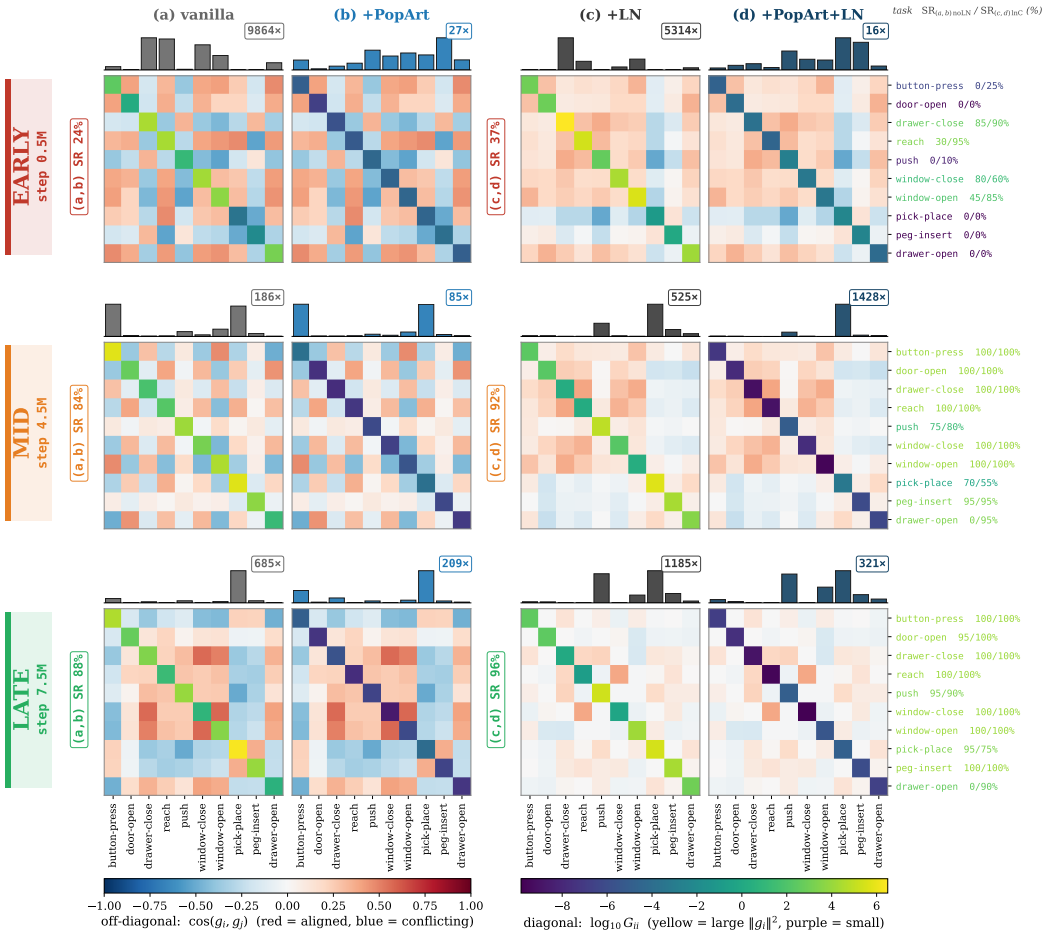


Figure D.4: **Critic Gram heatmap matrix: 3 stages (rows: early/mid/late) × 4 intervention conditions (cols: raw-unit reconstruction, +PopArt, +LN, +PopArt+LN).** Top sidebar = per-task mean-aggregator contribution $\|\mathbf{g}_i\|/K = \sqrt{\mathbf{G}_{ii}}/K$, in-bar badge = per-cell spread $\max_i \|\mathbf{g}_i\| / \min_i \|\mathbf{g}_i\|$; main grid off-diagonal = cosines $\mathbf{G}_{ij}/\sqrt{\mathbf{G}_{ii}\mathbf{G}_{jj}}$; diagonal color = $\log_{10} \mathbf{G}_{ii}$. PopArt (a→b, c→d) preserves cosines exactly and compresses the diagonal magnitude palette in early/late stages, with a transient mid-row spread inversion under LN-c ($525\times \rightarrow 1428\times$) tracked to Welford-lagged σ_i. LN (a→c, b→d) reduces absolute cosine similarity in the recorded representations while leaving the diagonal palette roughly intact. Archived MT10 artwork; the source snapshots are unavailable.

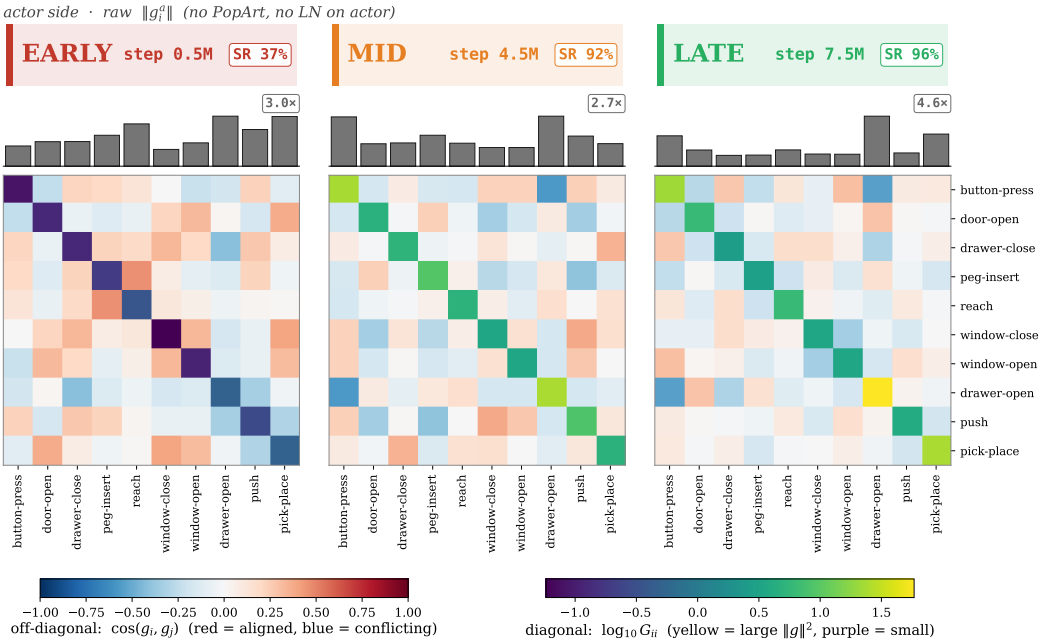


Figure D.5: **Actor Gram heatmaps at 3 training stages (EARLY 0.5M / MID 4.5M / LATE 7.5M steps; raw $\|\mathbf{g}_i^a\|$, no PopArt or LN on actor).** Top sidebar shows per-task gradient-norm bars with the in-bar badge giving the spread ratio $\max_i \|\mathbf{g}_i^a\| / \min_i \|\mathbf{g}_i^a\|$ ($3.0\times$, $2.7\times$, $4.6\times$); main grid plots off-diagonal cosines $\mathbf{G}_{ij}/\sqrt{\mathbf{G}_{ii}\mathbf{G}_{jj}}$ (red aligned, blue conflicting) with the diagonal colored by $\log_{10} \mathbf{G}_{ii}$ (yellow large, purple small). The mild 2.7–$4.6\times$ actor diagonal spread contrasts sharply with the raw-loss-unit critic reconstruction's $9864\times$ (no LN) and $5314\times$ (LN-c) early spreads in Figure D.4, while off-diagonals shift from early inter-task conflict to late near-orthogonal alignment. Archived MT10 artwork; the source snapshots are unavailable.

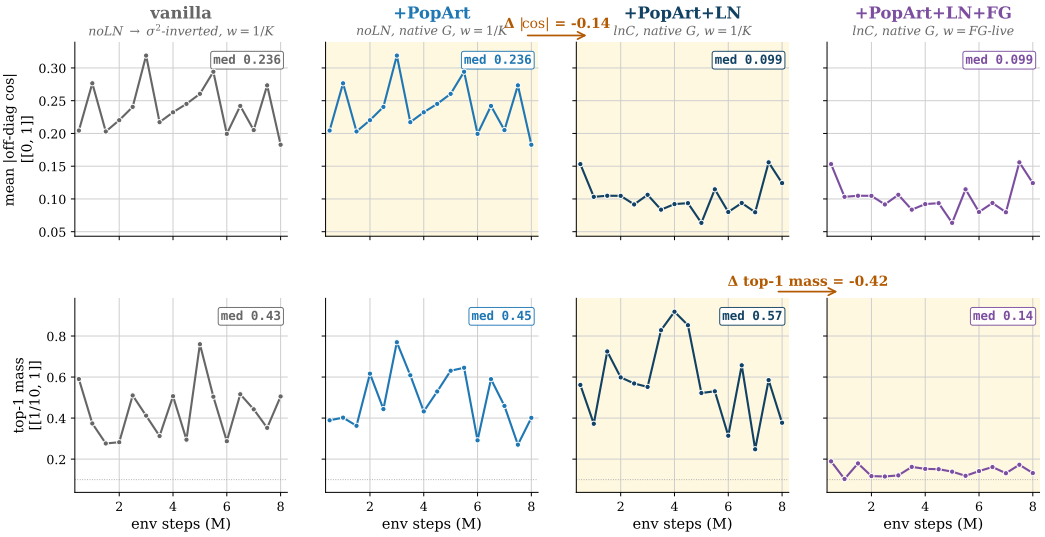


Figure D.6: **LN and FG act on algebraically orthogonal critic-Gram health metrics.** Top row: mean off-diagonal $|\cos|$; bottom row: top-1 weighted contribution mass. LN (col 2→3) cuts off-diag $|\cos|$ from 0.24 to 0.10 without reducing top-1 mass; FG (col 3→4) cuts top-1 mass from 0.57 to 0.14 while leaving cosine structure unchanged (FG modifies only $\mathbf{w}$, not $\mathbf{G}$). Archived MT10 artwork; the source snapshots are unavailable.

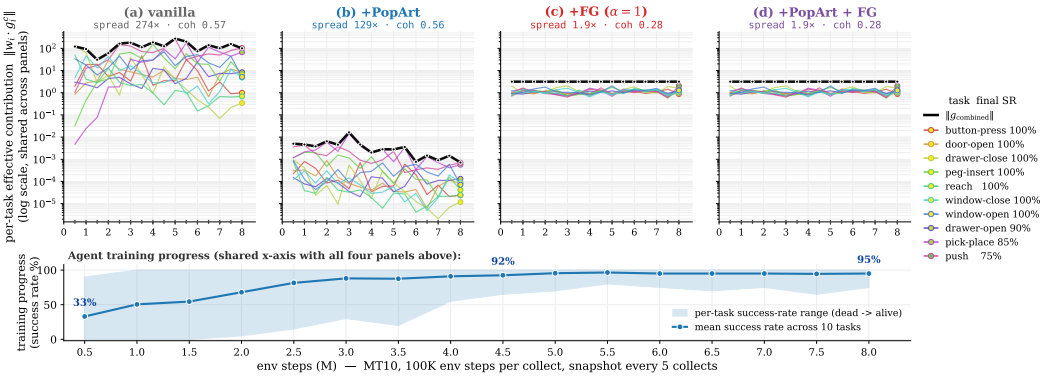


Figure D.7: **FairGrad** (α=1) **equalizes per-task contribution; PopArt's task-wise rescaling effect is absorbed at the aggregator (Corollary 1).** Per-task effective contribution $\|w_i \mathbf{g}_i^c\|$ across training, with spreads (a) raw-loss-unit reconstruction $\sim$ 274×, (b) +PopArt $\sim$ 129×, (c) +FG (α=1) on raw gradients $\sim$ 1.9×, and (d) +FG (α=1) on PopArt-rescaled gradients $\sim$ 1.9×. The (c)≡(d) coincidence illustrates the per-minibatch corollary of Theorem 1. Archived MT10 artwork; the source snapshots are unavailable.

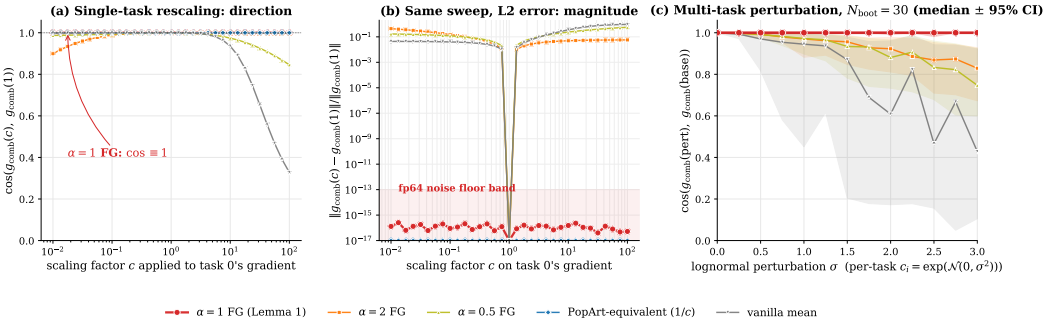


Figure D.8: Archived MT10 snapshot rescaling diagnostic; the source snapshot is unavailable. The panels show single-task direction, relative vector change, and repeated multi-task perturbations. The bands labeled "95% CI" in the artwork are perturbation percentiles, not confidence intervals for a training effect. The independently reproducible synthetic controls follow in Figure D.9.

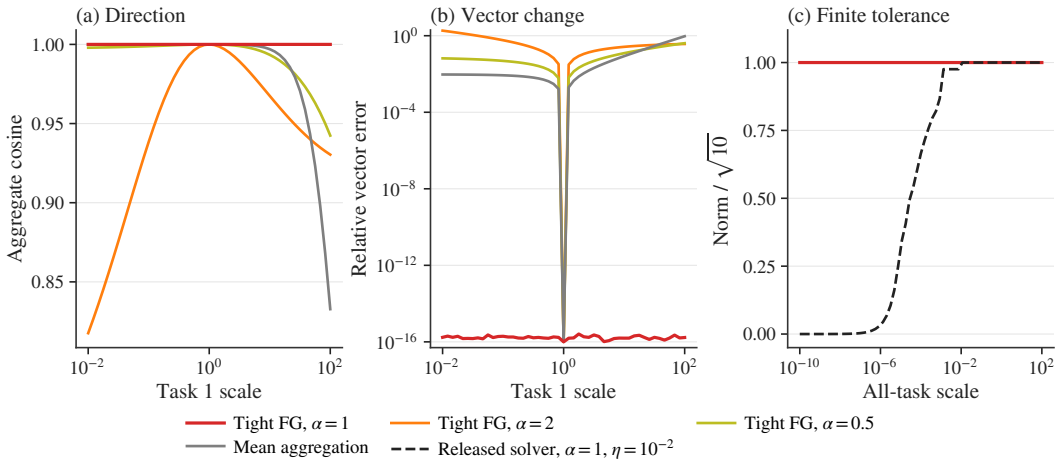


Figure D.9: Synthetic verification with $K = 10$ independent vectors in $\mathbb{R}^{32}$. (a,b) Positive rescaling of one task, with a fresh tight KKT solve in normalized coordinates for each perturbation: cosine to the unperturbed aggregate and relative vector change for tight FairGrad ($\alpha = 1, 2, 0.5$) and mean aggregation. The $\alpha = 1$ aggregate agrees to floating-point precision; errors below 10^{-16} are displayed at that floor. (c) Global rescaling of all tasks: aggregate norm divided by the exact reference $\sqrt{10}$ for the tight $\alpha = 1$ solve (solid) and the released solver at absolute tolerance $\eta = 10^{-2}$ with its numerical guards (dashed), which can depart from the reference. Colors for α follow Figure D.8. These are synthetic controls, separate from the training snapshots.

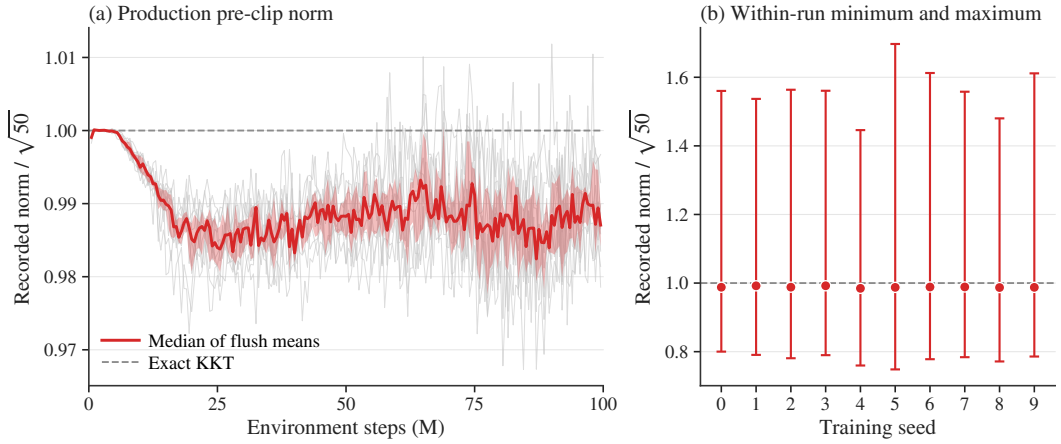


Figure D.10: Production critic aggregate norms in the ten MT50 V2 TOPPO seeds before global gradient clipping, divided by the exact-KKT norm $\sqrt{50}$ (dashed line at 1). (a) Per-flush mean norms: thin lines are seeds; the band and thick line are the across-seed interquartile range and median. (b) Per seed, bars span the recorded minibatch minimum and maximum over the run, and dots mark the median flush mean; the bars are extrema, not uncertainty intervals. Missing logger records are not imputed.

D.4 Headline V2 learning curves

Figure D.11 shows unsmoothed learning curves for the six intervention configurations, using complete recorded evaluation histories. Each curve uses only checkpoints recorded for all ten seeds in that group, without an imputed origin or held endpoints; the one exception is the MT50 V2 TOPPO curve before 6M, described next. The observed mean-curve peak is $97.92 \pm 2.23\%$ at 7.2M on MT10 and $91.26 \pm 1.63\%$ at 96M on MT50; these are distinct from per-seed best checkpoints. For TOPPO MT50 V2, the common recorded grid begins at 6M because two seeds lack earlier evaluations (one has none before 6M, the other only at 0M); the plotted points at 0, 2, and 4M average the nine, eight, and eight seeds logged there, and all crossings below use the ten-seed grid. On MT50, first observed crossings of the ARS final means occur at 12M (ARS), 18M (ARS-LN-400), 24M (ARS-LoRA), and 28M (ARS-LN-1024), and of the published MOORE final mean at 12M. Linear interpolation between checkpoints gives 11.7M, 16.6M, 22.1M, 27.7M, and 10.7M, respectively, the basis of the approximate times quoted in Section 5.2.

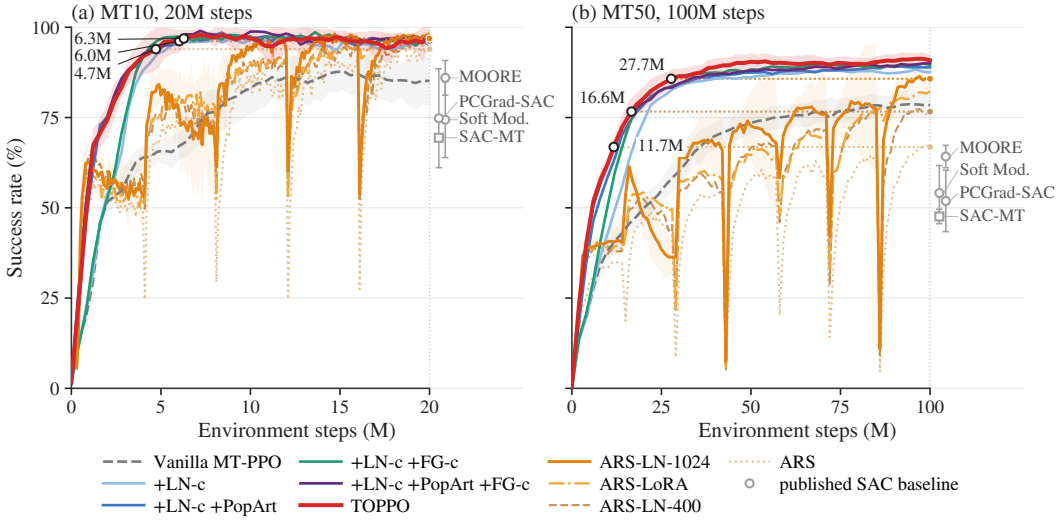


Figure D.11: MT10 (a) and MT50 (b) V2 learning curves of the six intervention configurations and the four ARS variants. Lines show ten-seed means on common recorded checkpoints, except that two MT50 TOPPO seeds lack some evaluation logs before 6M, so MT50 TOPPO points there average the seeds logged (nine at 0M, eight at 2M and 4M); bands show sample std for TOPPO, vanilla, and ARS-LN-1024. Hollow gray right-margin markers show published SAC-baseline final means $\pm$ std without training curves [Cho et al., 2025]. Open circles mark where TOPPO first reaches a comparator's final mean (ARS, ARS-LN-400, and ARS-LN-1024; on MT10, TOPPO's mean never reaches ARS-LoRA), interpolated between recorded checkpoints; dotted lines lead to that mean. TOPPO has 685K (MT10) and 717K (MT50) parameters (vanilla 684K/716K); ARS and ARS-LN-400 have 2.5M (MT10) and 2.6M (MT50), ARS-LoRA 3.9M and 16.1M, and ARS-LN-1024 16.1M and 16.3M. Final PPO results are in Table 2.

D.5 V1 reward sensitivity

Meta-World V1 rewards have substantially wider per-task scale heterogeneity than V2 [McLean et al., 2025]. We reran the same intervention rungs and the PCGrad-a headline on MT50 V1 (ten seeds each, 100M steps). The upper panel of Table D.3 reports final-checkpoint IQM $\pm$ untrimmed sample std alongside V2; the lower panel transcribes the Meta-World+ SAC-family results. The change in module marginals across reward versions is an empirical observation, rather than a quantitative prediction of Corollary 1.

PopArt's IQM marginal is larger on V1 both with and without FG-c (Table D.3). Within the V1 ladder, FG-c's marginal over LN-c+PopArt is 2.47 points, whereas adding FG-c without PopArt reduces IQM by 2.29 points. These comparisons do not identify which of value clipping, changing targets and statistics, optimizer history, or finite solver accuracy explains the difference. In particular,

Table D.3: **V1/V2 reward sensitivity on MT50.** Our rows use ten seeds, 100M transitions, and final-checkpoint IQM (25% integer trimming of seed means, retaining six of ten) with untrimmed sample std. The lower panel transcribes the published Meta-World+ results [McLean et al., 2025]. PopArt's IQM marginal over LN-c+FG-c is 17.01 points on V1 versus 0.32 on V2. This observed regime dependence does not establish which non-rescaling channel accounts for the change; the exact aggregation identity has the scope stated in Corollary 1.

Configuration	V1 IQM	V2 IQM	V1 → V2 gap
Our intervention cube (10 seeds, IQM ± std)			
Vanilla MT-PPO	45.2 ± 2.4	78.0 ± 3.3	+32.76
+LN-c	64.3 ± 3.1	87.7 ± 2.4	+23.43
+LN-c +PopArt	76.5 ± 2.0	89.0 ± 2.3	+12.51
+LN-c +FG-c	62.0 ± 2.7	89.4 ± 1.6	+27.39
+LN-c +PopArt +FG-c	79.0 ± 1.2	89.7 ± 2.3	+10.70
TOPPO	**79.3** ± 1.3	**90.8** ± 1.6	**+11.49**
Meta-World+ MT50 SAC-family baselines (10 seeds, IQM ± std) [McLean et al., 2025]			
MT-MH-SAC	31.9 ± 2.7	54.9 ± 1.1	+22.98
Soft Modularization	60.6 ± 3.9	65.8 ± 1.9	+5.19
MOORE	61.8 ± 2.7	72.0 ± 2.9	+10.22
PaCo	18.6 ±15.4	58.9 ± 4.6	+40.30
PCGrad-SAC	45.8 ± 5.9	69.5 ± 2.7	+23.65

Δ_{PopArt} IQM on V1: $+\mathbf{12.26}$ points without FG-c (rows 2→3) and $+\mathbf{17.01}$ points with FG-c (rows 4→5). On V2 the same two IQM deltas are $+1.35$ and $+0.32$ points, respectively.

large FairGrad weights on small gradients do not by themselves imply an unbalanced exact aggregate, because Theorem 1 compensates positive task-wise scaling. The clipping controls and alternative-normalizer experiments in Section E.2 directly test some of these implementation dependencies.

V1→V2 gap: narrower for our PopArt-equipped rows than for three of the five SAC baselines. Under matched final-checkpoint IQM (Table D.3), every row with PopArt on has a V1→V2 gain in a 10–13-point band (12.51 for +LN-c+PopArt, 10.70 for +LN-c+PopArt+FG-c, 11.49 for the headline). The Meta-World+ SAC-family baselines span 5.19 (Soft Modularization) to 40.30 points (PaCo) under the same V1→V2 reward switch, with three of the five methods gaining at least 20 points (MT-MH-SAC 22.98, PaCo 40.30, PCGrad-SAC 23.65). This narrower gap is associated with PopArt in the reported ladder: our *no*-PopArt rows (vanilla 32.76, +LN-c 23.43, +LN-c+FG-c 27.39 points) sit in a 23–33-point range, inside the 23–40-point range of the three SAC-family baselines that gain at least 20 points. Figure D.12 shows the corresponding V1 learning curves on the same axes for each intervention rung.

V1 worst-k tail tasks. The mean/IQM sensitivity above hides how much of V1 remains concentrated in the tail, so Table D.4 reports the same bottom-k diagnostic used for the V2 headline.

Table D.4 is the V1 sibling of Table 2; row-by-row reading is in the table. Three appendix-only points: (i) FG-c without PopArt is worst-k-indistinguishable from LN-c at every k, the worst-k analog of the FG-c-needs-PopArt-on-V1 finding from the mean column. (ii) The dead-task floor on V1 is thicker than V2 (V1 headline k=10 is 4.9 ± 5.1 vs. V2 56.5 ± 7.8), showing that these interventions leave substantial unresolved tail-task failure on V1. (iii) k=5 is uniformly 0 ± 0 across all six rows (every V1 seed has ≥ 5 tasks at zero), which is reported as a degenerate column and not bolded.

The V1 per-task table (Table D.7) and per-task learning curves (Figure D.15) are reported alongside the V2 per-task in Section D.6; they expose the FG-c-without-PopArt regression and the thicker V1 dead-task floor row-by-row.

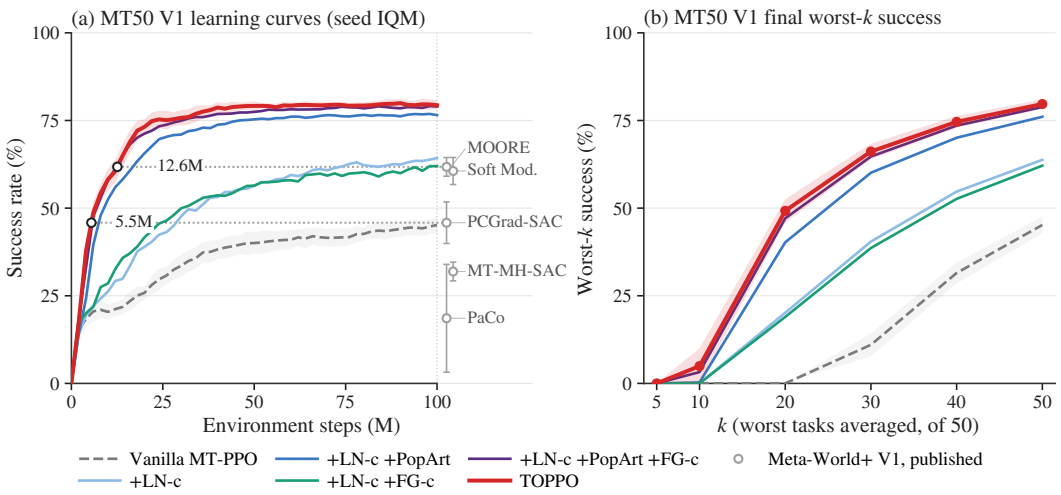


Figure D.12: MT50 V1 results for the six intervention configurations, ten seeds each. (a) Seed IQM learning curves on common recorded checkpoints, with untrimmed sample-standard-deviation bands for TOPPO and vanilla. Hollow gray right-margin markers show published Meta-World+ V1 IQM values with their reported uncertainty [McLean et al., 2025]. Open circles mark where TOPPO first reaches the published PCGrad-SAC and MOORE values, interpolated between recorded checkpoints; Table 3 reports first recorded crossings. (b) Final worst-k success, computed within each seed and averaged across seeds, with sample-standard-deviation bands for TOPPO and vanilla.

Table D.4: **Worst-k tail-tasks success rate on Meta-World MT50 under V1 rewards.** V1 sibling of the V2 worst-k panel in Table 2: per-seed worst-k average for $k \in \{5, 10, 20, 30, 40, 50\}$, then mean $\pm$ std across 10 seeds at the $[400\times3]$ MLP backbone, final-checkpoint, across the six intervention-stack rungs from Vanilla MT-PPO to TOPPO. PopArt is the dominant tail step on V1 and FG-c lifts the tail only once PopArt is on; TOPPO is best at every $k \geq 10$. **Bold** = column maximum; k=5 is degenerate (0 ± 0 across all rows) and unbolded.

	Average Worst-k Success Rate (%)					
Algorithm	k=5	k=10	k=20	k=30	k=40	k=50
Vanilla MT-PPO	0.0 ± 0.0	0.0 ± 0.0	0.0 ± 0.0	11.0 ± 3.3	31.5 ± 3.0	45.2 ± 2.4
+LN-c	0.0 ± 0.0	0.0 ± 0.1	20.2 ± 5.0	40.5 ± 4.7	54.7 ± 3.8	63.8 ± 3.1
+LN-c +PopArt	0.0 ± 0.0	0.3 ± 0.7	40.2 ± 5.0	60.1 ± 3.3	70.1 ± 2.5	76.1 ± 2.0
+LN-c +FG-c	0.0 ± 0.0	0.0 ± 0.1	19.0 ± 4.3	38.6 ± 4.0	52.6 ± 3.4	62.1 ± 2.7
+LN-c +PopArt +FG-c	0.0 ± 0.0	3.2 ± 2.8	47.1 ± 3.1	64.7 ± 2.1	73.5 ± 1.5	78.8 ± 1.2
TOPPO	0.0 ± 0.0	**4.9** ± 5.1	**49.2** ± 3.4	**66.1** ± 2.2	**74.6** ± 1.7	**79.7** ± 1.3

D.6 Per-task success rates

This appendix reports final-checkpoint per-task success (10 seeds, mean $\pm$ std) and the matching per-task learning curves for the three reported regimes: MT10 V2 (Table D.5 and Figure D.13), MT50 V2 (Table D.6 and Figure D.14), and MT50 V1 (Table D.7 and Figure D.15). All tables are sorted worst-first by the TOPPO column; the six columns compare the same intervention configurations used throughout the paper (Vanilla MT-PPO, +LN-c, +LN-c+PopArt, +LN-c+FG-c, +LN-c+PopArt+FG-c, TOPPO). Column definitions and bimodal-row ($\sigma > \mu$) reading guidance are in each table caption. The companion learning-curve figures share the same seeds and intervention ladder, so the trajectory leading to each table cell can be read directly — which tasks the Vanilla baseline never lifts off zero, at what step the LN-c rung begins to make hard tasks tractable, and where TOPPO's PopArt + FG-c + PCGrad-a stack pulls ahead.

MT50 V2 (Table D.6 and Figure D.14). Of the 5 hardest tasks under vanilla MT-PPO (assembly 0.0%, disassemble 0.2%, shelf-place 3.2%, stick-pull 8.6%, pick-place-wall 19.6%), 3/5 recover

to $\geq 70\%$ under TOPPO (shelf-place, stick-pull, pick-place-wall); disassemble partially recovers ($0.2 \rightarrow 19.6\%$); only assembly-v3 remains 0% in these experiments. TOPPO regresses on push-back ($30.0 \rightarrow 10.0\%$, bimodal $\sigma > \mu$). MT10 V2 is near ceiling on most tasks under any rung beyond Vanilla MT-PPO (Figure D.13), so rung-to-rung differences are visible only on `pick-place-v3`, `push-v3`, and `peg-insert-side-v3`; MT10 is reported for completeness while MT50 carries the load-bearing per-task evidence.

MT50 V1 (Table D.7 and Figure D.15). The same drilldown under V1 rewards exposes two V1 effects discussed in Section D.5. (i) *FG-c without PopArt*: the +LN-c+FG-c column tracks +LN-c rather than +LN-c+PopArt on most mid-difficulty tasks (e.g. `door-unlock`, `lever-pull`, `sweep`), the per-task realization of the -2.29-point V1 IQM regression. (ii) *Thicker dead-task floor*: every rung is pinned at 0% on `hand-insert`, `handle-pull`, `peg-insert-side`, `stick-pull`, `stick-push`, accounting for the k=5 degenerate column of Table D.4. Where PopArt does lift LN-c, the gain is consistent with setting-dependent effects beyond the fixed rescaling covered by Corollary 1.

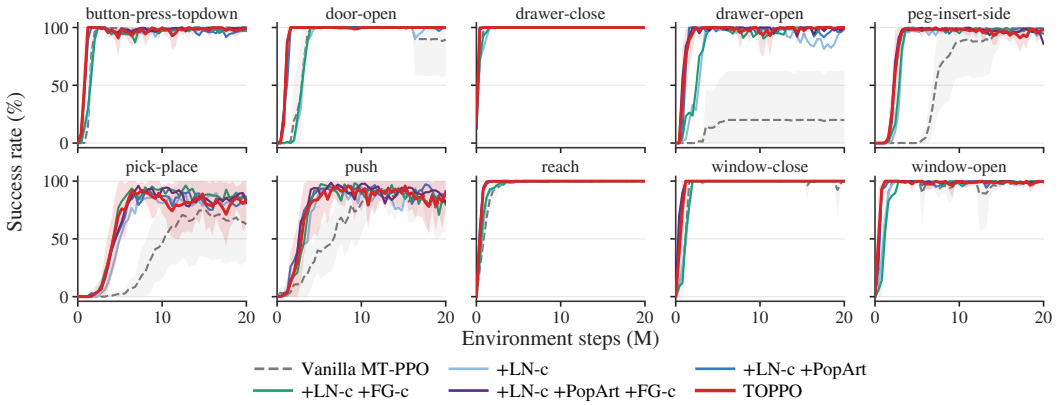


Figure D.13: Per-task MT10 V2 learning curves for the six intervention configurations. Lines are ten-seed means; shaded bands, drawn only for TOPPO and Vanilla MT-PPO, are sample standard deviations. Each configuration uses only evaluation checkpoints recorded for all ten seeds; the trajectories are unsmoothed. Companion to Table D.5.

Table D.5: **Per-task final-checkpoint success on MT10 V2 (10-seed mean ± std).** Rows are Meta-World MT10 tasks sorted worst-first by TOPPO; the six columns are the cumulative V2 intervention rungs Vanilla MT-PPO → +LN-c → +LN-c+PopArt → +LN-c+FG-c (α=1) → +LN-c+PopArt+FG-c → TOPPO (+PCGrad-a), matching the curves in Figure D.13. Rows with std > mean (e.g. `drawer-open-v3` Vanilla, 20.0 ± 42.2) are bimodal across seeds and should be read as a frequency-of-success summary.

Task	Vanilla MT-PPO	+ LN-c	+ LN-c + PopArt	+ LN-c + FG-c	+ LN-c + PopArt + FG-c	**TOPPO**
`pick-place-v3`	62.8 ±32.8	86.2 ±20.0	86.0 ±11.7	85.2 ±17.2	80.8 ±17.3	83.8 ±20.9
`push-v3`	83.2 ±27.1	81.6 ±28.4	87.6 ±19.5	79.8 ±25.2	81.8 ±24.2	90.8 ±14.8
`peg-insert-side-v3`	98.0 ± 5.7	97.4 ± 4.2	99.0 ± 1.4	94.8 ±10.5	85.8 ±25.6	98.4 ± 3.7
`button-press-topdown-v3`	99.8 ± 0.6	98.6 ± 3.3	97.0 ± 5.9	97.6 ± 5.4	100.0 ± 0.0	99.4 ± 1.3
`window-open-v3`	98.4 ± 5.1	99.4 ± 1.3	99.4 ± 1.3	99.4 ± 1.3	100.0 ± 0.0	99.6 ± 1.3
`door-open-v3`	89.6 ±31.5	100.0 ± 0.0	100.0 ± 0.0	100.0 ± 0.0	100.0 ± 0.0	100.0 ± 0.0
`drawer-close-v3`	100.0 ± 0.0	100.0 ± 0.0	100.0 ± 0.0	100.0 ± 0.0	100.0 ± 0.0	100.0 ± 0.0
`drawer-open-v3`	20.0 ±42.2	99.0 ± 3.2	98.6 ± 4.4	100.0 ± 0.0	100.0 ± 0.0	100.0 ± 0.0
`reach-v3`	99.8 ± 0.6	100.0 ± 0.0	100.0 ± 0.0	100.0 ± 0.0	100.0 ± 0.0	100.0 ± 0.0
`window-close-v3`	100.0 ± 0.0	100.0 ± 0.0	100.0 ± 0.0	100.0 ± 0.0	100.0 ± 0.0	100.0 ± 0.0

Table D.6: **Per-task success rate on MT50 V2 (final-checkpoint, 10-seed mean ± std).** Tasks sorted ascending by TOPPO mean (worst first). Columns trace the cumulative TOPPO build-up: *Vanilla MT-PPO* (default actor and critic aggregators, no PopArt, no LN), + *LN-c* (add LayerNorm on the critic), + *LN-c* + *PopArt* (add PopArt return rescaling), + *LN-c* + *FG-c* (instead add α=1 FairGrad on the critic), + *LN-c* + *PopArt* + *FG-c* (combine both interventions), and *TOPPO* = + LN-c + PopArt + α=1 FG-c + PCGrad-a (full method). Entries with std > mean (e.g. `push-back-v3` TOPPO (10.0 ± 31.6), `disassemble-v3` TOPPO (19.6 ± 40.8)) have a bimodal seed distribution (some seeds at $\sim 0\%$, some near 100%); the reported ±std should be read as a frequency-of-success summary rather than a Gaussian dispersion in those rows.

Task	Vanilla MT-PPO	+ LN-c	+ LN-c + PopArt	+ LN-c + FG-c	+ LN-c + PopArt + FG-c	**TOPPO**
assembly-v3	0.0 ± 0.0	0.0 ± 0.0	0.2 ± 0.6	0.0 ± 0.0	0.0 ± 0.0	0.0 ± 0.0
push-back-v3	30.0 ±48.3	50.0 ±52.7	0.0 ± 0.0	20.0 ±42.2	9.2 ±29.1	10.0 ±31.6
disassemble-v3	0.2 ± 0.6	8.0 ±25.3	9.4 ±29.0	19.0 ±40.1	18.6 ±39.3	19.6 ±40.8
coffee-pull-v3	75.6 ±22.8	91.4 ±13.0	82.6 ±16.3	88.4 ±10.3	83.2 ±18.6	72.4 ±30.6
shelf-place-v3	3.2 ±10.1	23.0 ±37.9	85.6 ±17.4	56.6 ±43.8	66.0 ±40.2	75.2 ±33.4
pick-place-wall-v3	19.6 ±41.3	11.2 ±31.4	84.8 ±30.8	93.4 ±10.7	66.6 ±46.3	77.2 ±40.9
stick-pull-v3	8.6 ±27.2	56.4 ±39.8	70.4 ±29.2	75.8 ±28.1	76.2 ±23.3	82.4 ±11.1
bin-picking-v3	27.4 ±43.7	90.0 ± 8.6	87.8 ± 8.9	82.4 ±29.6	85.0 ±16.7	83.4 ±29.8
soccer-v3	84.8 ± 9.6	91.4 ±10.3	74.2 ±13.0	91.8 ± 7.8	85.6 ±12.6	84.0 ±15.0
basketball-v3	34.4 ±34.3	72.4 ±20.9	75.0 ±25.1	76.8 ±13.5	80.4 ±15.9	85.0 ±16.8
coffee-push-v3	83.2 ±10.7	95.4 ± 5.4	94.6 ± 7.9	84.8 ±11.8	92.6 ±11.5	90.4 ± 9.2
button-press-topdown-wall-v3	98.0 ± 4.3	96.0 ± 6.0	92.4 ±14.0	82.0 ±16.1	98.0 ± 3.5	94.2 ± 8.9
dial-turn-v3	87.8 ±15.1	78.8 ±33.9	76.0 ±31.2	89.4 ±31.4	88.2 ±18.7	95.2 ± 4.4
button-press-topdown-v3	99.0 ± 2.2	96.4 ± 6.3	87.6 ±15.1	89.8 ± 9.6	98.0 ± 3.4	96.4 ± 5.1
pick-out-of-hole-v3	54.2 ±47.6	91.6 ± 7.0	85.0 ±15.2	87.6 ± 9.5	92.0 ±14.0	96.6 ± 6.4
handle-pull-side-v3	89.8 ±31.6	100.0 ± 0.0	100.0 ± 0.0	100.0 ± 0.0	100.0 ± 0.0	97.4 ± 8.2
box-close-v3	97.4 ± 3.0	97.0 ± 4.2	97.8 ± 3.9	97.2 ± 8.2	98.0 ± 5.0	97.8 ± 2.9
button-press-wall-v3	99.0 ± 2.5	96.2 ± 3.9	98.0 ± 3.8	99.8 ± 0.6	98.6 ± 1.9	98.0 ± 3.3
hand-insert-v3	98.4 ± 4.4	94.4 ± 5.2	99.4 ± 1.0	99.4 ± 1.0	97.8 ± 3.7	98.2 ± 3.5
push-wall-v3	96.2 ± 4.6	90.6 ±16.2	99.2 ± 1.4	87.4 ±12.4	90.6 ±16.1	98.6 ± 2.1
pick-place-v3	95.2 ± 5.9	94.8 ± 5.0	90.8 ±15.8	96.0 ± 5.5	95.2 ± 8.2	98.8 ± 1.9
sweep-into-v3	99.0 ± 2.2	96.6 ± 5.0	98.4 ± 1.8	95.8 ± 6.1	99.4 ± 1.9	98.8 ± 3.2
push-v3	90.6 ±11.5	90.0 ±10.3	95.4 ± 6.0	92.0 ± 8.3	97.0 ± 4.0	99.0 ± 1.4
hammer-v3	50.0 ±52.7	87.8 ±31.6	79.8 ±42.1	99.8 ± 0.6	98.2 ± 5.7	99.2 ± 1.4
peg-unplug-side-v3	99.0 ± 1.7	96.0 ± 8.6	96.2 ± 9.3	99.6 ± 0.8	97.0 ± 3.0	99.2 ± 1.4
faucet-open-v3	92.8 ±16.2	100.0 ± 0.0	96.0 ± 8.6	95.6 ± 7.9	95.8 ±13.3	99.4 ± 1.3
faucet-close-v3	99.2 ± 1.9	98.8 ± 2.1	99.6 ± 0.8	94.6 ±11.9	99.6 ± 0.8	99.6 ± 1.3
window-open-v3	97.8 ± 4.7	99.8 ± 0.6	100.0 ± 0.0	99.0 ± 1.9	100.0 ± 0.0	99.6 ± 1.3
coffee-button-v3	100.0 ± 0.0	99.0 ± 3.2	99.8 ± 0.6	97.8 ± 3.8	99.0 ± 3.2	99.8 ± 0.6
handle-press-v3	97.8 ± 4.9	99.8 ± 0.6	98.2 ± 2.9	97.6 ± 6.2	100.0 ± 0.0	99.8 ± 0.6
handle-pull-v3	99.8 ± 0.6	99.8 ± 0.6	99.8 ± 0.6	99.6 ± 0.8	99.8 ± 0.6	99.8 ± 0.6
lever-pull-v3	29.2 ±47.0	99.4 ± 1.9	100.0 ± 0.0	100.0 ± 0.0	100.0 ± 0.0	99.8 ± 0.6
peg-insert-side-v3	99.6 ± 0.8	99.6 ± 0.8	100.0 ± 0.0	99.2 ± 1.4	98.6 ± 3.1	99.8 ± 0.6
reach-wall-v3	98.2 ± 2.2	99.2 ± 1.9	99.8 ± 0.6	98.6 ± 2.1	99.4 ± 1.0	99.8 ± 0.6
sweep-v3	99.8 ± 0.6	99.4 ± 1.9	99.6 ± 0.8	99.4 ± 1.0	99.2 ± 1.4	99.8 ± 0.6
button-press-v3	100.0 ± 0.0	100.0 ± 0.0	100.0 ± 0.0	100.0 ± 0.0	100.0 ± 0.0	100.0 ± 0.0
door-close-v3	100.0 ± 0.0	100.0 ± 0.0	100.0 ± 0.0	100.0 ± 0.0	100.0 ± 0.0	100.0 ± 0.0
door-lock-v3	100.0 ± 0.0	100.0 ± 0.0	100.0 ± 0.0	99.8 ± 0.6	99.8 ± 0.6	100.0 ± 0.0
door-open-v3	99.4 ± 1.3	100.0 ± 0.0	100.0 ± 0.0	100.0 ± 0.0	100.0 ± 0.0	100.0 ± 0.0
door-unlock-v3	100.0 ± 0.0	100.0 ± 0.0	100.0 ± 0.0	100.0 ± 0.0	100.0 ± 0.0	100.0 ± 0.0
drawer-close-v3	100.0 ± 0.0	100.0 ± 0.0	100.0 ± 0.0	100.0 ± 0.0	100.0 ± 0.0	100.0 ± 0.0
drawer-open-v3	30.0 ±48.3	89.0 ±31.4	97.6 ± 6.3	97.4 ± 7.5	100.0 ± 0.0	100.0 ± 0.0
handle-press-side-v3	99.2 ± 1.9	97.8 ± 4.7	99.4 ± 1.9	100.0 ± 0.0	100.0 ± 0.0	100.0 ± 0.0
plate-slide-back-side-v3	100.0 ± 0.0	100.0 ± 0.0	100.0 ± 0.0	100.0 ± 0.0	100.0 ± 0.0	100.0 ± 0.0
plate-slide-back-v3	100.0 ± 0.0	100.0 ± 0.0	100.0 ± 0.0	100.0 ± 0.0	100.0 ± 0.0	100.0 ± 0.0
plate-slide-side-v3	100.0 ± 0.0	100.0 ± 0.0	100.0 ± 0.0	100.0 ± 0.0	100.0 ± 0.0	100.0 ± 0.0
plate-slide-v3	100.0 ± 0.0	100.0 ± 0.0	100.0 ± 0.0	100.0 ± 0.0	100.0 ± 0.0	100.0 ± 0.0
reach-v3	99.8 ± 0.6	100.0 ± 0.0	100.0 ± 0.0	100.0 ± 0.0	100.0 ± 0.0	100.0 ± 0.0
stick-push-v3	60.0 ±51.2	100.0 ± 0.0	94.8 ±11.0	99.8 ± 0.6	100.0 ± 0.0	100.0 ± 0.0
window-close-v3	99.4 ± 1.9	100.0 ± 0.0	100.0 ± 0.0	100.0 ± 0.0	100.0 ± 0.0	100.0 ± 0.0

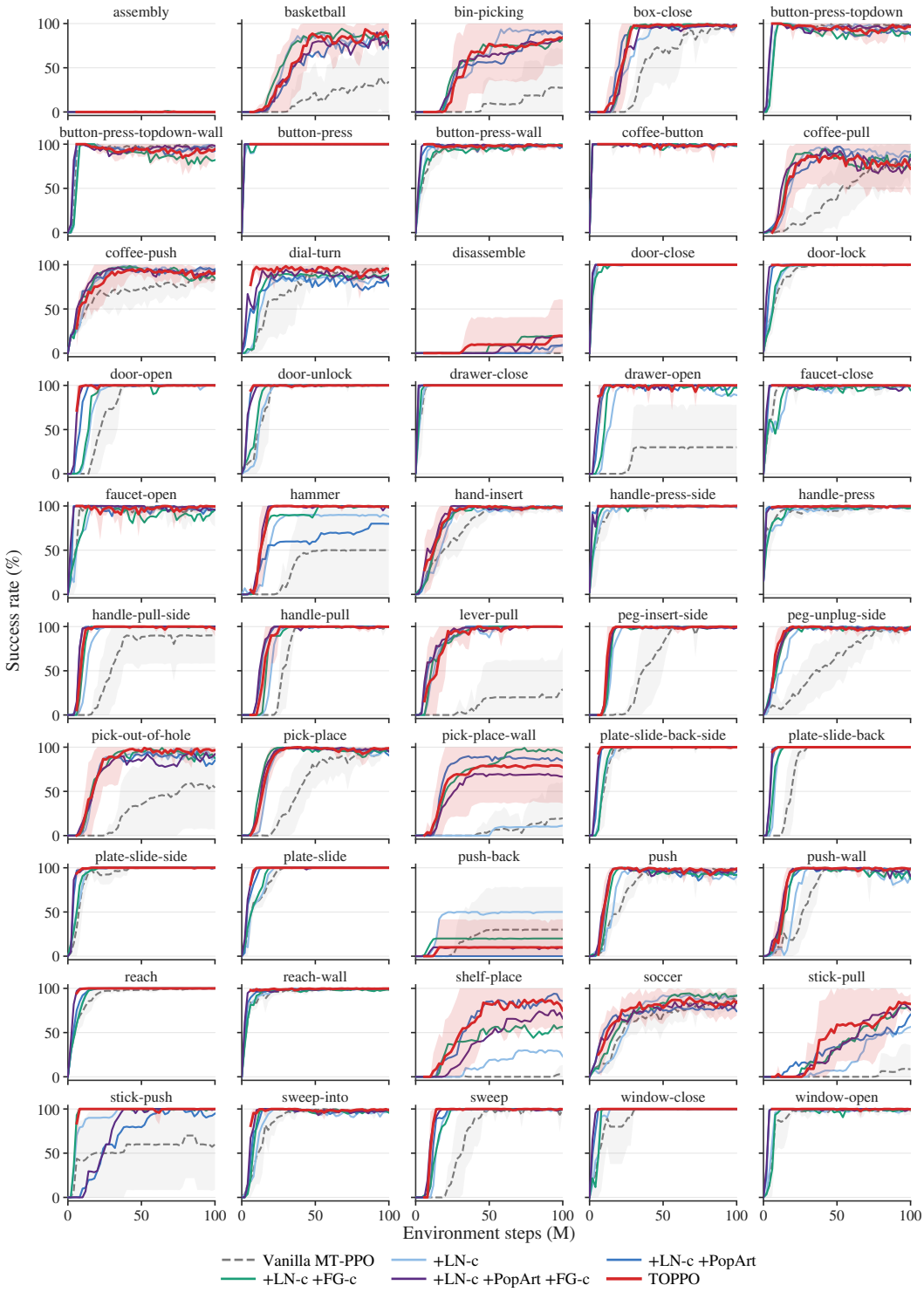


Figure D.14: Per-task MT50 V2 learning curves across all 50 tasks for the six intervention configurations. Lines are ten-seed means; shaded bands, drawn only for TOPPO and Vanilla MT-PPO, are sample standard deviations. Each configuration uses only evaluation checkpoints recorded for all ten seeds; the trajectories are unsmoothed.

Table D.7: **Per-task final-checkpoint success on MT50 V1 (10-seed mean ± std).** Rows are Meta-World MT50 tasks sorted worst-first by TOPPO (V1); the six columns are the cumulative V1 intervention rungs Vanilla MT-PPO → +LN-c → +LN-c+PopArt → +LN-c+FG-c (α=1) → +LN-c+PopArt+FG-c → TOPPO (V1) (+PCGrad-a), matching the curves in Figure D.15; V1's wider per-task reward scale [McLean et al., 2025] produces a thicker dead-task floor (Table D.4) and the FG-c-without-PopArt regression of Section D.5. Rows with std > mean (e.g. `plate-slide-back-v3` Vanilla, 30.0 ± 48.3) are bimodal across seeds and should be read as a frequency-of-success summary.

Task	Vanilla MT-PPO	+ LN-c	+ LN-c + PopArt	+ LN-c + FG-c	+ LN-c + PopArt + FG-c	**TOPPO (V1)**
box-close-v3	0.0 ± 0.0	7.4 ±11.1	2.2 ± 7.0	0.4 ± 1.3	0.0 ± 0.0	0.0 ± 0.0
hand-insert-v3	0.0 ± 0.0	0.0 ± 0.0	0.0 ± 0.0	0.0 ± 0.0	0.0 ± 0.0	0.0 ± 0.0
handle-pull-v3	0.0 ± 0.0	0.0 ± 0.0	0.0 ± 0.0	0.0 ± 0.0	0.0 ± 0.0	0.0 ± 0.0
peg-insert-side-v3	0.0 ± 0.0	0.0 ± 0.0	0.0 ± 0.0	0.0 ± 0.0	0.0 ± 0.0	0.0 ± 0.0
stick-pull-v3	0.0 ± 0.0	0.0 ± 0.0	0.0 ± 0.0	0.0 ± 0.0	0.0 ± 0.0	0.0 ± 0.0
stick-push-v3	0.0 ± 0.0	0.0 ± 0.0	0.0 ± 0.0	0.0 ± 0.0	0.0 ± 0.0	0.0 ± 0.0
disassemble-v3	0.0 ± 0.0	0.0 ± 0.0	0.0 ± 0.0	17.8 ±37.6	20.0 ±42.2	8.6 ±27.2
assembly-v3	0.0 ± 0.0	7.8 ±19.4	6.2 ±17.5	8.4 ±18.3	18.2 ±38.5	18.2 ±38.1
handle-pull-side-v3	0.0 ± 0.0	0.0 ± 0.0	10.0 ±31.6	0.0 ± 0.0	30.0 ±48.3	20.0 ±42.2
basketball-v3	0.0 ± 0.0	3.4 ± 7.5	5.6 ±11.7	1.0 ± 1.9	14.4 ±23.5	29.6 ±34.2
coffee-pull-v3	18.6 ±27.5	40.2 ±34.7	7.8 ±24.0	30.6 ±33.5	40.0 ±37.4	68.2 ±38.4
hammer-v3	13.0 ±24.8	66.4 ±36.0	77.2 ±23.5	90.2 ±14.3	85.4 ±12.1	84.2 ±13.3
soccer-v3	60.8 ± 5.4	65.6 ±10.1	88.6 ± 8.0	59.4 ±11.7	87.2 ±12.6	93.0 ± 7.0
pick-place-wall-v3	0.0 ± 0.0	75.4 ±21.0	97.6 ± 3.4	66.0 ±29.6	96.8 ± 3.2	94.8 ± 4.2
bin-picking-v3	0.0 ± 0.0	59.8 ±17.5	91.8 ± 7.9	69.2 ±18.2	94.2 ± 6.4	95.4 ± 5.0
coffee-push-v3	67.4 ± 9.2	79.2 ±12.7	94.6 ± 4.9	83.4 ± 6.3	89.8 ±11.8	95.6 ± 5.1
button-press-topdown-v3	100.0 ± 0.0	91.8 ±16.8	99.6 ± 1.3	84.8 ±17.7	98.4 ± 2.5	95.8 ±11.9
button-press-topdown-wall-v3	100.0 ± 0.0	84.2 ±31.2	98.6 ± 2.7	86.6 ±15.0	97.0 ± 4.6	96.0 ±10.0
pick-out-of-hole-v3	0.0 ± 0.0	69.8 ±24.8	72.4 ±40.1	70.8 ±24.2	97.2 ± 6.9	96.2 ± 5.8
push-v3	40.8 ±10.1	88.6 ± 9.0	98.4 ± 2.6	93.8 ± 6.0	96.2 ±10.1	97.6 ± 5.6
sweep-into-v3	83.8 ±14.1	80.8 ±13.1	96.0 ± 6.2	78.0 ±12.2	99.6 ± 0.8	97.8 ± 3.8
shelf-place-v3	0.0 ± 0.0	20.4 ±34.8	77.2 ±40.9	32.2 ±35.5	98.8 ± 1.7	98.2 ± 3.3
pick-place-v3	0.0 ± 0.0	77.8 ±14.4	89.2 ±31.4	72.2 ±15.4	97.6 ± 2.5	98.6 ± 2.5
sweep-v3	6.4 ±20.2	53.0 ±24.0	99.2 ± 1.4	46.4 ±21.1	96.8 ± 4.6	98.8 ± 2.7
button-press-wall-v3	71.6 ±10.8	81.0 ±17.6	98.6 ± 4.4	67.0 ±13.7	98.8 ± 3.2	99.2 ± 2.5
door-lock-v3	87.8 ±14.3	60.4 ±27.6	100.0 ± 0.0	69.6 ±23.7	99.6 ± 1.3	99.2 ± 1.7
push-back-v3	0.0 ± 0.0	76.8 ±18.0	97.0 ± 8.8	54.8 ±21.1	99.8 ± 0.6	99.8 ± 0.6
push-wall-v3	24.0 ± 8.1	79.6 ±21.4	97.8 ± 2.7	72.6 ±20.1	98.0 ± 3.8	99.8 ± 0.6
reach-wall-v3	96.4 ± 1.8	98.4 ± 1.8	99.8 ± 0.6	93.8 ± 7.3	100.0 ± 0.0	99.8 ± 0.6
button-press-v3	100.0 ± 0.0	100.0 ± 0.0	100.0 ± 0.0	94.2 ±14.1	99.0 ± 3.2	100.0 ± 0.0
coffee-button-v3	100.0 ± 0.0	100.0 ± 0.0	100.0 ± 0.0	100.0 ± 0.0	100.0 ± 0.0	100.0 ± 0.0
dial-turn-v3	84.8 ±17.5	95.4 ±10.1	99.8 ± 0.6	86.0 ± 8.5	100.0 ± 0.0	100.0 ± 0.0
door-close-v3	100.0 ± 0.0	84.0 ±22.8	100.0 ± 0.0	78.4 ±20.7	100.0 ± 0.0	100.0 ± 0.0
door-open-v3	0.0 ± 0.0	84.0 ±31.2	99.6 ± 1.3	82.0 ±30.5	100.0 ± 0.0	100.0 ± 0.0
door-unlock-v3	16.2 ±13.9	3.2 ±10.1	99.4 ± 1.0	2.4 ± 5.1	99.6 ± 0.8	100.0 ± 0.0
drawer-close-v3	100.0 ± 0.0	100.0 ± 0.0	100.0 ± 0.0	100.0 ± 0.0	100.0 ± 0.0	100.0 ± 0.0
drawer-open-v3	86.8 ±31.7	93.0 ±11.6	100.0 ± 0.0	95.4 ±10.1	100.0 ± 0.0	100.0 ± 0.0
faucet-close-v3	76.8 ±41.0	76.8 ±27.1	100.0 ± 0.0	74.0 ±23.9	100.0 ± 0.0	100.0 ± 0.0
faucet-open-v3	100.0 ± 0.0	97.6 ± 5.0	100.0 ± 0.0	75.4 ±33.1	100.0 ± 0.0	100.0 ± 0.0
handle-press-side-v3	100.0 ± 0.0	100.0 ± 0.0	100.0 ± 0.0	99.8 ± 0.6	100.0 ± 0.0	100.0 ± 0.0
handle-press-v3	93.0 ± 6.2	84.0 ±12.1	99.6 ± 1.3	94.2 ±10.5	99.8 ± 0.6	100.0 ± 0.0
lever-pull-v3	25.4 ±31.2	49.0 ±41.3	100.0 ± 0.0	35.6 ±44.6	100.0 ± 0.0	100.0 ± 0.0
peg-unplug-side-v3	14.8 ±17.3	81.4 ±14.5	99.6 ± 0.8	85.6 ± 7.5	99.4 ± 1.9	100.0 ± 0.0
plate-slide-back-side-v3	18.8 ±39.7	100.0 ± 0.0	100.0 ± 0.0	99.0 ± 3.2	100.0 ± 0.0	100.0 ± 0.0
plate-slide-back-v3	30.0 ±48.3	100.0 ± 0.0	100.0 ± 0.0	100.0 ± 0.0	90.0 ±31.6	100.0 ± 0.0
plate-slide-side-v3	76.4 ±40.8	100.0 ± 0.0	100.0 ± 0.0	100.0 ± 0.0	100.0 ± 0.0	100.0 ± 0.0
plate-slide-v3	86.2 ±13.8	98.2 ± 4.5	100.0 ± 0.0	97.0 ± 5.4	100.0 ± 0.0	100.0 ± 0.0
reach-v3	100.0 ± 0.0	99.8 ± 0.6	100.0 ± 0.0	97.6 ± 3.0	100.0 ± 0.0	100.0 ± 0.0
window-close-v3	90.0 ±31.6	97.8 ± 7.0	100.0 ± 0.0	97.8 ± 3.2	100.0 ± 0.0	100.0 ± 0.0
window-open-v3	90.0 ±31.6	76.4 ±18.5	99.6 ± 1.3	62.0 ±25.1	100.0 ± 0.0	100.0 ± 0.0

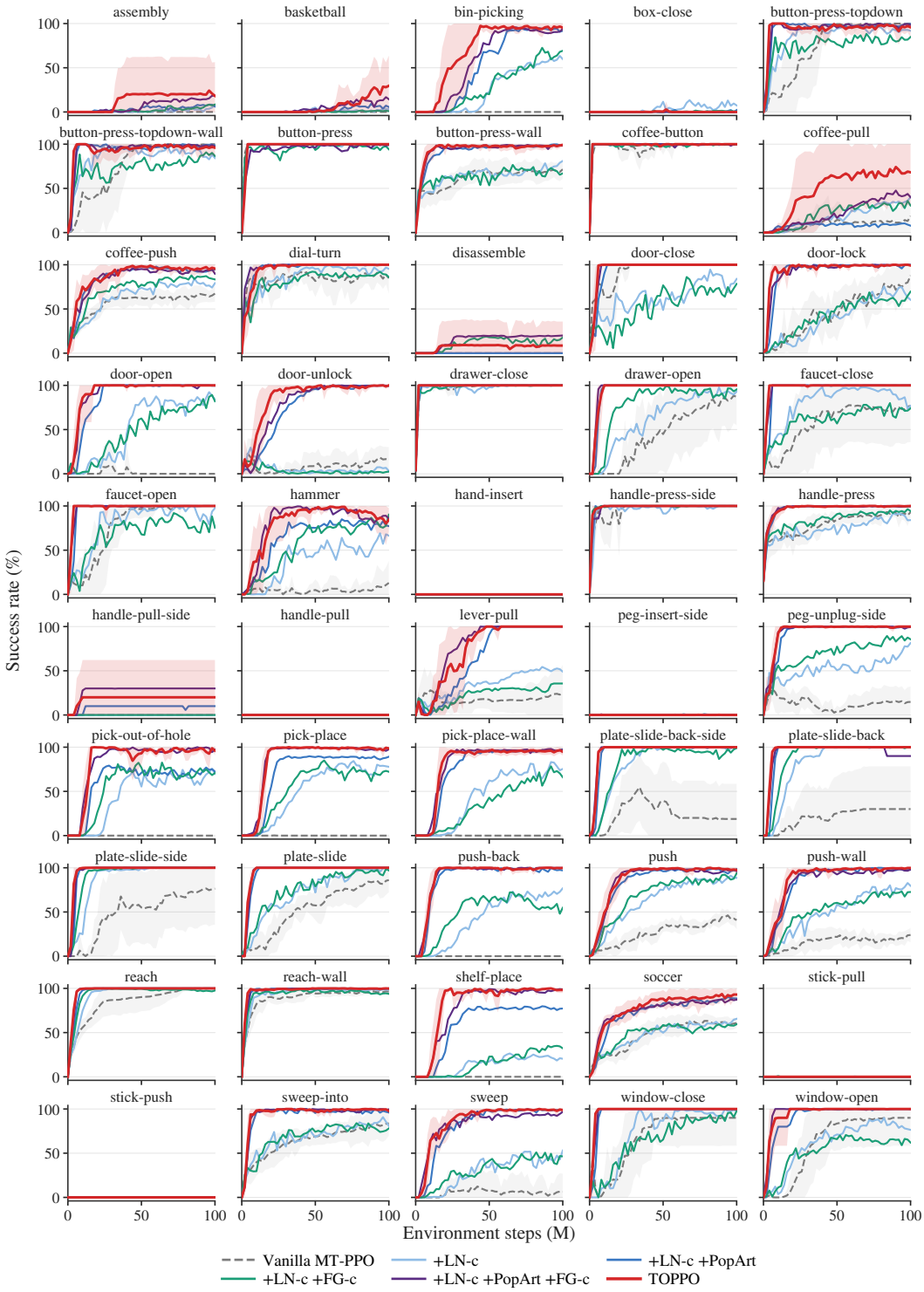


Figure D.15: Per-task MT50 V1 learning curves across all 50 tasks for the six intervention configurations under V1 rewards. Lines are ten-seed means; shaded bands, drawn only for TOPPO and Vanilla MT-PPO, are sample standard deviations. Each configuration uses only evaluation checkpoints recorded for all ten seeds; the trajectories are unsmoothed.

D.7 Cross-paper reporting-protocol map

Reporting conventions across the MTRL literature are not standardized: papers differ on the aggregator (final-checkpoint vs. mean-curve peak vs. best-per-seed), the central statistic (mean vs. IQM), the dispersion measure (std vs. SEM), the seed count, and the V1/V2 reward semantics. Table D.9 maps each cited baseline to its source paper's choices and Table D.8 verifies step-budget alignment; Tables D.10 and D.11 report the four-metric breakdown and per-seed best-checkpoint-step distribution for our headline configurations so readers can convert to any baseline's protocol. Headline-relevant points beyond what those captions already disclose:

- **SEM versus std.** The mtrl-codebase family (CAGrad / CARE / FAMO / FairGrad) reports SEM, not std; SEM $\equiv$ std/$\sqrt{n}$ is roughly $3.16\times$ tighter at n=10 and is paired with mean-curve-peak aggregation, which is upward-biased. Worked conversions for direct verification: FairGrad MT10 0.84 ± 0.07 SEM $\equiv \pm 0.22$ std; CAGrad MT10 0.83 ± 0.045 SEM $\equiv \pm 0.142$ std; CAGrad MT50 0.52 ± 0.023 SEM $\equiv \pm 0.073$ std.
- **Step-budget alignment is exact.** All cited baselines except Soft Modularization (15M/50M paper-original; we cite the MW+ 20M/100M re-run instead) train at our 20M/100M budget, so step budgets need no renormalization. The unannotated Meta-World+ MT50 numbers are validated against the companion `metaworld-algorithms` repo configs (including the misnamed `paco_mt10.py` file whose internal config is verbatim MT50 K=20); details in Table D.8 caption. Evaluation protocols still differ (Table D.9 caption, Section E.1).
- **Reward versions must match.** Older gradient-method reports use V1 rewards, whereas our default setting uses V2. A V1-baseline/V2-TOPPO contrast would favor TOPPO through the reward change and cannot isolate an algorithmic difference. We therefore use the reward-matched V2 rows in Table 2 and the separate V1 comparison in Table 3.

Table D.8: **Step-budget alignment across cited baselines.** We normalize every paper's reporting convention — "per-task", "per mtrl-iteration", "epochs $\times$ batch" — to total environment steps (every parallel-env step counts $+1$) and verify all rows train at our 20M / 100M budget except Soft Modularization (15M / 50M paper-original; we cite its Meta-World+ re-run instead), so cross-paper comparison in Table 2 requires no renormalization.

Paper	Reported	Total MT10	Total MT50	Verification
Ours (PPO)	20M / 100M (total)	20M	100M	baseline
Original Meta-World (2020)	500 epochs $\times$ batch	20M	100M	verified from garage scripts
CAGrad (2021)	2M (mtrl iter)	20M	100M	`num_envs` = `num_tasks`
CARE (2021)	2M per task	20M	100M	explicit
FAMO (2023)	follows CAGrad exactly	20M	–	MT10 only
FairGrad (2024)	2M / batch 1280	20M	–	MT10 only
PaCo (2022)	20M total / 100M total	20M	100M	explicit
MOORE (2024)	20 ep $\times$ 100K vec $\times$ envs	20M	100M	verified from `VecCore`
ARS (2025)	$2{\cdot}10^7$ / 10^8	20M	100M	matches ours exactly
Soft Modularization (2020)	15M / 50M	**15M**	**50M**	outlier; verified from JSON configs
Meta-World+ (2025) multi-task	not explicitly tabulated	20M	100M	inferred from companion repo (Section D.7)

Table D.9: **Reporting protocol across cited baselines.** For each cited paper we tabulate seed count, aggregator (A: final-checkpoint average; B: best-per-seed then average; C: mean-curve peak; D: late-window mean; E: other), dispersion measure (std / SEM / IQM), eval episodes per task, and reward version, so readers can align cross-paper comparisons in Tables 2 to 3 with the matching column of Table D.10. V1* marks rows inferred from a pinned pre-V2 Meta-World commit; † Meta-World+ Appendix D scalar tables carry no explicit dispersion label, the paper's main text only commits to 95% CIs for the IQM-through-training plots, and the companion `metaworld-algorithms` repository contains no table-generation / cross-seed aggregation script – so whether the reported ± is std, SEM, or a 95% CI cannot be verified from primary sources. We treat it as std throughout the paper (Tables 3 and D.3, the V1 head-to-head); this is a working assumption. Matching the step budget and reporting statistic does not match the evaluation protocol: published ARS results use stochastic evaluation on 10 sampled goals per task, sampled training goals, and a different MuJoCo binding, whereas our reruns use our deterministic protocol on the 50 fixed benchmark goals (Section E.1).

Paper	Seeds	Aggreg.	Description	Disp.	Eval eps.	Reward
Ours (PPO)	10	all of A/B/C/D	best/peak/final/late, all reported	std	50	V2
MT-SAC (orig 2020)	10	(E)	max-over-time per (seed,task)	none	5	V1
Soft-Mod (2020)	3	(E)	final-policy 100-ep dedicated pass	(graphical only)	100	V1
PCGrad (2020)	?	–	figure eyeball, no num table	–	?	V1
CAGrad (2021)	10	(C)	mean-curve peak (App B.3)	**SEM**	1	V1*
CARE (2021)	10	(C)	mean-curve peak	SEM	5	V1
PaCo (2022)	10	(A)	final 20M, explicit anti-peak	std	10	**V2**
FAMO (2023)	10	(C)	inherits CAGrad	SEM	1	V1*
MOORE (2024)	10	(A)	final ckpt (20M MT10 / 100M MT50)	std	10	**V2**
FairGrad (2024)	10	(C)	mean-curve peak (§5.3)	SEM	1	V1*
Meta-World+ (2025)	10	(A/B)[?]	IQM (final-step or best ckpt; ambiguous)	IQM, ± unspec.[†]	50	V1+V2
ARS (2025)	**8**	(A)	final EvalFinalSR	std	10	**V2**
Our SAC-MT / ARS reruns	10	(A)	final ckpt, our evaluation protocol	std	50	V2

Table D.10: **Four-metric disclosure for our headline configurations.** Each row reports MT10 and MT50 success (%, mean ± std over 10 seeds at 20M / 100M total environment steps) under four aggregators that span the conventions used by cited baselines: *best* (per-seed argmax then averaged), *peak* (argmax of the mean curve), *final* (terminal step), and *late* (mean of the last 10% of steps). Reporting all four lets readers convert our numbers to any baseline's protocol (Table D.9).

	MT10				MT50			
Configuration	best	peak	final	late	best	peak	final	late
Vanilla MT-PPO	89.5 ± 4.6	87.8 ± 5.1	85.2 ± 6.5	85.1 ± 5.7	79.6 ± 3.2	78.7 ± 3.7	78.5 ± 3.3	78.5 ± 3.5
+LN-c	99.5 ± 0.3	97.9 ± 1.6	96.2 ± 3.4	95.3 ± 1.9	89.2 ± 1.9	88.3 ± 1.9	87.5 ± 2.4	87.7 ± 2.2
+LN-c +PopArt	99.9 ± 0.2	98.5 ± 1.2	96.8 ± 1.5	96.4 ± 2.3	90.7 ± 1.8	89.2 ± 2.2	88.9 ± 2.3	89.0 ± 1.8
+LN-c +FG-c	99.8 ± 0.2	98.6 ± 0.7	95.7 ± 4.0	96.2 ± 2.4	91.2 ± 1.6	89.9 ± 1.7	89.7 ± 1.6	89.6 ± 1.5
+LN-c +PopArt +FG-c	99.8 ± 0.2	99.0 ± 0.6	94.8 ± 5.1	96.7 ± 2.0	91.2 ± 2.1	90.1 ± 2.3	90.1 ± 2.3	89.7 ± 2.2
TOPPO	99.6 ± 0.4	97.9 ± 2.2	97.2 ± 3.1	96.0 ± 1.6	92.1 ± 1.7	91.3 ± 1.6	90.9 ± 1.6	91.0 ± 1.7

Table D.11: **Per-seed best-checkpoint step distribution** (median, IQR, min–max in env-step millions across 10 seeds, per configuration). These steps relate our runs to the peak-based reporting conventions in Table D.9; all success comparisons in the paper use the final checkpoint.

Configuration	Bench.	Budget (M)	Median (M)	IQR (M)	min–max (M)
Vanilla MT-PPO	MT10	20	15.0	[13.4, 17.2]	10.0–19.6
+LN-c	MT10	20	11.8	[10.9, 16.4]	6.8–20.0
+LN-c +PopArt	MT10	20	13.4	[9.7, 15.9]	6.4–17.6
+LN-c +FG-c	MT10	20	8.4	[6.7, 9.7]	5.6–19.2
+LN-c +PopArt +FG-c	MT10	20	8.4	[7.0, 9.8]	6.4–12.4
TOPPO	MT10	20	12.6	[9.4, 17.2]	7.2–19.6
Vanilla MT-PPO	MT50	100	93.5	[89.0, 97.2]	83.0–99.0
+LN-c	MT50	100	77.0	[72.0, 86.5]	48.0–96.0
+LN-c +PopArt	MT50	100	88.0	[67.0, 92.0]	40.0–96.0
+LN-c +FG-c	MT50	100	84.0	[70.0, 97.0]	58.0–100.0
+LN-c +PopArt +FG-c	MT50	100	86.0	[66.0, 97.5]	40.0–100.0
TOPPO	MT50	100	84.0	[51.0, 93.5]	46.0–96.0

E Extended Experiments and Robustness Checks

The additional experiments examine whether the headline results hold against SAC-MT and the ARS family run under our protocol, whether other normalizers can fill PopArt's role, and whether the critic-side interventions extend to an off-policy learner and a second control setting. They keep the Meta-World headline configuration fixed and distinguish its results from the explicitly labeled alternative configurations below. Unless specified otherwise, success rates are final-checkpoint percentages at 100M total environment steps over 10 seeds, and every $\pm$ denotes the sample standard deviation across seeds. For V1, IQM denotes the paper's 25%-trimmed mean of per-seed mean success rates, accompanied by the untrimmed sample standard deviation. Paired tests use the untrimmed scores for shared training seeds; consequently, a reported paired difference need not equal the difference between two printed IQMs.

E.1 SAC-family baselines under a common evaluation protocol

We rerun the ARS-family implementations and MTSAC (SAC-MT in Table 2) using Meta-World 3.0.0, V2 rewards, a 500-step horizon, and 20M (MT10) or 100M (MT50) total training interactions, including SAC's random exploration warmup. All of these runs use TOPPO's evaluation protocol: deterministic policies, one episode for each of the 50 benchmark goals per task, success if achieved at any point in the episode, and 10 seeds. Worst-10 is computed within each seed by averaging its ten lowest task success rates, then summarized across seeds. For the published rows in Table 2, worst-k is the bottom-k score reported by Cho et al. [2025], whose aggregation is not fully specified; the worst-5 zeros of the published non-ARS methods are inferred from their zero worst-10 scores.

The reruns differ from the published ARS setup in the MuJoCo binding, fixed benchmark training goals, deterministic rather than stochastic evaluation, and 50 rather than 10 evaluation goals; published ARS results use 8 seeds (unstated for ARS-LN-1024). We therefore retain the published and rerun numbers separately in Tables 2 and E.1. ARS-LoRA's attach-versus-reset decision also reads this deterministic evaluation signal at its decision point (85.8M steps on MT50, 16M on MT10), so the protocol affects that arm's training as well as its measurement. On MT50, the most recent per-seed evaluation (at 85M steps) ranges from 71.5% to 82.8%, 6.5–17.8 points above the 65% attach threshold; on MT10, the 16M evaluation ranges from 85.4% to 99.2% against the 80% threshold, so all ten seeds attach the adapters on both benchmarks. We retain the released baseline hyperparameter recipes without per-arm tuning.

Table E.1: MT50 V2 ARS-family comparisons. Published values are from Tables 2 and 6 of Cho et al. [2025], which report no ARS-LN-1024 worst-10 score. Published values use 8 seeds, except ARS-LN-1024 (Table 6), whose seed count is not stated. Our runs match the corresponding rows of Table 2. All entries are percentages, mean $\pm$ sample std.

	Published		Our runs (n=10)	
Method	Mean	Worst-10	Mean	Worst-10
ARS	65.9 ± 2.9	9.1 ± 6.6	66.84 ± 4.81	0.62 ± 1.64
ARS-LN-400	78.3 ± 3.7	21.0 ± 11.4	76.64 ± 5.67	11.70 ± 9.57
ARS-LN-1024	88.9 ± 2.6	—	85.75 ± 3.23	43.26 ± 9.77
ARS-LoRA	83.2 ± 1.8	29.3 ± 7.7	82.28 ± 3.09	19.04 ± 11.56
TOPPO (headline)	—	—	90.88 ± 1.59	56.50 ± 7.76

On MT50, against the strongest baseline, ARS-LN-1024, TOPPO improves the final mean by 5.14 points and worst-10 by 13.24 points (differences of unrounded means; Tables 2 and E.1). These comparisons support the headline MT50 result without attributing the differences between published and our baseline scores to any single protocol change. Against published values, TOPPO's worst-10 gap to ARS-LoRA is 27.2 points, but the published worst-k task-ordering and aggregation convention is not fully specified.

Porting the stack to MTSAC. MTSAC uses the ARS backbone hyperparameters with adaptive reward scaling disabled. Its critic-balancing variant adds LN-c, PopArt, and FairGrad-c at α=1; the full-stack variant additionally uses actor-side PCGrad. The port uses EMA PopArt with coefficient

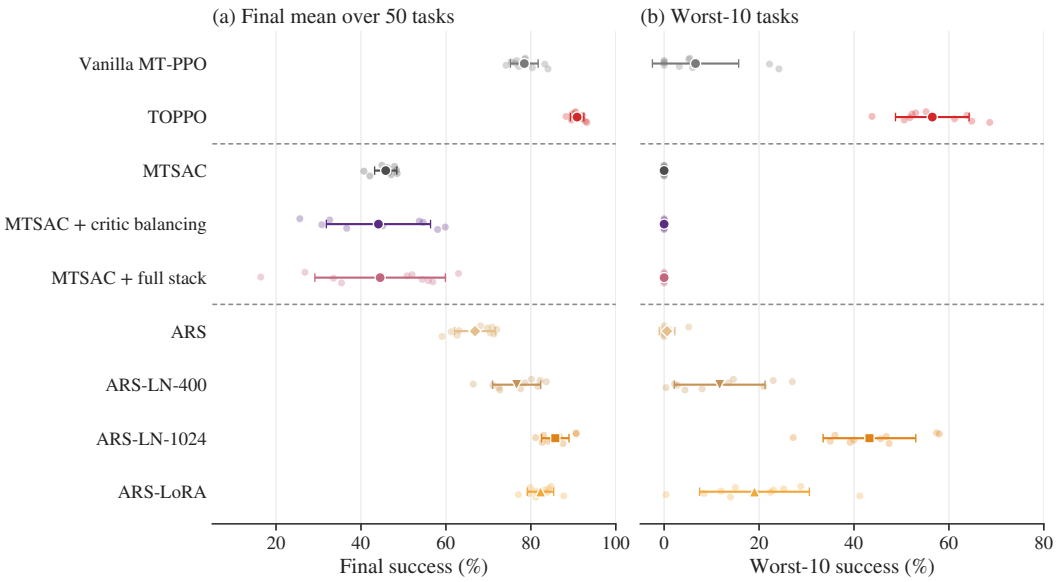


Figure E.1: Final MT50 V2 success of our PPO and baseline runs, ten seeds each at 100M transitions: (a) final mean over 50 tasks and (b) worst-10 success. Pale points are the ten seeds, large markers the means, and whiskers sample std; dashed lines separate the PPO, MTSAC, and ARS families. Published baseline numbers are listed separately in Table E.1. The critic-balancing and full-stack MTSAC ports show much greater seed dispersion without a reliable mean improvement.

3×10^{-4}, the upstream SAC LayerNorm parameterization, and entropy temperature in normalized value units, so it is an adaptation to SAC rather than an identical implementation across learner families.

Table E.2: MT50 V2 transfer to MTSAC at 100M steps, 10 seeds. The first row is SAC-MT from Table 2. Neither port improves the final mean; both increase seed dispersion.

Method	Final mean	Final worst-10
SAC-MT (MTSAC), ARS hyperparameters	45.82 ± 2.61	0.00 ± 0.00
MTSAC + critic balancing	44.11 ± 12.27	0.00 ± 0.00
MTSAC + full stack	44.51 ± 15.37	0.00 ± 0.00

The final mean changes by -1.71 points for critic balancing and -1.31 points for the full stack relative to MTSAC, with seed standard deviations increasing by factors of 4.7 and 5.9, respectively (Table E.2). The full-stack port therefore provides no reliable final-budget gain beyond the critic-only port. These results limit the empirical claim to the studied PPO setting; they do not establish that critic balancing cannot benefit other off-policy implementations.

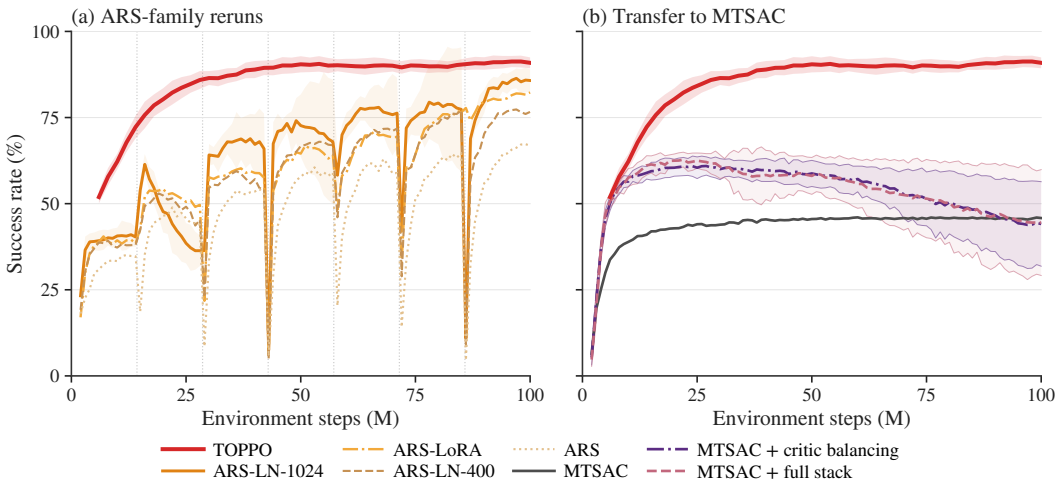


Figure E.2: Recorded MT50 V2 trajectories, ten seeds per configuration. (a) TOPPO and the ARS family. (b) TOPPO, MTSAC, and MTSAC with critic balancing or the full stack. Lines show means on each group's common recorded evaluation grid; bands show sample std for TOPPO and ARS-LN-1024 in (a) and for TOPPO and the two MTSAC ports in (b), where thin edges separate the two overlapping port bands. Curves are not smoothed. Dotted vertical lines in (a) mark the scheduled ARS learner resets every 14.3M transitions; the drops after them are genuine evaluation results, verified against native metrics. LoRA follows its configured reset/attach rule.

E.2 Normalizer alternatives and value clipping

At the LN-c rung, with both gradient combiners set to their default mean, we compare PopArt with per-task reward normalization, return-based scaling [Schaul et al., 2021], and the HL-Gauss categorical value loss [Farebrother et al., 2024]. Reward normalization divides rewards by a running standard deviation of discounted returns and clips normalized rewards to $[-10, 10]$. Return-based scaling instead rescales the value-loss residual while retaining raw value units. HL-Gauss replaces scalar regression with cross-entropy against Gaussian-smoothed targets on a fixed categorical support. This campaign trains 120 runs and reuses completed reference runs where configurations coincide. Its final scores are reconstructed from the per-run evaluation CSVs; this avoids incomplete final summaries in 12 of the 120 online run histories.

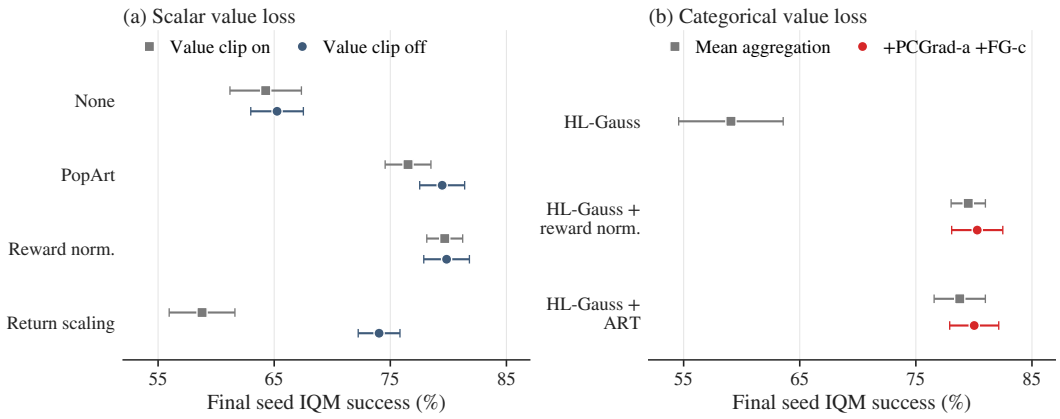


Figure E.3: MT50 V1 normalizer controls, ten seeds at 100M steps (seed IQM $\pm$ untrimmed std). (a) Scalar value loss, value clipping on (gray) or off (slate). (b) HL-Gauss critics with mean aggregation (gray) or +PCGrad-a +FG-c (red); bins differ by row (Table E.4); ART: PopArt-style target rescaling.

Matched clipping controls. The headline PPO configuration clips value changes by 0.2 in the units used by its value loss. Those units differ between raw-return, normalized-return, and PopArt

critics. HL-Gauss structurally requires value clipping to be disabled. We therefore compare all five V1 critic settings with value clipping disabled and report the clip-on scalar controls alongside them in Table E.3.

Table E.3: MT50 V1 normalizer comparison at the LN-c rung, 10 seeds and 100M steps. IQM is computed across per-seed mean success rates; std uses all seeds. Worst-20 is the per-seed lower-tail mean, averaged across seeds. The matched comparison is the clip-off column.

Normalizer	Clip off: IQM $\pm$ std	Clip on: IQM $\pm$ std	Clip-off worst-20
None	65.25 ± 2.27	64.27 ± 3.08	19.49 ± 3.72
PopArt	79.47 ± 1.94	76.53 ± 1.97	48.95 ± 4.77
Reward normalization	79.85 ± 1.97	79.69 ± 1.55	49.97 ± 4.91
Return-based scaling	74.03 ± 1.80	58.79 ± 2.83	37.39 ± 4.34
HL-Gauss	59.07 ± 4.50	—	5.30 ± 5.27

Under matched clip-off conditions, reward normalization and PopArt differ by only $+0.43$ points in paired untrimmed means (p=0.64); this is an absence of a detected difference, not an equivalence test. Their larger clip-on difference ($+3.61$ points) should consequently not be read as an intrinsic advantage of reward normalization. Removing value clipping improves PopArt by 3.49 points (p=0.0027) and return-based scaling by 15.78 points (p=8.3×10^{-8}); both survive Bonferroni correction over the four within-normalizer clipping comparisons. Thus the PopArt ablations of the intervention ladder establish gains over an unnormalized critic, rather than superiority over all normalization alternatives.

On V2, mean success is 87.54 ± 2.42 without a normalizer, 88.90 ± 2.26 with PopArt, 89.49 ± 1.98 with reward normalization, 89.08 ± 1.77 with return-based scaling, and 87.74 ± 2.12 with HL-Gauss. No alternative differs significantly from the no-normalizer control at the nominal 0.05 level. The only nominally significant pair among all ten comparisons, reward normalization versus HL-Gauss (p=0.036), does not survive Bonferroni correction (p_{adj}=0.36). These V2 rows mix clip-on scalar critics with clip-off HL-Gauss; a matched V2 clipping study was not run, so they do not isolate loss form from clipping.

Return scaling and time-limit truncation. In this benchmark, episodes end by time-limit truncation and bootstrap rather than entering a true terminal state. The discount-variance term in return-based scaling therefore vanishes: measured $\mathrm{Var}[\gamma_t] \simeq 3.9 \times 10^{-13}$, so its scale estimate reduces to reward variance. A diagnostic variant that counts truncations as terminal for the scale estimator restores variance to 1.956×10^{-3}, close to $0.99^2/500$, but changes final success by only $+1.72$ points (p=0.25) in the clip-on V1 setting. This control identifies a benchmark-specific limitation of that scale estimator without establishing a general failure of return-based scaling.

Alternative normalization in the full stack. With PCGrad-a and FG-c enabled, reward normalization reaches V1 IQM 82.22 ± 2.86, compared with 80.03 ± 2.61 for a PopArt-EMA reference. The paired untrimmed mean difference is $+2.49$ points (p=0.066), which is not statistically significant. This comparison uses EMA PopArt rather than the headline's Welford statistics, and the runs span heterogeneous GPU hosts.

E.3 Composing a categorical critic with scale normalization

The standalone HL-Gauss result does not imply that categorical critics are unsuitable for multi-task PPO. We additionally compose HL-Gauss with either per-task reward normalization or PopArt-style adaptive target rescaling (ART). The latter normalizes value targets before categorical projection but omits PopArt's output-preserving reparameterization, for which this categorical implementation has no exact analog. Both compositions disable value clipping. Their support and bin count are calibrated from preliminary return statistics, so they introduce additional choices beyond the headline scalar-critic configuration.

At the LN-c rung, HL-Gauss with reward normalization raises V1 IQM from 59.07 to 79.51 (Table E.4); its paired untrimmed improvement is 20.93 points (p=5.8×10^{-7}). It does not differ significantly from matched scalar reward normalization (-0.26 points, p=0.76) or matched scalar

Table E.4: MT50 V1 categorical-critic compositions, 10 seeds and 100M steps. All rows use LN-c and disable value clipping. The final two rows add PCGrad-a and FairGrad-c at α=1. IQM is accompanied by untrimmed sample std; worst-20 is mean $\pm$ sample std.

Configuration	Bins; support	IQM $\pm$ std	Worst-20
HL-Gauss alone	101; $[-8\times10^5, 1.6\times10^6]$	59.07 ± 4.50	5.30 ± 5.27
HL-Gauss + reward normalization	1000; $[-10, 30]$	79.51 ± 1.48	49.42 ± 3.69
HL-Gauss + ART	2400; $[-10, 60]$	78.78 ± 2.21	47.02 ± 5.46
Full stack + HL-Gauss + reward norm.	1000; $[-10, 30]$	80.29 ± 2.20	51.49 ± 5.50
Full stack + HL-Gauss + ART	2400; $[-10, 60]$	80.03 ± 2.11	50.62 ± 5.27

PopArt ($+0.17$ points, p=0.71). The large improvement over standalone HL-Gauss survives Bonferroni correction over these three comparisons; the composition jointly changes target scaling, support, and bin count, so it does not isolate any single change. On V2, the corresponding 600-bin composition on $[-4, 32]$ reaches mean 89.95 ± 1.92 and worst-10 54.24 ± 7.85; its $+2.21$-point paired mean difference from standalone HL-Gauss is not significant (p=0.061).

A smaller 101-bin reward-normalized control reaches mean 79.89 ± 1.24 over three seeds, with a $+1.15$-point paired difference from the 1000-bin composition on the same seeds (p=0.45). This control uses support $[-6, 25]$, and 25 of 50 tasks have target standard deviation below one bin. Thus a count of tasks with sub-bin target variation is insufficient to explain the standalone critic's failure. The control changes support as well as resolution, has only three seeds, and does not reproduce the most extreme raw-scale resolution deficits; it does not establish that resolution is irrelevant.

Both compositions remain viable in the full stack, but adding the two gradient combiners yields no statistically reliable extra gain: $+0.87$ points for reward normalization (p=0.085) and $+1.46$ points for ART (p=0.151) over their respective LN-c rungs. Comparisons to scalar full-stack references additionally change value clipping, and the categorical runs use CPU PCGrad projections rather than the CUDA path used by some reference runs. These results support scale-aware composition.

E.4 Measured computation cost

We time 10M training interactions per configuration on an RTX 3090 with an AMD EPYC 7313 CPU, allocating 16 CPU cores and 64GB host memory. Table E.5 reports the resulting linear extrapolation to 100M interactions. Evaluation is disabled, and each configuration is measured once; these measurements describe this implementation and hardware rather than a distribution of full-run training times.

Table E.5: Training time extrapolated from 10M measured interactions on an RTX 3090, with evaluation disabled and one measurement per configuration. The three additional combiner rows apply the named method to both actor and critic, with LN-c and PopArt enabled.

Configuration	Hours/100M	Configuration	Hours/100M
Vanilla MT-PPO	8.7	FairGrad on both sides	16.5
+ LN-c	8.8	CAGrad on both sides	16.9
+ LN-c + PopArt	8.9	PCGrad on both sides	23.9
+ LN-c + PopArt + FG-c	15.6	MTSAC	7.2
TOPPO (also PCGrad-a)	19.8	ARS	7.5
		ARS-LN-1024	17.9

LN-c and PopArt add approximately 2% to the vanilla training time in this measurement; extracting and combining per-task gradients accounts for the larger overhead. Among the measured symmetric combiners, FairGrad is the least expensive, while PCGrad takes approximately 45% longer. TOPPO takes approximately 10% longer per environment interaction than ARS-LN-1024 on this rig, so fewer interactions to reach a baseline's final mean should not be interpreted as an end-to-end wall-clock speedup.

The stratified MT50 sampler produces 31 minibatches per repeat, giving 16×31=496 combiner calls per rollout collection and 99,200 per 100M-step seed. In the production critic telemetry of

the headline MT50 V2 runs, Gram formation plus the FairGrad solve averages 6.9–7.4 ms per call over training on the RTX 3090 hosts of seeds 3–9 and 0.8–0.9 ms on the H200 NVL host of seeds 0–2; this timer excludes gradient extraction and recombination. At 99,200 calls per 100M-step seed, the RTX 3090 rate amounts to 11–12 minutes, about 1.0% of the 19.8-hour estimate measured on the same GPU model. The solve-only benchmark on 1,984 real training Gram matrices is reported separately in Section C.5.

The timing comparisons have four further limits. Configurations run on the same CPU/GPU model but not uniformly on the same physical node; in particular, the PopArt-to-FG-c ladder step crosses nodes. SAC and PPO use different software frameworks, and logging is offline for SAC but disabled for PPO. SAC replay warmup is included in the 10M measurement, so linear extrapolation need not reproduce its full-run average throughput. Finally, evaluation and its different checkpoint cadence are excluded, and all measurements use $K=50$; no measured claim about scaling with task count follows.

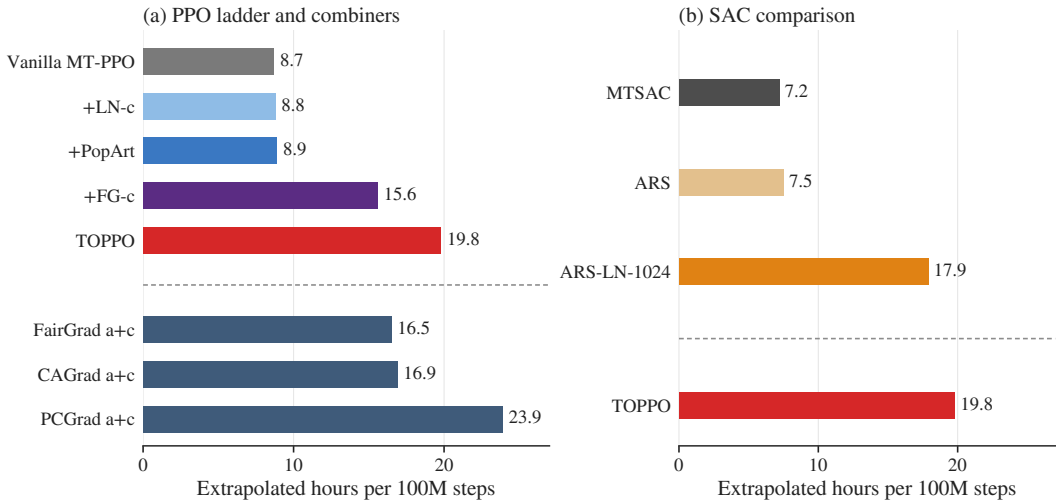


Figure E.4: Training-loop time on RTX 3090/EPYC 7313 hardware with evaluation disabled; each bar is one 10M-step measurement extrapolated to 100M steps, so there are no seed intervals. (a) The PPO intervention path and, below the dashed line, FairGrad, CAGrad, and PCGrad applied to both actor and critic (a+c). (b) MTSAC, ARS, and ARS-LN-1024, with TOPPO for reference. These are whole-loop estimates, distinct from the solve-only speedup.

E.5 AMP humanoid: a two-objective control stress test

We also study humanoid walk steering with an adversarial motion prior (AMP) [Peng et al., 2021], combining task-tracking and motion-style rewards through a shared critic trunk. Our implementation extends MimicKit [Peng, 2025], which provides the humanoid character, steering environment, and AMP agent; the reference walking clip comes from the public DeepMimic motion data [Peng et al., 2018], and all training and evaluation runs use the Newton physics simulator [The Newton Contributors, 2025]. This is a two-objective mechanism stress test rather than a second multi-task benchmark suite. The broader campaign comprises 25 configurations with 10 shared training seeds each; the configurations in Table E.6 all train for 100M samples. Each policy is evaluated on 4,096 episodes under a common environment configuration, using 8,192 motion-style samples.

Our style metric is the squared Fréchet distance after a fixed 64-dimensional random projection of AMP observation features standardized by demonstration statistics. It uses the same feature definition across arms and does not score each policy with its own learned discriminator. We report task return alongside style distance because improving motion similarity can trade off against task tracking. All uncertainty in Table E.6 is sample standard deviation across training seeds, and inference pairs those seeds rather than individual evaluation episodes.

The PPO full stack reduces mean style FID by 76.0% relative to the base policy, with improvement in all ten seeds (paired $p=4.7\times10^{-6}$; 95% CI for the relative mean difference $[-93.8\%, -58.2\%]$;

Table E.6: AMP humanoid walk steering, 100M samples and 10 seeds per arm. Style FID is a squared distance; lower is better. Values are mean ± sample std. The PPO FairGrad row also disables critic gradient clipping, and the full stack retains that change.

Family	Configuration	Task return	Style FID
PPO	Base	533.56 ± 20.74	$(5.477 \pm 1.327) \times 10^4$
PPO	Two-component critic + LN + PopArt	534.99 ± 16.89	$(3.855 \pm 0.871) \times 10^4$
PPO	Above + FG-c, no critic grad clip	550.63 ± 9.01	$(3.635 \pm 3.943) \times 10^4$
PPO	Full stack (also PCGrad-a)	521.11 ± 14.64	$(1.315 \pm 0.088) \times 10^4$
SAC	Base	573.77 ± 4.03	$(5.596 \pm 1.522) \times 10^6$
SAC	Full stack	575.33 ± 2.57	$(4.486 \pm 1.108) \times 10^6$

significant after Bonferroni correction across 25 comparisons). This is evidence for the complete intervention under this protocol. It does not identify independent module effects: introducing FairGrad also disables critic gradient clipping, and the additional PCGrad step is not statistically significant relative to the FairGrad rung (p=0.098; paired difference -2.32×10^4, 95% CI $[-5.16, 0.52] \times 10^4$). Moreover, the full-stack policy walks more slowly: the paired change in projected speed is -0.416 (from 1.169 to 0.753; 95% CI $[-0.529, -0.303]$), while the speed-error change is not significant (95% CI $[-0.119, 0.023]$). The style gain therefore should not be interpreted as a uniform improvement across motion and task objectives.

The SAC full stack reduces mean style FID by 19.8%, but the paired effect is not statistically reliable at n=10 (p=0.078; 95% CI for the relative mean difference $[-42.4\%, 2.8\%]$). The interval establishes neither a reliable benefit nor equivalence to the base policy. Cross-family module comparisons also differ in implementation: the SAC FairGrad path uses a preconditioned fp32 Gram, whereas the PPO path differs, and these arms do not match the aggregate gradient magnitude to a direction-only control. Consequently, the experiment supports a PPO endpoint result while leaving individual mechanisms and general SAC transfer unresolved.

A separate short H200 timing run adds 4.2% end-to-end time for the PPO full stack (189.5 to 197.5s), compared with 49.5% for SAC (287.6 to 430.1s). These are single measurements over approximately 8M samples, not full-budget run-time estimates. Evaluation spans multiple GPU types; repeated evaluations of the same checkpoints show at most 0.994% drift in style FID in the audited cross-device groups.

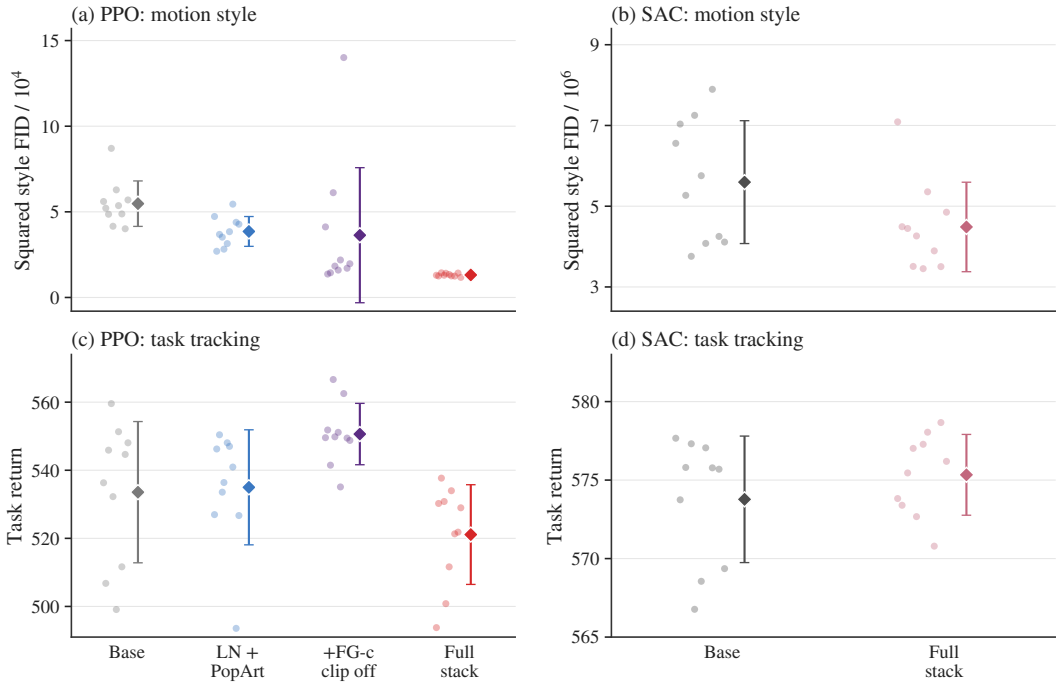


Figure E.5: AMP walk steering, ten seeds per arm at 100M samples. Pale points are seeds; filled diamonds and whiskers show the mean and sample std. (a, b) Motion style as squared Fréchet distance in a common fixed feature space (lower is better; PPO in units of 10^4, SAC in units of 10^6). (c, d) Task return, showing the accompanying tradeoff. The PPO +FG-c arm also disables critic gradient clipping, a change retained by the full stack.

E.6 Actor aggregation and fairness sensitivity

We extend the actor-side comparison with eight choices at a fixed critic configuration: the default mean, PCGrad, CAGrad with c=0.5, and FairGrad with $\alpha_a \in \{0.5, 1, 2, 5, 10\}$. The critic uses LayerNorm and FairGrad at α_c=1 throughout. This study uses EMA PopArt with update coefficient 3×10^{-4}, value clipping enabled, and the same $[400, 400, 400]$ actor and critic architectures. Each of the 16 actor-by-reward-regime cohorts contains 10 completed seeds at 100M environment steps. We report this EMA sensitivity study separately from the Welford-PopArt headline configuration.

Table E.7: Actor aggregation sensitivity on MT50, final checkpoint at 100M steps, 10 seeds per cell. All uncertainties are untrimmed sample standard deviations. V1 IQM uses the paper's seed-trimming convention: sort the ten per-seed mean success rates, discard the two lowest and two highest, and average the remaining six. The Welford reference is the separate headline cohort and is excluded from the EMA actor comparisons.

Actor aggregation	V1 mean ± std	V1 IQM ± std	V2 mean ± std
EMA PopArt study; fixed LN-c and FG-c (α_c=1)			
Default mean	78.32 ± 1.95	78.42 ± 1.95	90.38 ± 1.90
PCGrad	79.94 ± 2.61	80.03 ± 2.61	89.86 ± 1.79
CAGrad (c=0.5)	79.60 ± 1.99	79.71 ± 1.99	90.64 ± 1.91
FairGrad (α_a=0.5)	81.03 ± 2.34	81.09 ± 2.34	89.58 ± 2.04
FairGrad (α_a=1)	81.04 ± 2.38	80.82 ± 2.38	91.10 ± 1.37
FairGrad (α_a=2)	80.00 ± 1.74	80.09 ± 1.74	90.54 ± 2.08
FairGrad (α_a=5)	80.45 ± 2.05	80.47 ± 2.05	89.19 ± 1.80
FairGrad (α_a=10)	80.29 ± 1.84	80.20 ± 1.84	89.70 ± 2.17
Welford PopArt: headline reference			
PCGrad (TOPPO)	79.69 ± 1.35	79.35 ± 1.35	90.88 ± 1.59

Within the EMA cohort, PCGrad is not the highest-scoring actor choice in either reward regime (Table E.7 and Figure E.6). Actor FairGrad at $\alpha_a{=}1$ exceeds PCGrad's untrimmed mean by 1.10 points on V1 and 1.24 points on V2, with paired two-sided Student-t p-values of 0.126 and 0.064, respectively. Across the seven comparisons against PCGrad in each regime, none reaches even nominal $p < 0.05$; the smallest p-values are 0.057 on V1 and 0.064 on V2, and none survives Bonferroni correction within its seven-comparison family. These comparisons are exploratory and do not establish equivalence between actor methods. They show that the headline actor choice is one workable member of a broader set rather than a unique optimum.

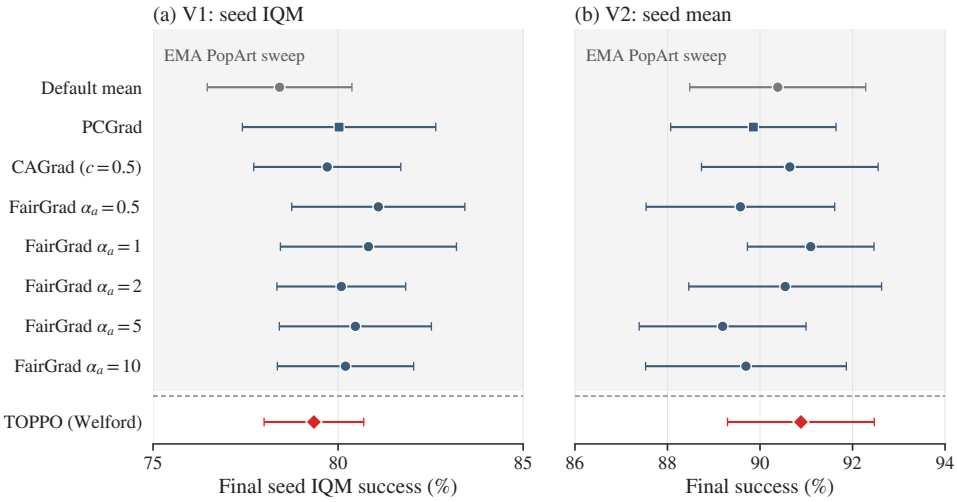


Figure E.6: Actor aggregation on MT50, ten seeds at 100M transitions: (a) V1 seed IQM and (b) V2 seed mean of final success; whiskers are untrimmed sample std. Shaded rows use EMA PopArt, LN-c, and FG-c ($\alpha_c{=}1$) and vary only the actor aggregator: the default mean (gray) and seven alternatives (slate; PCGrad as a square). The red diamond is the separate Welford-PopArt TOPPO headline.